Spring 2019

Beneficial Effects of Resveratrol Against Colitis and Colorectal Cancer Mediated by the Host Microbiome, Epigenome, and Immune Response

Haider Rasheed Daham Alrafas

BENEFICIAL EFFECTS OF RESVERATROL AGAINST COLITIS AND COLORECTAL CANCER MEDIATED BY THE HOST MICROBIOME, EPIGENOME, AND IMMUNE RESPONSE

by

Haider Rasheed Daham Alrafas

Bachelor of Science
University of Basrah, 2004

Master of Science
University of Basrah, 2010

Submitted in Partial Fulfillment of the Requirements

For the Degree of Doctor of Philosophy in

Biomedical Science

School of Medicine

University of South Carolina

2019

Accepted by:

Mitzi Nagarkatti, Major Professor

Prakash Nagarkatti, Committee Member

Traci Testerman, Committee Member

Susan K. Wood, Committee Member

Sofia Lizarraga, Committee Member

Cheryl L. Addy, Vice Provost and Dean of the Graduate School

DEDICATION

This work is dedicated to everyone who has helped me throughout my life, particularly my colleagues who shared this journey with me. I want to also dedicate this work to all my family and friends for offering their much appreciated love and support.

ACKNOWLEDGEMENTS

I would like to thank my mentors, Dr. Mitzi Nagarkatti and Dr. Prakash Nagarkatti, for their support and leadership. I want to thank my committee members, Dr. Traci Testerman, Dr. Susan K. Wood, and Dr. Sofia Lizarraga for their guidance and support. I would like to acknowledge Dr. Philip Brandon Busbee for his help and guidance as both a colleague and friend. Thank you to Nicole Holt, Lee Ann Faulling, Tina Akers, and Margaret Whisenant for their service to our department. I want to thank my fellow graduate students, postdocs, and faculty members from our laboratory for their wisdom and friendship. Thank you Dr. Esraah Al-Harris, Amira Mohammed, Kathryn Miranda, Dr. Hasan Al-Ghetaa , Osama Abdulla, Muthanna Sultan, William Becker and Zinah Al-Gheiz, Dr. Alexa Gandy, Dr. Marpe Bam, Wurood Neamah, and Nicholas Dopkins. I would like to thank my beloved country of Iraq for sending me to the United States and allowing me to complete my Ph.D. here.

Last, but most certainly not least, I want to thank and acknowledge my family in Iraq: my father, Rasheed; my mother; Batool; my brothers, Akra, Mohammad, and Moshtaq; my sister, Eqbal; and my wife, Marwa, and my kids Batool, Mostafa, and Sarah. Most of the good I do and the person I am are in large part due to all of you in so many ways. I thank you all for being there for me, through the good and bad, and I want you to know how lucky of a person I consider myself for having you all in my life.

ABSTRACT

Resveratrol, a natural polyphenol compound found in red wine, the skins of grapes, and other plant products, has been used as a traditional medicine for thousands of years throughout human history, but current research has revealed this natural component is capable of modulating a variety of immunological, microbial, and epigenetic mechanisms to improve overall health and well-being of hosts that consume it. Colitis, an inflammatory bowel disease characterized by chronic inflammation in the colon and rectum, which has been associated with colon cancer. This cancer incidence is rising in younger adults in the US. Thus, newer approaches to prevent colitis and colon cancer are critical. In this dissertation, data and evidence is presented which demonstrate that resveratrol, natural polyphenol can attenuate murine models of colitis and prevent colitis-associated colon cancer. In addition, in-depth mechanistic studies will provide evidence that resveratrol suppresses inflammation in the colon by regulating the host-gut microbiome, as well as inducing epigenetic changes via modulation of small noncoding RNA molecules that target key gene transcripts involved in key immunologic processes.

TABLE OF CONTENTS

LIST OF TABLES

LIST OF FIGURES

LIST OF ABBREVIATIONS

AhR ..... Aryl Hydrocarbon Receptor

BUT ..... Sodium Butyrate

CMC ..... Carboxymethyl Cellulose

CRC ..... Colorectal Cancer

DSS ..... Dextran Sodium Sulfate

ELISA ..... Enzyme-linked Immunosorbant Assay

FT ..... Fecal Transfer

HDAC ..... Histone Deacetylase

IBD ..... Inflammatory Bowel Disease

MDSCs ..... Myeloid-derived Suppressor Cells

miR/miRNA ..... MicroRNA

OTU ..... Operational Taxonomic Unit

PAS ..... Periodic Acid Schiff

PCA ..... Principal Component Analysis

PCR ..... Polyermase Chain Reaction

SCFA ..... Short Chain Fatty Acid

Th ..... T Helper Cell

TNBS ..... 2,4,6-Trinitrobenzenesulfonic Acid

Treg ..... Regulatory T Cell

CHAPTER 1

INTRODUCTION

1.1 COLITIS AND COLITIS-ASSOCIATED COLON CANCER

Inflammatory bowel diseases (IBDs), such as ulcerative colitis (UC) and Crohn's disease (CD), are chronic digestive diseases defined by often uncontrollable inflammation along the gastrointestinal tract and colon (Singh et al., 2014b). The incidence and prevalence of these diseases has risen since 1980 in many parts of the world, particularly in the United States (Molodecky et al., 2012), and there is an alarming trend of these diseases increasing in the pediatric population (Ong et al., 2018; Sykora et al., 2018). Even more concerning is the link between colitis and an increased susceptibility to developing colorectal cancer (CRC) in animal models and the human patient population (Al Bakir et al., 2018; Foersch et al., 2012; Yang et al., 2018a). Colitis, as a form of IBD, has a complex etiology often attributed to many interrelated genetic, dietary, and other environmental factors (Hart, 2019; Mikhailov and Furner, 2009). Current conventional treatment options (e.g. steroids and immunosuppressive drugs) often have adverse side-effects, or in some cases, colitis patients are non-responsive to these conventional therapies (Antonelli et al., 2018). With increasing incidence, a link to development of CRC, and lack of effective treatment options, more studies are focusing on preventative measures to decrease colitis incidence.

Recent advances in next-generation sequencing technology have shown that IBD may also result from alterations in the composition and function of gut microbiota,

referred to as dysbiosis. The gut microbiota also interact closely with dietary components to maintain normal immune system homeostasis in the gut. Whether dietary supplements that are effective against colonic inflammation mediate their effects through modulation of gut microbiota is an area of investigation that is novel and highly significant.

Colorectal cancer (CRC), which is characterized by tumor development in the large intestine, ranks as third among cancer incidences and fourth in cancer-related mortalities worldwide (Global Burden of Disease Cancer et al., 2015). Despite an overall decrease in CRC incidence in the United States among all race and ethnic groups due to standardized screening guidelines (Edwards et al., 2014), there has been a rise in prevalence of this disease among young adult patients which prompted the American Cancer Society to suggest the recommended age for CRC screening be lowered from 50 to 45 (Pittman, 2018). Even with conventional chemotherapy options, which have major negative side-effects, patients often show chemo-resistance (Bose et al., 2011). It is for this reason, the emphasis has been on prevention of CRC development and regular screening to detect and cure at an early stage. CRC development, is also associated with chronic inflammation and high levels of circulating inflammatory biomakers (Lopez et al., 2018; Song et al., 2018). Recent reports have shown that inflammation induced by certain types of diet and alterations in the microbiome is associated with increased risk of CRC development in men and women (Liu et al., 2018; Tabung et al., 2018). By the same token, diet and life styles that promote chronic inflammation in the gut is associated with dysregulation in the microbiome and development of colon tumorigenesis (Chen et al., 2017; Song et al., 2015). Together, such studies suggest that use of preventative

agents against colonic inflammation, or colitis, could be beneficial in reducing the incidence of CRC.

1.2 RESVERATROL

Resveratrol (3,4,5-trihydroxy-trans-stilbene) is a natural polyphenol produced by several plants in response to injury or when the plant is under attack by pathogens such as bacteria or fungi (Singh et al., 2007). Resveratrol has been extensively studied for its therapeutic benefits against a wide array of diseases including cancer, cardiovascular, neurological and inflammatory diseases (Altamemi et al., 2014; Cui et al., 2010; de la Lastra and Villegas, 2005; Guan et al., 2012; Rieder et al., 2012; Singh et al., 2007; Singh et al., 2010; Wu et al., 2005). Resveratrol mediates these anti-inflammatory effects through multiple pathways (Rieder et al., 2012). For example, resveratrol has been shown to attenuate colitis by upregulating of silent mating type information regulation-1 (SIRT1) in immune cells which is associated with the T regulatory cells (Treg) induction and activation of hypoxia-inducible Factor 1α (HIF-1α)/MTor signaling pathway (Singh et al., 2010; Yao et al., 2015). Resveratrol has also been shown to induce unique microRNA that trigger anti-inflammatory pathways as well as induce myeloid-derived suppressor cells (MDSCs) (Altamemi et al., 2014; Cui et al., 2010; Singh et al., 2010; Singh et al., 2012). While resveratrol has been shown to alter the gut microbiome in various disease models (Diaz-Gerevini et al., 2016; Etxeberria et al., 2015; Jung et al., 2016; Tung et al., 2016), these studies have captured only an association between resveratrol-induced modulations in gut microbiota and the disease outcome. Thus, conclusive evidence, such as through fecal transfer, is lacking to connect resveratrol-

induced modulation in gut microbiota and its beneficial effects against disease pathogenesis.

In addition, resveratrol has been shown to be a promising preventive measure to suppress chronic inflammation leading to tumor development (Busbee et al., 2013). Resveratrol has already been shown by our lab, as well as others, to possess a myriad of anti-cancer effects, including those related to CRC. This natural compound has been shown to be effective at preventing the proliferation and survival of human CRC cells as well decrease CRC disease severity and tumor development in relevant animal CRC models (Busbee et al., 2013; Elshaer et al., 2018; Hofseth et al., 2010). Some of the mechanisms by which resveratrol has been shown to prevent colon cancer cell proliferation and invasion metastasis include regulation of key cellular signaling pathways such as NF-Kb-dependent cellular processes (Buhrmann et al., 2017), PI3K/Akt signaling (Zeng et al., 2017), modulation of histones and sirtuins (San Hipolito-Luengo et al., 2017), inhibition of cyclooxygenase-2 (Cox-2) expression (Gong et al., 2017), and alterations in gene-regulating microRNAs (miR) (Yang et al., 2015). Previous reports from our lab have shown that resveratrol is able to alter expression of certain miRs (miR-101b and miR-455) that target inflammatory mediators such as interleukin-6 (IL-6), tumor necrosis factor alpha (TNF-α), and COX-2 in the dextran sodium sulfate (DSS)-induced colitis-associated tumorigenesis Apc(Min/+) mouse model (Altamemi et al., 2014). In addition, in the AOM/DSS CRC model, we have shown that resveratrol downregulates inflammatory stress markers such as p53 to modulate the T cell response (Cui et al., 2010). However, while the regulation of these host-derived cellular mechanisms play an important role in resveratrol-mediated CRC treatment, recent

research has shown the gut microbiome is also a key player in both CRC disease development and progression (Chen, 2018). Nonetheless, whether the ability of resveratrol to suppress CRC is related to its action on gut microbiota remains a possibility that needs to be explored.

1.3 THE GUT MICROBIOME

The gut microbiome, a diverse ecosystem consisting of gut commensals including bacteria and fungi, has been shown to have a great impact on human health and disease, particularly in CRC (Jobin, 2017; Rezasoltani et al., 2017; Zou et al., 2018). For example, patients diagnosed with CRC were found to have distinct microbiome profiles compared to healthy controls, and this microbial signature was found to be altered after treatment with probiotics (Hibberd et al., 2017). Interestingly, after oral administration of antibiotics to deplete the gut microbiome, tumor burden was decreased in a CRC murine model, but this effect was negated in Rag-deficient mice that lacked mature T cells and B cells (Sethi et al., 2018). This study highlights the importance of the interplay between the host immune defense the microbiome. While resveratrol has been shown to modulate the host immune response to promote anti-inflammation as previously discussed and has been shown to alter the microbiome in other disease models (Chen et al., 2016; Kim et al., 2018; Qiao et al., 2014; Zhao et al., 2017), there currently are no reports determining if resveratrol-mediated alterations in the gut microbiome can influence the immune response to protect against CRC development caused by chronic colitis.

1.4 MICRORNA

microRNA (miRNA or miR) are small 18-25 nucleotide non-coding RNAs that regulate the expression of several protein-encoding genes post-transcriptionally by either

inhibiting translation of targeted-miR or leading to the degradation of certain targeted-mRNA transcripts, and even though they make up only 3% of the human genome, it has been estimated that these non-coding RNAs regulate around 90% of genes (Guo et al., 2018). Canonical miR biogenesis begins in the nucleus when miR genes are transcribed by either RNA polymerase II or III to produce primary miRNA transcripts (pri-miRNAs). While still in the nucleus, pri-miRNA is cleaved by a class 2 RNAase III enzyme, called Drosha, to create a 60-70 nucleotide hairpin structured precursor (pre-miRNA). The pre-RNA is then shuttled from the nucleus to the cytoplasm by Exportin 5 (Exp5), where it is released by Exp5 when GTP on the Exp5-associated Ran cofactor is converted to GDP. While in the cytoplasm, another RNase called dicer cleaves pre-miRNA into a duplex intermediate. The duplex intermediate is bound to an Argonaute (AGO) protein to form a AGO:mature miRNA strand complex, where one strand of the intermediate is discarded (Catalanotto et al., 2016).

miRs were found to be important in both the development and progression of colitis, particularly in terms of regulating inflammation, serving as disease biomarkers, and responding to therapies (Feng et al., 2018; Lopetuso et al., 2018; Minacapelli et al., 2019; Morilla et al., 2018; Schonauen et al., 2018; Singh et al., 2014a). The importance of miRs in regulating colitis was highlighted in our previous report showing that deficiency in only one miR (miR-155) was able to protect mice from developing severe colitis symptoms by a reduction in the inflammatory T helper (Th) type responses (Singh et al., 2014a).

1.5 PROBLEM AND HYPOTHESIS

IBD patients represent a high risk group for developing colitis-associated CRC, and these diseases, which currently has no cure, result in an overall decrease in quality of life and an increase in health care costs. There is need to seek out new and novel treatments to combat the inflammatory response initiated by colitis and colitis-associated colorectal cancer. Therefore, we examined how the use of natural product, resveratrol, could prevent colitis-induced T cell activation and inflammation which could lead to colorectal cancer. Based on recent findings that resveratrol has anti-inflammatory and anti-microbial properties, we hypothesized that resveratrol would be a novel treatment for colitis and colitis-associated CRC in relevant mouse models through alterations in gut microbiota and regulating certain miRs during inflammation.

CHAPTER 2

RESVERATROL MODULATES THE GUT MICROBIOTA TO PREVENT MURINE COLITIS DEVELOPMENT THROUGH INDUCTION OF TREGS AND SUPPRESSION OF TH17 CELLS

2.1 ABSTRACT

Inflammatory diseases of the gastrointestinal tract are often associated with microbial dysbiosis. Thus, dietary interactions with intestinal microbiota, to maintain homeostasis, play a crucial role in regulation of clinical disorders such as colitis. In the current study, we investigated if resveratrol, a polyphenol found in a variety of foods and beverages, would reverse microbial dysbiosis induced during colitis. Administration of resveratrol attenuated colonic inflammation and clinical symptoms in the murine model of TNBS-induced colitis. Resveratrol treatment in mice with colitis led to an increase in CD4+FOXP3+ and CD4+IL-10+ T cells, and a decrease in CD4+IFN-γ+ and CD4+IL-17+ T cells. 16S rRNA gene sequencing to investigate alterations in the gut microbiota revealed that TNBS caused significant dybiosis, which was reversed following resveratrol treatment. Analysis of cecal flush revealed that TNBS administration led to an increase in species such as *Bacteroides acidifaciens,* but decrease in species such as *Ruminococcus gnavus* and *Akkermansia mucinphilia,* as well as a decrease in SCFA i-butyric acid. However, resveratrol treatment restored the gut bacteria back to homeostatic levels, and increased production of i-butyric acid. Fecal transfer experiments confirmed the protective role of resveratrol-induced microbiota against colitis inasmuch as such

recipient mice were more resistant to TNBS-colitis and exhibited polarization towards CD4+FOXP3+ T cells and decreases in CD4+IFN-γ+ and CD4+IL-17+ T cells. Collectively, these data demonstrate that resveratrol-mediated attenuation of colitis results from reversal of microbial dysbiosis induced during colitis and such microbiota protect the host from colonic inflammation by inducing Tregs while suppressing inflammatory Th1/Th17 cells.

2.2 INTRODUCTION

Here, we demonstrate that during colitis, microbial dysbiosis takes place in the host, which leads to the activation and differentiation of inflammatory effector T cells and inhibition of Tregs. However, upon treatment with resveratrol, these changes are reversed, leading to the development of an anti-inflammatory Treg response. More importantly, we conclusively prove that this mechanism is driven by resveratrol-mediated alterations in the gut microbiome by performing fecal transplant experiments, thereby not only reinforcing the notion that resveratrol is a potential therapeutic against colitis, but also providing a key mechanism through which resveratrol mediates its effects.

2.3 MATERIALS AND METHODS

Animals. Female BALB/c mice (aged 6-8 weeks) were purchased from the Jackson Laboratories (Bar Harbor, ME). All mice were housed at the AAALAC-accredited animal facility at the University of South Carolina, School of Medicine (Columbia, SC). All procedures were performed according to NIH guidelines under protocols approved by the Institutional Animal Care and Use Committee.

Effects of resveratrol on colitis in mice. To test the efficacy of treatment with resveratrol in an *in vivo* TNBS-induced colitis mouse model, we used TNBS, purchased

from Sigma-Aldrich (St. Louis, MO). After lightly anesthetizing the mice with controlled isoflurane vaporizer chamber (5% isoflurane with 75% CO2/25% O2), TNBS was administered intrarectally one time into female BALB/c mice at a dose of 1 mg dissolved 0.1 ml of 50% ethanol using a 38 mm catheter, as previously reported (Elson et al., 1996). For treatment groups resveratrol, purchased from Sigma-Aldrich (St. Louis, MO), was administered orally using a 30 mm oral gavage needle at 100 mg/kg, a dose established in our previous studies (Singh et al., 2010), in a total volume of 100µl in appropriate vehicle of 1% carboxymethyl cellulose (CMC). Resveratrol was given 24 hours prior to TNBS injection and given daily this way until completion of the experiment (5 days). Two control groups were used for this study. One control group only received appropriate vehicle (CMC), while the other control group received 100 mg/kg resveratrol dissolved in CMC vehicle. Neither of these control groups received injection of TNBS. The evaluation of colitis clinical signs was done by measuring the weight of mice in all groups daily and performing colonoscopy every other day after TNBS-colitis induction. Colonoscopy scores were determined using a scoring system previously published (Kodani et al., 2013). In addition, blood was collected prior to experimental endpoint and serum samples were separated and stored at -20°C for colitis-associated biomarker detection. All experimental mice studied were also given intrarectal injections of 50% ethanol to ensure changes in the gut were due to either TNBS or treatment and not attributed to alterations by ethanol. Resveratrol efficacy was also tested in the dextran sodium sulfate (DSS) model of colitis. DSS (3%) was used to induce disease as previously reported (Cui et al., 2010), and treatment groups (DSS+Resveratrol)

were given oral administration of 100 mg/kg of the compound daily throughout the 14-day experiment.

Histology analysis. Animals were euthanized 5 days after injection of TNBS using the drop jar method containing 5% isoflurane (260 mL in 1 L drop jar) for overdose inhalation, and the proximal portion of colons were excised and cleaned by saline flushing. The length of colon was measured before fixing the excised tissue with 4% paraformaldehyde. Colon pieces were embedded in paraffin, cut into 5μm sections, deparaffinized in xylene, serially diluted in decreasing concentrations of ethanol, and stained with hematoxylin-eosin (H&E) for histopathological examination and Periodic Acid Schiff (PAS) staining to assess mucosal mucin production and presence of goblet cells. Histological scoring of colon sections was determined using previously published criteria (Akgun et al., 2005).

Serum evaluation by enzyme-linked immunoabsorbant assay (ELISA). Acute phase serum amyloid A (SAA), Lipocalin-2 (Lcn2), myeloid peroxidase (MPO), and interleukin-10 (IL-10) levels in the serum were measured by using enzyme-linked immunosorbent assay (ELISA) kits. SAA ELISA kit was purchased from Abcam (Cambridge, United Kingdom), Lcn-2 ELISA kit was purchased from Thermo-Scientific (Waltham, Massachusetts, USA), MPO ELISA kit was acquired from LifeSpan BioSciences (Seattle, WA) and the IL-10 Luminex ELISA kit was purchased from Biolegend (San Diego, CA). All kits were used in accordance with the respective manufacturer's protocol.

Flow cytometry staining and analysis. Cells from mesenteric lymph nodes were isolated and the red blood cells were lysed using lysis buffer (Sigma, St Louis, MO). Cell

suspensions were filtered using sterile 70 micron filters (Sigma, St Louis, MO). Four-color flow cytometric analysis was performed following blocking with Fc receptor. All cells were washed with FACS staining buffer (PBS with 1% fetal bovine serum), then stained with FITC-labeled anti-CD3, PE-labeled anti-CD8 and PE-CY7-labeled anti-CD4 at manufacturer suggested concentrations (Biolegend, San Diego, CA). For intracellular staining, cells previously stained for membrane proteins were fixed and permeabilized using a Fix/Perm kit (Biolegend, San Diego, CA). Cells were stained with PE-Cy7-labeled CD4, PE-labeled Foxp3, FITC-labeled IL10, PE-labeled IFN-γ, and FITC-labeled IL-17 (Biolegend, San Diego, CA). Flow cytometry data was analyzed using a CXP FC500 flow cytometer (Beckman Coulter, Brea, CA) and the gating strategy for shown represented plots is shown in Figure 2.1.

Genomic DNA extraction and 16S rRNA gene sequencing. Colonic flushes were used for pyrosequencing analysis to characterize the gut microbiome composition. The extraction of genomic DNA from colonic flushes was carried out using the QIAamp DNA Stool Mini Kit (Qiagen, Hilden, Germany) according to the manufacture's instruction. The DNA concentration were determined using a NanoDrop ND-1000 spectrophotometer and stored at −20°C until further processing. Amplification of the 16S rRNA V3-V4 hypervariable gene region was carried out using the 16S V3 314F forward (5′TCGTCGGCAGCGTCAGATGTGTATAAGAGACAGCCTACGGGNGGCWGCAG 3′) and V4 805R reverse primers (5′GTCTCGTGGGCTCGGAGATGTGTATAAGAGACAGGACTACHVGGGTATCT AATCC3′) with added Illumina adapter overhang nucleotide sequences. The PCR conditions used were as follows: 3 minutes (min) at 95°C, follow by 25 cycles of 30

seconds (s) at 95°C, 30 s at 55°C and 30 s at 72°C, and a final extension at 72°C for 5 min. Each reaction mixture (25 µl) contained 50 ng of genomic DNA, 0.5 µl of amplicon PCR forward primer (0.2 µM), 0.5 µl of amplicon PCR reverse primer (0.2 µM) and 12.5 µl of 2× KAPA Hifi Hot Start Ready Mix. Each reaction was cleaned up with Agencourt AMPure XP beads (Beckman Coulter, Indianapolis, IN). Attachment of dual indices and Illumina sequencing adapters was performed using 5 µl of amplicon PCR DNA product, 5 µl of Illumina Nextera XT Index Primer 1 (N7xx), 5 µl of Nextera XT Index Primer 2 (S5xx), 25 µl of 2× KAPA HiFi Hot Start Ready Mix, and 10 µl of PCR-grade water in this case. Amplification was carried out under the following conditions: 3 min at 95°C, followed by 8 cycles of 30 s at 95°C, 30 s at 55°C, and 30 s at 72°C, and a final extension at 75°C for 5 min. Constructed 16S rRNA gene libraries were purified with Agencourt AMPure XP beads and quantified with Quant-iT PicoGreen dsDNA Assay kit (Thermo Fisher Scientific, Waltham, MA). Library quality control and average size distribution were determined with the Agilent Technologies 2100 Bioanalyzer (Agilent, Santa Clara, CA). Libraries were normalized and pooled to 40 nM based on quantified values. Pooled samples were denatured and diluted to a final concentration of 6 pM with a 30% PhiX (Illumina, San Diego, CA) control. Amplicons were subject to pyrosequencing using the MiSeq Reagent Kit V3 in the Illumina MiSeq System.

Microbial 16S rRNA gene analysis of sequencing data. The online 16S analysis software from National Institute of Health (NIH, Baltimore, MD), known as Nephele (https://nephele.niaid.nih.gov/), was used to analyze sequencing data collection from the Illumina MiSeq platform. FASTQ sequences were uploaded to Nephele and the 16S metagenomics application was performed. Groups of related DNA sequences were

assigned to operational taxonomic units (OTUs), and Nephele-generated output files were analyzed to determine gut microbial composition. Linear Discrimination Analysis Effect Size (LEfSe) was performed on Nephele-generated OTU output data in order to determine microbial biomarkers among experimental groups as previously described (Segata et al., 2011).

Quantitative Real-Time PCR. For validation of bacteria identified by 16S rRNA gene analysis, qRT-PCR was used. DNA was extracted from cecal samples using the QIAamp DNA Stool Mini Kit (Qiagen, Hilden, Germany). Samples were analyzed by PCR using primers designed to amplify bacterial 16S rRNA genes. For quantification of *Ruminococcus gnavus* (5′AGAGGGATGTCAAGACCAGGTA, 3′TACTAGGTGTCGGGTGGAAAAG), *Akkermansia muciniphila* (5′GTATCTAATCCCTTTCGCTCCC, 3′GACTAGAGTAATGGAGGGGGAA), and *Bacteroides acidifaciens* (5′GTATGGGATGGGGATGCGTT, 3′CTGCCTCCCGTAGAGTTTGG) the StepOnePlus Real-Time PCR system was used. Fold changes from PCR analysis were obtained by using the delta-delta CT method with comparison to the control group (Vehicle).

SCFAs identification and quantification. Colonic flushes were collected immediately after euthanasia by excising colon tissues and flushing them with PBS. Samples were collected into in 2 ml Eppendorf tubes under anaerobic conditions. Samples collected were immediately frozen at −80 °C for future analysis. Samples were analyzed for SCFA concentrations using 2-Ethylbutyric acid as internal standard as previously described (Chitrala et al., 2017). Briefly, the cecal samples (100 mg) were suspended and homogenized in water. After centrifugation for 10 min at 12,000 rpm, the

supernatant was acidified by addition 25% metaphosphoric acid. The internal standard was added into the supernatant. SCFAs were identified and quantified using a HP 5890 gas chromatograph configured with flame-ionization detectors (GC-FID) and SCFAs were identified using control standard compounds purchased from Sigma-Aldrich.

Fecal transfer experiment. Fecal material from TNBS+Vehicle or TNBS+Resveratrol mice was collected 48 hours after the last day of oral gavage treatment in the experimental model (day 5) from colonic flushes under anaerobic conditions (using anerobic glove box chamber) prior to inoculation into recipient mice in 200 µl of PBS. Fecal material was collected 48 hours after the last treatment to ensure that resveratrol had been absorbed in the tissues and eliminated from the feces prior to collection, as studies have shown this natural compound is rapidly absorbed and eliminated after consumption (Busbee et al., 2013). Before the fecal transfer, recipient mice (6 weeks old) were treated with streptomycin and penicillin to deplete endogenous gut microbiota. Penicillin (1g/L) and streptomycin (1g/L) were dissolved in sterile water and 100 µl were fed into mice by oral gavage once a day for four consecutive weeks, as previously described (Khosravi et al., 2014). Depletion of microbiota was validated by PCR analysis using 16S rRNA gene Eubacteria primer (5′ATTACCGCGGCTGCTGGC, 3′ACTCCTACGGGAGGCAGCAGT). Colitis induction was performed as previously described. Briefly, on the last day of antibiotic treatment, prior to disease induction, recipient mice were given feces (5g/L stocks from disease and treated groups) by oral gavage (100 µl) for 5 days. Body weights were measured daily and colonoscopy was performed every other day. At the end of experiment, the mice were sacrificed and colon tissues were taken for histopathology analysis by staining with H&E and PAS as

described already. Mesenteric lymph nodes were taken and T cell phenotyping was performed using flow cytometry as described above.

Statistical Analysis. GraphPad Prism software (San Diego, CA) was used for all statistical analysis. For the *in vivo* mouse experiments, groups of 5-10 mice were used per experimental group. For *in vitro* assays, all experiments were performed in triplicate. For statistical differences, one-way ANOVA was used for each experiment, and Tukey's post-hoc test was performed to analyze differences between groups, unless otherwise indicated. A p value of at least ≤ 0.05 was used to determine statistical significance.

2.4 RESULTS

Resveratrol attenuates TNBS-induced colitis

In the current study, we tested the ability of resveratrol to attenuate a well-characterized TNBS-mediated murine model of colitis (Kim and Berstad, 1992). We used 4 groups of mice: Vehicle alone, resveratrol alone, TNBS+Vehicle, and TNBS+Resveratrol. TNBS administration caused colitis with significant decrease in body weight (~20%) when compared to Vehicle- or resveratrol-treated only groups, as depicted in Figure 2.2A. However, in the TNBS+Resveratrol group, the weight loss was significantly reversed (~8%). Additionally, the TNBS+Vehicle group showed ~60% survival, while TNBS+Resveratrol group showed 100% survival (Figure 2.2B). Colitis-induction caused an overall decrease in the colon length in TNBS+Vehicle groups compared to those treated with either Vehicle or Resveratrol alone, as shown in Figure 2.2C-D. However, TNBS+Resveratrol groups showed a significant increase in colon length when compared with the disease group (TNBS+Vehicle). Colitis is also characterized by large productions of inflammatory biomarkers such as SAA, Lcn2, and

increased MPO activity, which are often used in the diagnosis of the severity of colitis (Martinez-Moya et al., 2012; Singh et al., 2012). The level of these biomarkers were significantly elevated in the TNBS+Vehicle group (Figure 2.2E-G), but TNBS+Resveratrol showed significant decreases in the levels of all those inflammatory biomarkers, collectively showing that resveratrol was able to ameliorate the colonic inflammatory response induced by TNBS. Similar results were obtained in DSS-induced colitis model with the current resveratrol treatment regimen. Oral administration of resveratrol prevented DSS colitis-induced weight loss (Figure 2.3A) and colon shortening (Figure 2.3B-C).

Colonoscopic examination at 3 different time points (days 0, 3, and 5) during the experiment gave a clear picture of the development of colitis-associated lesions and tissue sloughing after TNBS injection (TNBS+Vehicle), but TNBS+Resveratrol mice showed marked decrease in tissue disruption (Figure 2.2H-I). Histological examination of formalin-fixed colon tissues stained with H&E was also performed (Figure 2.4A), which showed a significant amount of cellular infiltration and loss of mucosal architecture in the TNBS+Vehicle group compared to naive mice treated with either just Vehicle or resveratrol alone. In contrast, TNBS+Resveratrol mice showed marked reduction in cellular infiltration, resembling the control groups. We also performed PAS staining on fixed colon tissue to determine normal arrangement and distribution of mucin and goblet cells within the colon mucosa. Mice challenged with TNBS showed high reduction in the number of goblet cells and mucin thickness, which was greatly returned to normal levels and size of mucin thickness in colons excised from TNBS+Resveratrol mice, similarly to naïve mice treated with Vehicle or resveratrol only (Figure 2.4B). Histological scores of

colons from TNBS mice treated with resveratrol (TNBS+Resveratrol) showed a significant decrease in disease parameters compared to TNBS+Vehicle mice, which had much higher scores than the controls groups (Figure 2.4C). These data suggested that resveratrol prevents the colonic tissue damage induced by TNBS, which includes loss of the naturally-occurring protective mucous layer.

Resveratrol treatment reduces inflammatory T cell subsets and increases anti-inflammatory Tregs

In order to examine the T cell subsets during disease and treatment states, we isolated cells from the mesenteric lymph node of all groups and phenotyped these cells using flow cytometry. First, we looked at expression of the general T cell marker (CD3) which showed a significant increase in the percentage in TNBS+RES mice, while TNBS+Resveratrol treatment led to a marked decrease (Figure 2.5A). We next looked at both T helper ($CD4^+$) and cytotoxic ($CD8^+$) T cell subset populations and showed significant increases in both $CD4^+$ and $CD8^+$ T cells in TNBS+Vehicle mice compared with those that were treated with Vehicle or resveratrol alone (Figure 2.5B), but this was effectively reduced in TNBS+Resveratrol groups. We then performed intracellular/intranuclear staining to identify the effect of resveratrol on specific $CD4^+$ T cells subsets which include inflammatory IFNγ- and IL17-producing $CD4^+$ T cells, in addition to anti-inflammatory $CD4^+FOXP3^+$ and $CD4^+IL10^+$ populations. The data showed a significant increase in percentages of both anti-inflammatory $CD4^+FOXP3^+$ and $CD4^+IL10^+$ cells population in the TNBS+Resveratrol group when compared TNBS+Vehicle, and this increase in $CD4^+FOXP3^+$ populations were also observed in naïve mice treated with resveratrol (Figure 2.5C-D). In contrast, intracellular staining for

$CD4^+IFN\gamma^+$ and $CD4^+IL17^+$ showed significant increases in both percentage and absolute cell number in TNBS+Vehicle mice, while those in the TNBS+Resveratrol had a reversal in this effect (Figure 2.5E-F). Absolute cell numbers of T cells and T cell subsets in the MLN confirmed these findings (Figure 2.5G). Collectively, these data showed that resveratrol treatment reduces the inflammatory T cell response during TNBS-induced colitis, while promoting the production of anti-inflammatory T cell subsets, mainly Tregs and IL-10-producing $CD4^+$ cells. This increase in Tregs was also observed in naïve mice that were treated only with resveratrol alone.

Alterations in gut microbiota and SCFA composition in colitis-induced mice treated with resveratrol

Next, we analyzed the gut microbiota from the all experimental groups to determine whether or not resveratrol altered the gut microbial composition during colitis. From colonic flushes, we isolated genomic DNA and performed 16S rRNA gene sequencing, analyzing the sequenced reads with the NIH-based Nephele online analysis tool. Nephele analysis output showed that the alpha diversity, represented as chao1, in naïve mice treated with resveratrol had the most diverse gut microbial compositions when to the other groups (Figure 2.6A). In terms of beta diversity, depicted as a PCA plot, samples clustered within their respective groups, with TNBS+Vehicle samples showing more dissimilarity compared to Vehicle-treated, or those groups treated with resveratrol (Resveratrol or TNBS+Resveratrol) (Figure 2.6B). 16s rRNA gene sequencing analysis from Nephele allowed sample reads to be classified into OTUs from phylum to the species level, and output data up to the genus level is summarized in Figures 2.7-2.9. In order to determine the most divergent and potential microbial biomarkers within

experimental groups, LeFSe analysis was performed with comparisons of TNBS+Vehicle vs TNBS+Resveratrol (Figure 2.6C-D). The results showed that TNBS+Vehicle mice had increased abundance of *Bacteroides acidifaciens* compared to the other groups (Figure 2.6E), while naïve or TNBS-induced colitis mice treated with resveratrol had enrichment of bacteria belonging to the genus *Ruminococcus* (Figure 2.6C). At the species level, *Ruminococcus gnavus* and *Akkermansia muciniphila* showed a significant increase in TNBS+Resveratrol groups when compared to TNBS+Vehicle groups (Figure 2.6F-G). It is interesting to note that mice treated with resveratrol alone also showed increases in *Ruminococcus gnavus* (Figure 2.6F). In order to validate our sequencing results at the species level, we performed PCR using bacterial species-specific primers. As shown in Figure 2.6H-J, *Bacteroides acidifaciens* was increased in the TNBS+Vehicle group compared to naïve mice treated with Vehicle or resveratrol only, but this species was reduced in the TNBS+Resveratrol group (Figure 2.6H). In addition, *Ruminococcus gnavus* and *Akkermansia muciphila* species showed significant increases in abundance in groups treated with resveratrol (Resveratrol or TNBS+Resveratrol) when compared to those treated with only vehicle (Vehicle or TNBS+Vehicle) (Figure 2.6I-J).

Lastly, we measured the SCFA production in response to these changes in the gut microbiome composition (Figure 2.10). The data showed that acetic acid and i-butyric acid concentrations were significantly reduced in the TNBS+Vehicle groups when compared to Vehicle, while naïve mice treated with resveratrol and TNBS+RES groups showed significant increases in these SCFAs (Figure 2.10A, 2.10C). However, propionic acid, n-butyric acid, i-valeric acid, n-valeric acid, and n-copric acid showed no significant changes among the various groups (Figure 2.10B, 2.10D-F). Together, these

data suggested that treatment with resveratrol, particularly in colitis induced conditions, significantly altered both the gut microbiome composition and SCFA production.

Fecal transfer from resveratrol-treated groups attenuates TNBS-induced colitis and alters the immune response

In order to determine whether or not resveratrol-induced alterations in the gut microbiome contributes to the altered immune response in colitis, we performed fecal transfer experiments following treatment of mice with antibiotics to deplete the existing gut microbiota. While there were no significant differences observed in body weight of mice in the wild-type and antibiotic-treated mice (Figure 2.11A), PCR for the universal Eubacteria 16S rRNA gene confirmed that the microbiome was depleted in antibiotic-treated mice prior to inoculation with fecal material (Figure 2.11B-C). TNBS-exposed mice were inoculated with either feces from TNBS-treated mice ((FT) TNBS+Vehicle), or inoculated with feces from TNBS+Resveratrol-treated mice ((FT) TNBS+Resveratrol). (FT) TNBS+Vehicle mice showed a gradual decrease in body weight until the termination of the experiment (Figure 2.11D). However, (FT) TNBS+Resveratrol mice showed resistance to loss of body weight. TNBS-induced colitis mice transferred with feces from TNBS+Vehicle also had shorter colons when compared those receiving fecal transfers from TNBS+Resveratrol-treated mice (Figure 2.11E-F). Looking at colitis-associated inflammatory biomarkers such as SAA, Lcn2, and MPO, we found that the (FT) TNBS+Resveratrol group had significantly lower levels of these inflammatory biomarkers compared to the (FT) TNBS+Vehicle group (Figure 2.11G-I). In addition, colonoscopy examination showed increased ulceration and sloughing in portions of the colon in (FT) TNBS+Vehicle mice, while (FT) TNBS+Resveratrol groups showed

reduced presence of colon tissue destruction (Figure 2.11J, top panel). Colonoscopy and histological examination of formalin-fixed colon tissues stained with H&E also showed that (FT) TNBS+Resveratrol mice showed no signs of cellular infiltration and tissue destruction, while (FT) TNBS+Vehicle mice had these colitis-associated observations (Figure 2.11J-K).

Lastly, we performed T cell $CD4^+$ phenotyping of the mesenteric lymph nodes in these fecal transfer experiments. The data showed that there was significant increases in $CD4^+FOXP3^+$ Tregs (Figure 2.11L), though not in $CD4^+IL10^+$ (Figure 2.11M), populations in the (FT) TNBS+Resveratrol group compared to (FT) TNBS+Vehicle, and the inflammatory Th1 ($CD4^+IFN\gamma^+$) and Th17 ($CD4^+IL17^+$) numbers were significantly reduced in these mice as well (Figure 2.11N-O). In order to confirm that relevant species were in fact altered during the FT experiments, PCR validation was performed on colonic flushes from these experimental FT groups. PCR validation showed that mice (FT) TNBS+Resveratrol mice did have increased levels of *Akkermansia muciniphila* (Figure 2.11P) and *Ruminococcus gnavus* (Figure 2.11Q) when compared to (FT) TNBS+Vehicle mice. In addition, there was significantly lower levels of *Bacteroides acidifaciens* in (FT) TNBS+Resveratrol groups compared to (FT) TNBS+Vehicle (Figure 2.11R), confirming that prominent species from the sequencing data were transferred successfully. Together, the fecal transfer experiments demonstrated that microbiota from (FT) TNBS+Resveratrol groups provide significant protection from colitis through enhancement of Tregs and suppression of Th17 and Th1 cells.

2.5 DISCUSSION

Resversatrol is a potent anti-inflammatory agent. Studies from our lab and elsewhere have shown the ability resveratrol to reduce the symptoms associated with colitis, in different murine models (Martin et al., 2006; Singh et al., 2012; Wagnerova et al., 2017; Yao et al., 2015; Youn et al., 2009), as well as in human patient populations (Samsami-Kor et al., 2015). Resveratrol is known to act through multiple pathways. In our previous reports, we were able to reveal some of the mechanisms that made this natural compound such a successful treatment. For example, in the genetic IL-10-/- model of colitis, we showed that resveratrol treatment was able to induce immunosuppressive MDSCs that led to a reduction in clinical parameters in addition to the reduction in CXCR3 expressing T cells (Singh et al., 2012). The ability of resveratrol to induce these anti-inflammatory MDSCs has been shown in our lab in other disease models (Altamemi et al., 2014; Guan et al., 2012; Rieder et al., 2012), and been confirmed by others as well (Chen et al., 2015a; Hong et al., 2017). Other studies have shown that the beneficial effects of resveratrol against colitis can be attributed to other mechanisms, such as targeting sphingosine kinase 1 (SphK1) and apoptosis, restoring nitric oxide levels, reducing neutrophil infiltration, inhibiting nuclear factor-kappaB activation, acting as an anti-oxidant, as well as inhibiting adhesion molecules (Abdallah and Ismael, 2011; Abdin, 2013; Yao et al., 2011). Resveratrol is also well-known to be a ligand for the aryl hydrocarbon receptor (AhR), and our lab and others have shown this natural compound's ability to shift T cell differentiation from Th17 to Tregs, which is dependent on this receptor-ligand interaction (Singh et al., 2007; Wang et al., 2013). Classically, Th1 and Th2 cells were thought to characterize Crohn's disease and ulcerative colitis respectively, however, Th17 cells are now known to play an important

role in gut immunity and inflammation, particularly in regards to IBDs such as colitis (Ueno et al., 2018). Genome-wide association (GWAS) studies in IBD patients found that IL-17 regulating genes are greatly altered in the disease state, thus suggesting the importance of this factor in IBD such as colitis (Ueno et al., 2018). In fact, both animal models of colitis and human IBD patients are characterized by increased presence and development of Th17 cells at sites of inflammation (Galvez, 2014; Jiang et al., 2014; Lee et al., 2012). Th17 plasticity towards inflammatory (IFN-γ-producing Th1) or anti-inflammatory (Treg) phenotypes make it a very unique cell population involved in intestinal homeostasis (Galvez, 2014). Interestingly, recent research has shown that Th17 cells are greatly influenced by the microenvironment such as the microbiome and microbial-derived byproducts (Ueno et al., 2018).

More recent studies have shown that resveratrol may protect against many clinical disorders by modulating the gut microbiota (Bird et al., 2017; Chen et al., 2016; Sung et al., 2017). However, such studies did not perform fecal transfer experiments to demonstrate that the microbiota altered by resveratrol treatment could lead to suppression of colitis-associated inflammation. In the present report, we therefore performed fecal transfer experiments, which conclusively demonstrated that resveratrol-mediated modulations in the gut microbiota is indeed responsible for attenuating colonic inflammation. It is becoming apparent that the gut microbiome contributes significantly to the development and progression of various diseases, particularly in the case of colitis (Autenrieth and Baumgart, 2017; Conte et al., 2006; Kanauchi et al., 2003; Nishikawa et al., 2009; Rapozo et al., 2017). With the gut microbiome playing such an important role in this disease, recent research is even focused on fecal transfer experiments as a

therapeutic option (Meighani et al., 2017; Paramsothy et al., 2017). In addition, potential treatments against colitis are being examined more thoroughly to determine what, if any, effects these possible therapeutics have on the gut microbiome (Jang et al., 2017; Yang et al., 2017).

In the current study, we were able to show that bacteria, such as those belonging to the Genus *Ruminococcus*, are increased during resveratrol treatment, which is consistent with animal studies and human fecal transplant experiments in which bacteria such as *Ruminococcus* and others were found to be anti-inflammatory, restoring and maintaining normal gastrointestinal tract function and integrity (Satokari et al., 2014). In fact, *Ruminococcus gnavus* and *Akkermansia muciniphilia* are mucolytic bacteria that are found to be reduced in both ulcerative colitis and Crohn's Disease patients when compared to normal patient controls (Png et al., 2010). Therefore, restoration of these bacteria, which we noted in our data after naïve mice or TNBS-induced colitis mice were treated with resveratrol, could help in restoring or maintaining gut homeostasis, particularly after the microbiome is altered during colitis due to microbial dysbiosis. On the other hand, the current study shows that resveratrol can effectively reduce *Bacteroides acidifaciens*, which was found to be significantly increased in TNBS-induced colitis, a finding also seen in a murine DSS model (Kang et al., 2013). *B. acidifaciens* have several features which could lead to the progression and development of colitis. This species is known to degrade mucin (Miyamoto and Itoh, 2000), the protective layer in the colon producing the host epithelial surface from luminal-bound bacteria. *B. acidifaciens* is also known to increase SCFA production of acetic and succinic acids (Miyamoto and Itoh, 2000), both of which can contribute to colitis-

associated inflammation. Acetic acid, given in high concentrations, can induce colitis in murine models (Karakoyun et al., 2017). Succinic acid, which is produced by members of *Bacteroidacea*e, like *B. acidifaciens*, was found to be increased in the colons of colitis-induced mice and when administered by enemas can produce ulcers in the colon (Ariake et al., 2000). *B. acidifaciens* resembles closely another member of the same genus *B. fragilis*, and these bacteria have been shown in the literature to trigger a strong inflammatory cascade response, including activation of IL-17-dependent pathways (Chung et al., 2018). By decreasing the presence of these bacteria during colitis-induction, resveratrol might be able to suppress the Th17 response which would normally lead to resident tissue destruction and microbial dysbiosis.

From our present study, we were also able to show that not only does resveratrol alter gut microbial composition during colitis disease induction, but these changes in the gut microbiome lead to alterations in the production of SCFAs. In particular, we found that i-butyric acid was significantly upregulated in resveratrol-treated mice during colitis induction and slightly in naïve mice treated with resveratrol compared to those treated only with Vehicle. From the literature, we know that butyrate/butyric acid has potent anti-inflammatory properties (Dai et al., 2017; van der Beek et al., 2017; Wang et al., 2017). There are studies that also show that butyrate plays an important role in regulating the development of colitis, or acting as an agent to mitigate its deleterious effects (Cobo et al., 2017; Zhang et al., 2016c). For example, oral administration of sodium butyrate into DSS-induced colitis mice led to reduction of inflammation (Simeoli et al., 2017). Butyrate deficiency was shown to increase susceptibility to the development of colitis (Meisel et al., 2017). Therefore, the fact that resveratrol was able to increase production

of this SCFA, particularly during colitis-induced conditions, provides a better understanding of the mechanisms that promote its efficiency against colitis, as well as other inflammatory disorders. Interestingly, we saw an increase in acetic acid in resveratrol treatment only after colitis induction, and this SCFA is often used to induce colitis (Sadraei et al., 2017). It is possible that the increase in butyric acid was able to either negate the effects of increased acetic acid in our model. The uniqueness of our findings lie in the fact that we were able to show through 16S rRNA gene sequencing and fecal transfer experiments that the effectiveness of resveratrol against colitis could be explained by the ability of this natural product to alter and reverse microbial dysbiosis and SCFA production to promote an anti-inflammatory effect (induction of Treg/IL-10) and suppress the inflammatory (Th1/Th17) T cell response, something that has not been reported in the literature thus far. It is particularly interesting to note that the poor bioavailability of resveratrol during oral consumption, which is attributed to the weak aqueous solubility of the compound, has always been an issue in terms to suggesting this natural product as a treatment of various disease (Peng et al., 2018). In fact, this observation has led to a wealth of research focusing on how to increase the bioavailability of this potent anti-inflammatory natural product so that it can be absorbed and circulated to various affected organs, such as by way of encapsulation in nanoparticles or some other vehicle (Borges et al., 2018; Zu et al., 2018). However, our findings suggest that resveratrol alters the microbiome directly and this leads to the anti-inflammatory effects during colitis, even before it becomes bioavailable to various organs after oral consumption.

In summary, the current study demonstrates the efficacy of resveratrol to attenuate colitis may result from its ability to alter gut microbiota that promotes anti-inflammatory T cell induction while suppressing pro-inflammatory T cells as summarized in Figure 2.12.

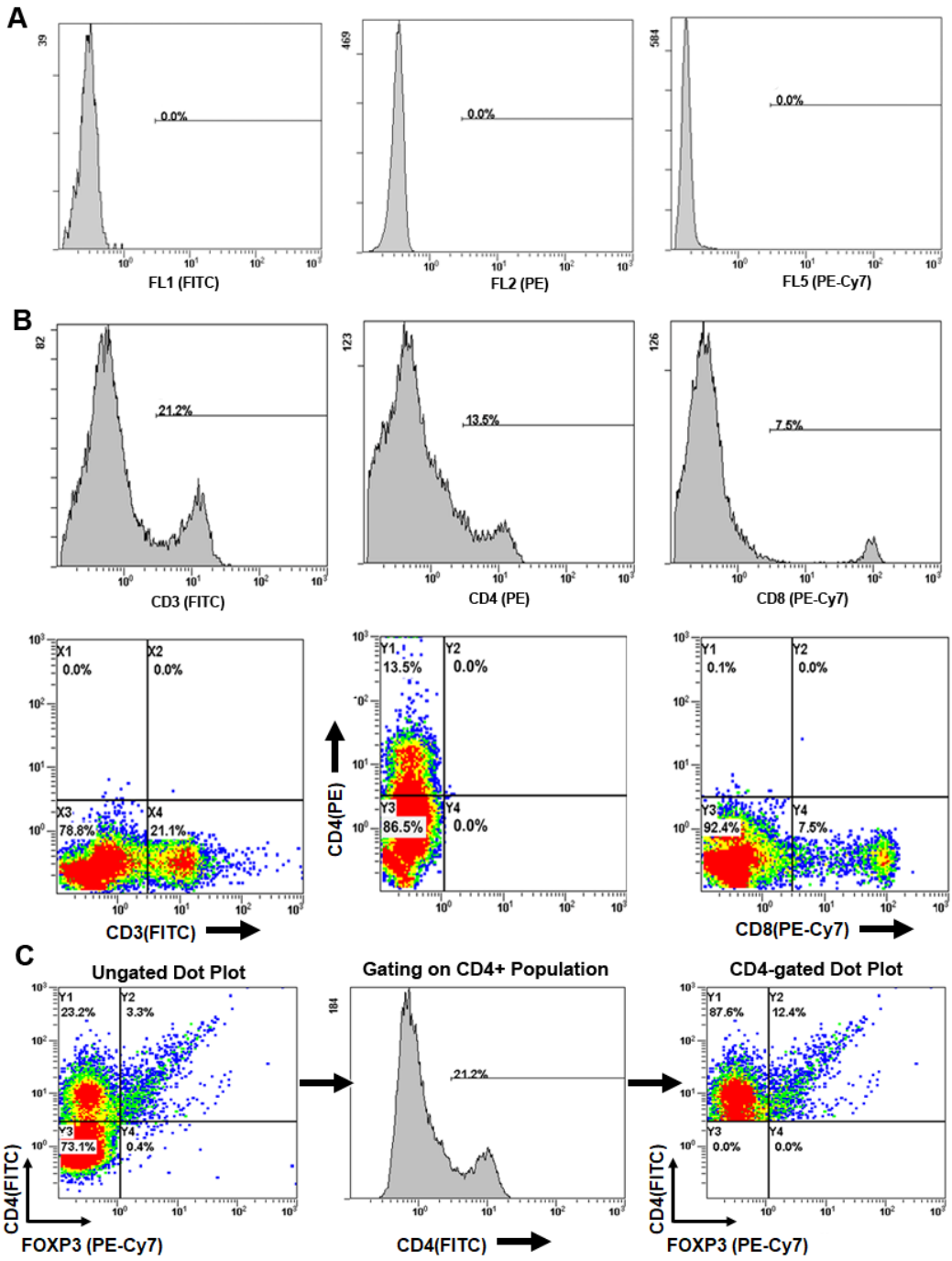

Figure 2.1 Gating strategy for flow cytometry. MLN lymph nodes from control (Vehicle) mice were stained and examined by flow cytometry using the following gating strategy: (A) Unstained negative controls were used to eliminate any non-specific false positive signal. (B) Single color controls were stained with either CD3 (FITC), CD4 (PE), or CD8 (PE-Cy7) to determine appropriate gating for histogram (top) and color dot plots (bottom). (C) Intracellular staining of CD4+ cells was gated as shown and represented in Figure 2.5.

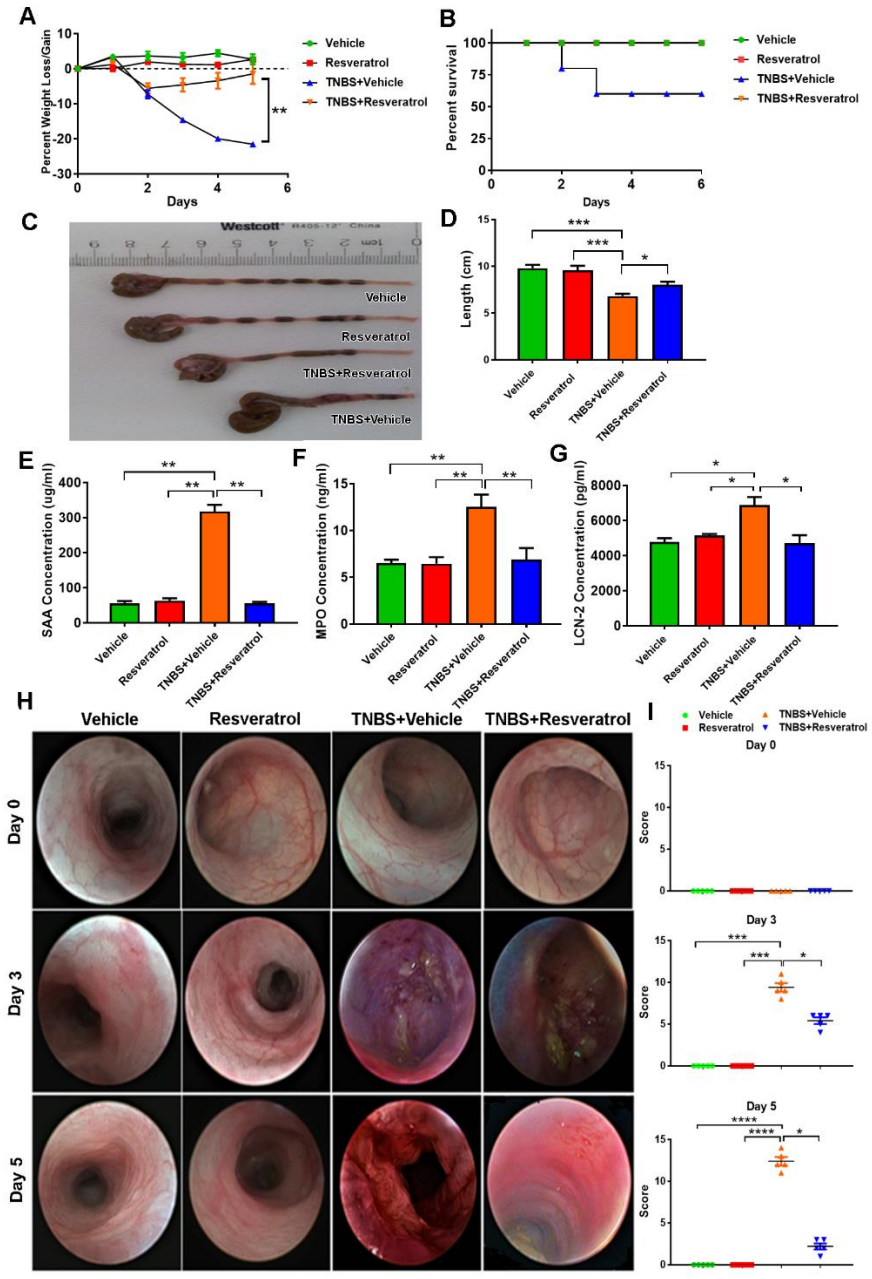

Figure 2.2 Treatment with resveratrol reduces clinical symptoms associated with TNBS-induced colitis murine model. Balb/c mice were administered intrarectally with 1mg of TNBS to induce colitis. Four groups of mice were used: Vehicle, Resveratrol, TNBS+Vehicle and TNBS+Resveratrol. The percent weight loss (A) was determined over the course of the study. (B) Survival curve of mice up to day 6 with colitis and those treated with RES. Colon lengths (C-D) were measured upon sacrifice (Day 5). Serum levels of SAA (E), MPO (F) and Lcn2 (G) were evaluated by ELISA. Endoscopy (H) was performed on mice on days 0, 3, and 5. Colonoscopy scores are provided (I). Significance (p-value: *<0.05, **<0.01, ***<0.005, ****<0.001) was determined by using one-way ANOVA and post-hoc Tukey's test. In all data presented in the figure, 5 mice were used in each group. Data presented is representative of at least 3 independent experiments.

Figure 2.3 Treatment with resveratrol reduces clinical symptoms associated with DSS-induced colitis murine model. C57BL/6 mice were given 7 days of 3% DSS ad libitum followed by regular drinking water for 7 more days. Four groups of mice (n=5 per group) were used: Vehicle, Resveratrol, DSS+Vehicle and DSS+Resveratrol. The percent weight loss (A) was determined over the course of the study. Colon lengths (B-C) were measured upon sacrifice (Day 10). Significance of the bar graphs (p-value: *<0.05, **<0.01, ***<0.005, ****<0.001) were determined by using one-way ANOVA followed by Tukey's post-hoc multiple comparisons test.

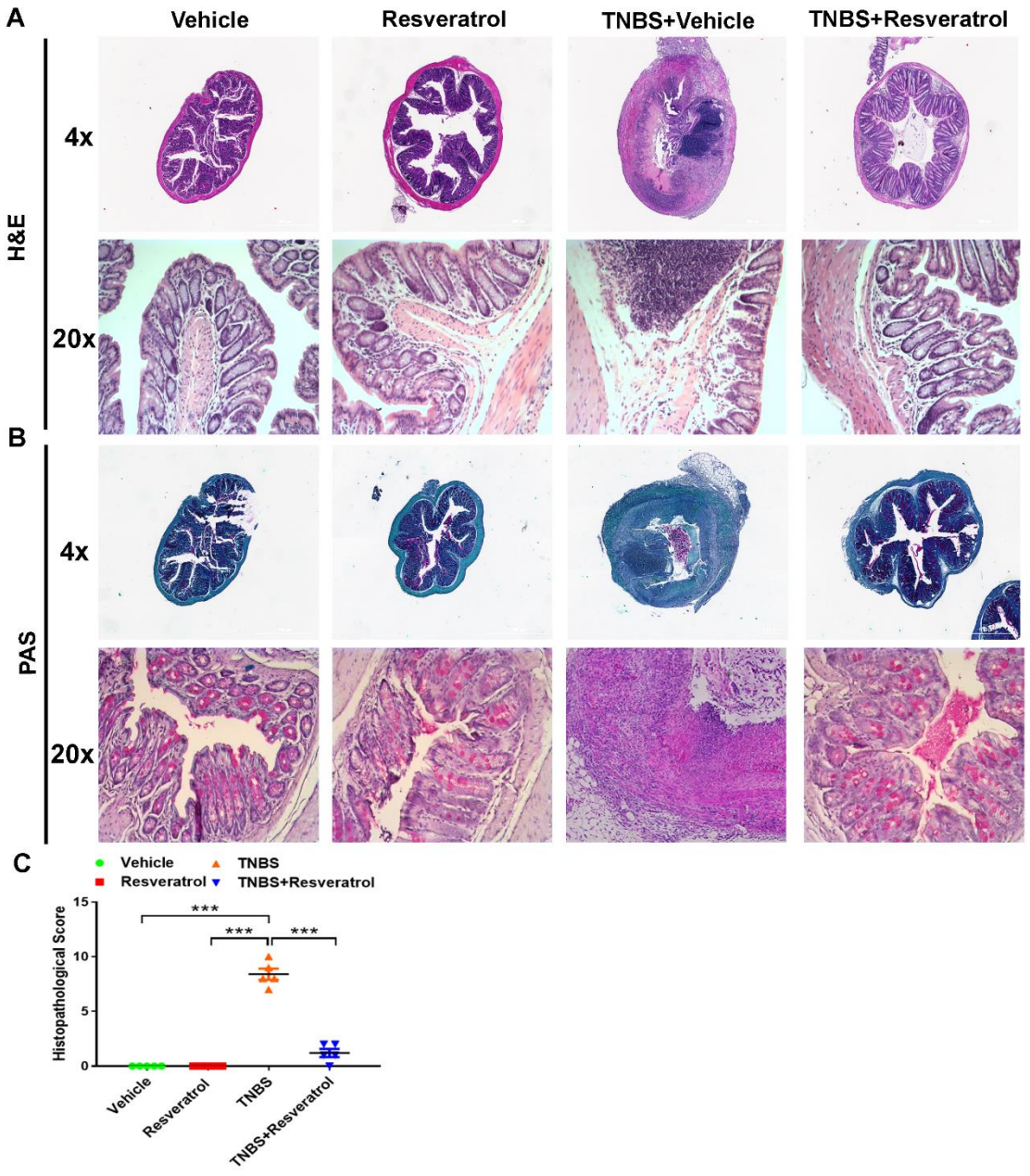

Figure 2.4 Treatment with resveratrol prevents cellular infiltration and mucin degradation and maintains colon gut structural architecture in TNBS model. The study was designed as described in Figure 2.2 legend. Colons (n=5) were excised from experimental mice at the endpoint of experiment, fixed in 10% formaldehyde, and embedded in paraffin blocks. Cross-section slides containing colons from experimental groups were stained using H&E (A) or PAS (B) for histological evaluation. Images of stained tissue were taken using both 4x and 20x objectives, and histological scores were provided (C). Scale bars (white) depicted are at 100 µM. Data is representative of at least 3 independent experiments.

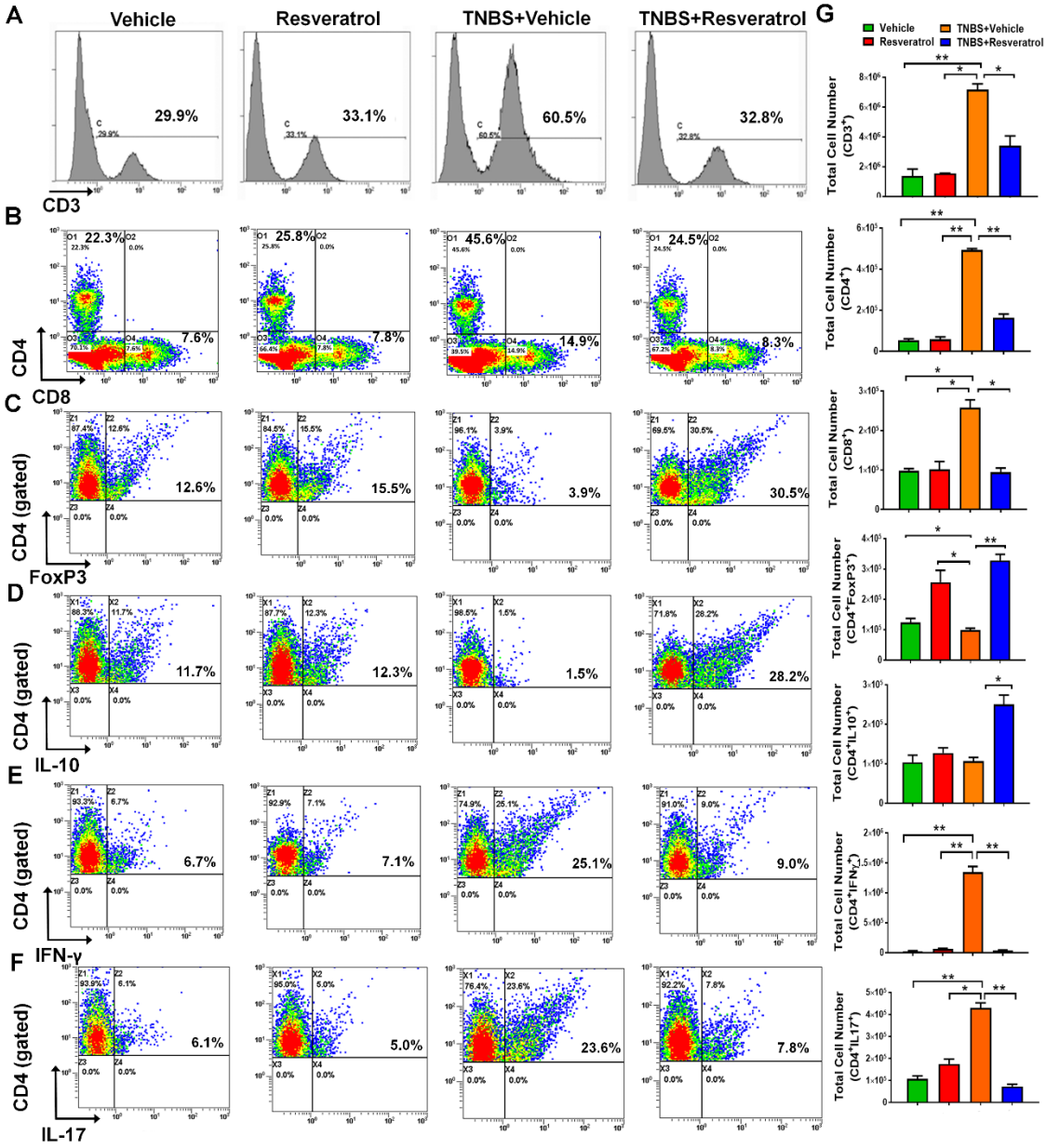

Figure 2.5 Resveratrol alters T cell subsets during TNBS colitis. The study was designed as described in Figure 2.2 legend. Flow cytometry histograms/dot plots are shown for the following T cell subsets: CD3+ (A), CD4+ or CD8+ cells (B), CD4+FOXP3+ (C), CD4+IL10+ (D) and CD4+IFNγ+ (E), and CD4+IL-17+ (F) expressing cells. For Figures C-F, cells were gated on the CD4+ population. The gating strategy for the CD4+ populations is detailed in Figure 2.1. Quantitative bar graphs depicting absolute cell numbers of the T cell subsets is provided (G) Each experimental group had at least 5 mice included, and significance (p-value: *<0.05, **<0.01, ***<0.005, ****<0.001) was determined for absolute cell numbers by using one-way ANOVA followed by Tukey's post-hoc multiple comparisons test. Data is representative of at least 3 independent experiments.

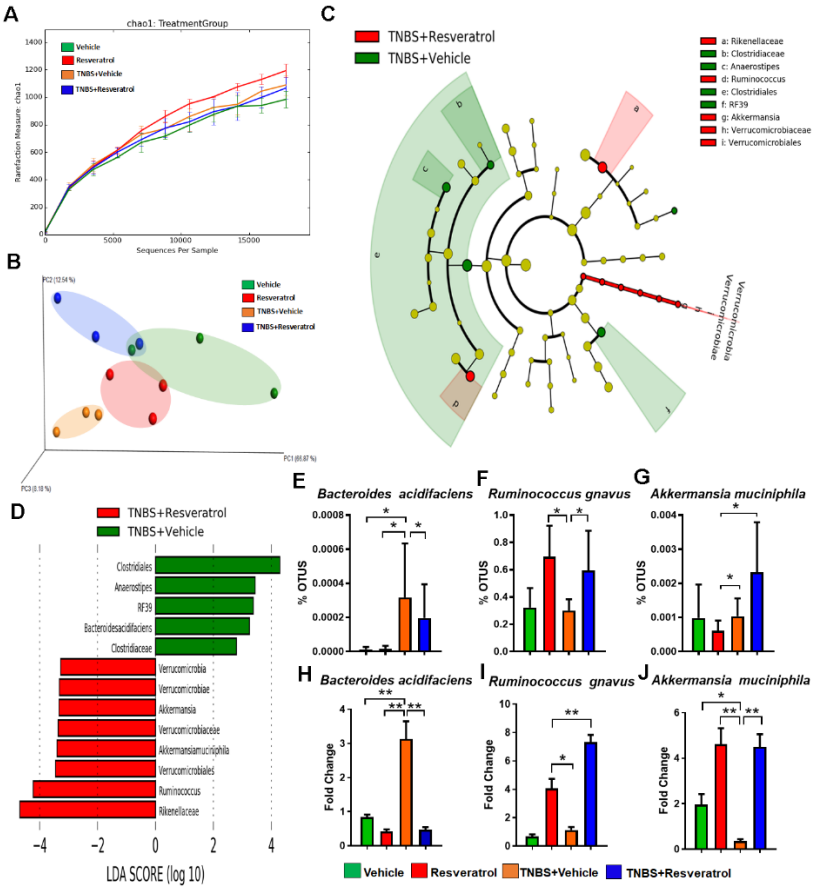

Figure 2.6 16S rRNA gene sequencing analysis. The study was designed as described in Figure 2.2 legend. Gut microbiome samples were collected from experimental groups by performing cecal flushes. Genomic DNA was isolated and V3-V4 regions of 16S rRNA gene subunit were sequenced. Three randomly selected mice from each group (n=3) were used for these experiments. All sequencing samples were analyzed using Nephele software 16S metagenomics provided at Nephele website (nephele.niaid.nih.gov). Alpha diversity (A), and Beta diversity (B) are depicted. LeFSe analysis of the Nephele OTU output files generated the cladogram (C) and LDA score bar graph (D) depicting microbial biomarkers among TNBS+Vehicle vs. TNBS+RES groups. OTU percent abundances are shown for the species Bacteroides acidifaciens (E) Ruminococcus gnavus (F) and Akkermansia muciphila (G). Validation of these significantly-altered bacterial species were performed using PCR and the fold changes are calculated using the delta-delta CT method with comparison to Vehicle controls (H-J). For 16S rRNA gene sequencing, 3 representative cecal flushes from each experimental group were processed and sequenced. For PCR validation, 10 mice were used in each group and fold changes were calculated using the delta-delta CT method compared to Vehicle control. Significance (p-value: *<0.05, **<0.01, ***<0.005, ****<0.001) was determined by using one-way ANOVA followed by Tukey's post-hoc multiple comparisons test. Experiments are representative of 3 independent experiments.

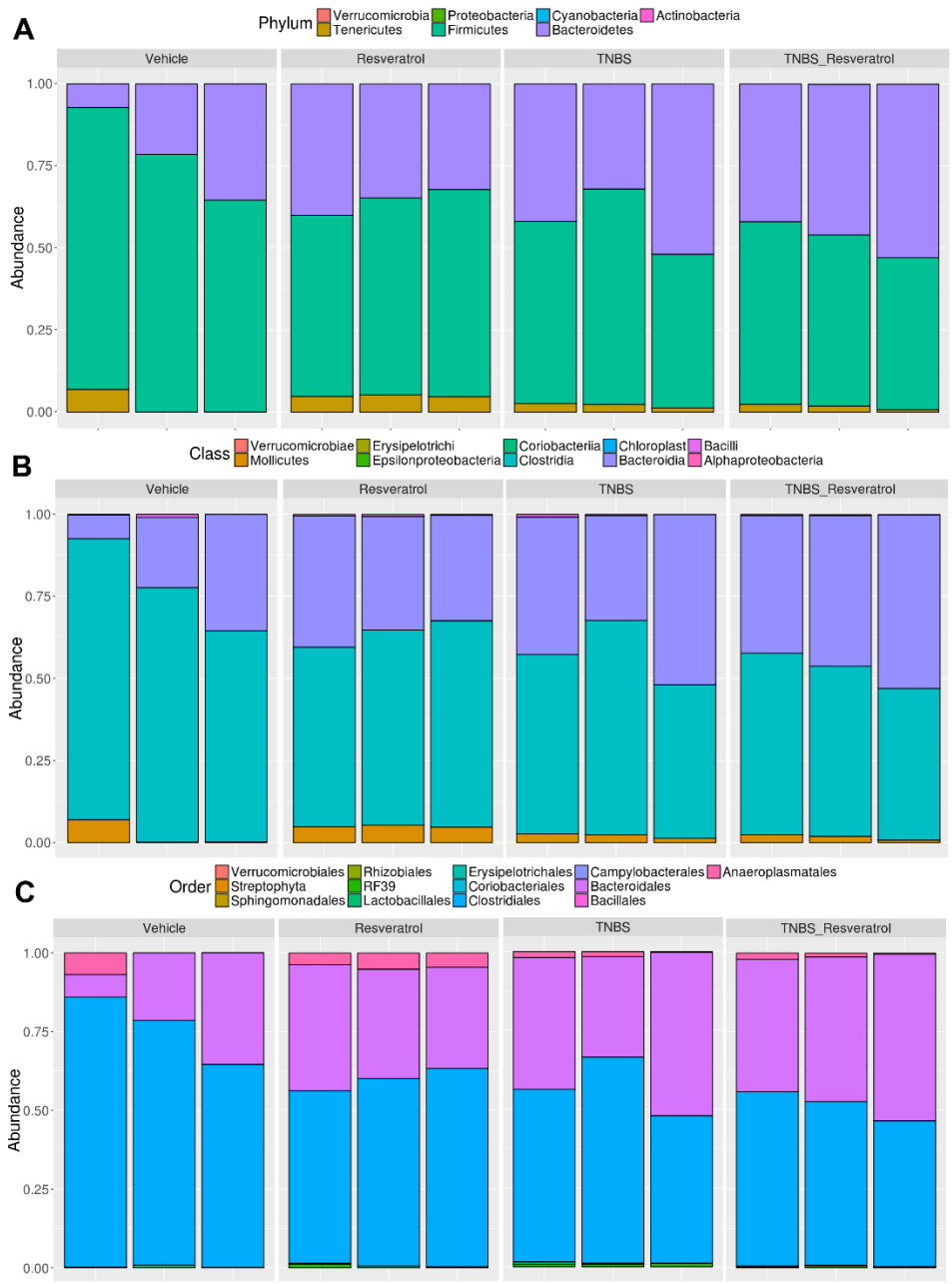

Figure 2.7 16S rRNA sequencing analysis at the phylum to order level. Gut microbiome samples (n=3 per group) were collected from experimental groups (Vehicle, Resveratrol, TNBS+Resveratrol, TNBS+Vehicle) by performing cecal flushes. Genomic DNA was isolated and V3-V4 regions of 16S rRNA subunit were sequenced. Three randomly selected mice from each group were used for these experiments. All sequencing samples were analyzed using Nephele software 16S metagenomics provided at Nephele website (nephele.niaid.nih.gov). Stacked bar charts depicting OTU relative expression with corresponding color-coded legend for the following levels: phylum (A), class (B), and order (C).

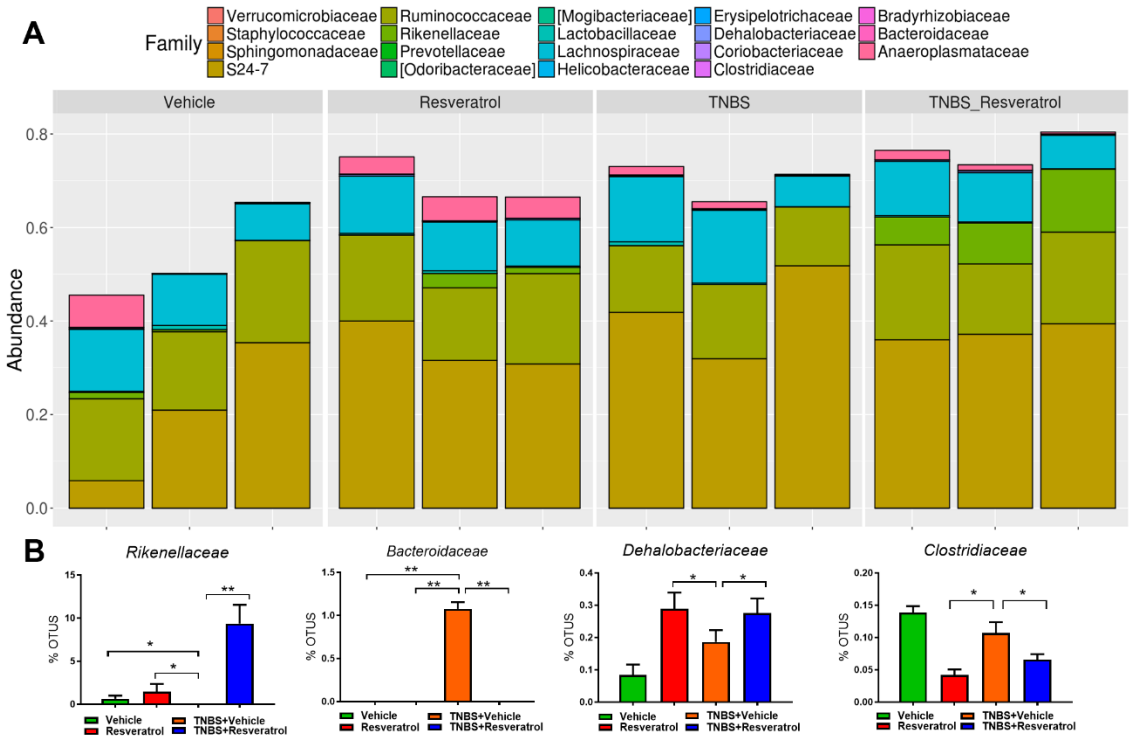

Figure 2.8 16S rRNA sequencing analysis at the family level. Gut microbiome samples were collected from experimental groups (Vehicle, Resveratrol, TNBS+Resveratrol, TNBS+Vehicle) by performing cecal flushes. Genomic DNA was isolated and V3-V4 regions of 16S rRNA subunit were sequenced. Three randomly selected mice from each group were used for these experiments. All sequencing samples were analyzed using Nephele software 16S metagenomics provided at Nephele website (nephele.niaid.nih.gov). (A) Stacked bar charts depicting OTU relative expression with corresponding color-coded legend. (B) Bar graphs representing percent OTU abundance. Significance of the bar graphs (p-value: *<0.05, **<0.01, ***<0.005, ****<0.001) were determined by using one-way ANOVA followed by Tukey's post-hoc multiple comparisons test.

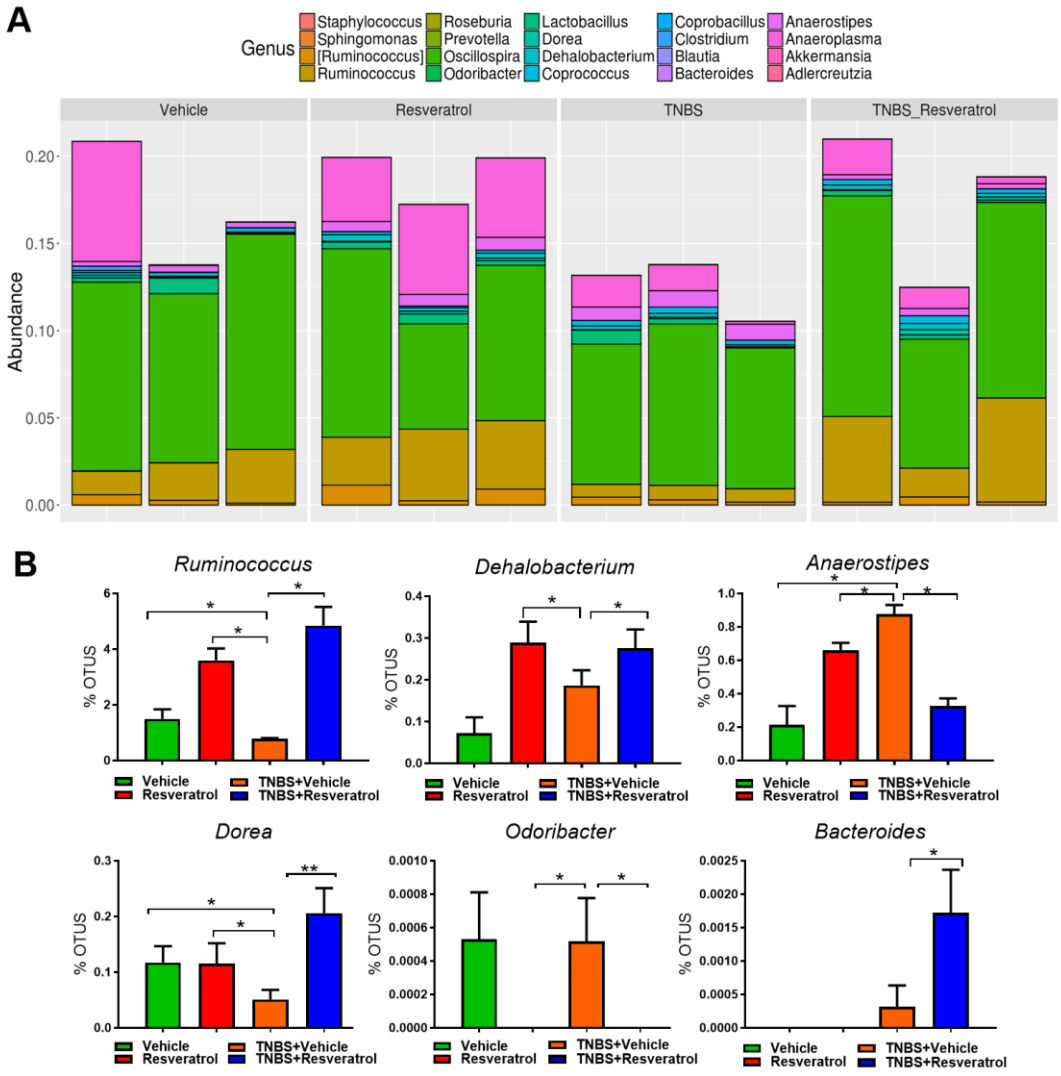

Figure 2.9 16S rRNA sequencing analysis at the genus level. Gut microbiome samples were collected from experimental groups (Vehicle, Resveratrol, TNBS+Resveratrol, TNBS+Vehicle) by performing cecal flushes. Genomic DNA was isolated and V3-V4 regions of 16S rRNA subunit were sequenced. Three randomly selected mice from each group were used for these experiments. All sequencing samples were analyzed using Nephele software 16S metagenomics provided at Nephele website (nephele.niaid.nih.gov). (A) Stacked bar charts depicting OTU relative expression with corresponding color-coded legend. (B) Bar graphs representing percent OTU abundance. Significance of the bar graphs (p-value: *<0.05, **<0.01, ***<0.005, ****<0.001) were determined by using one-way ANOVA followed by Tukey's post-hoc multiple comparisons test.

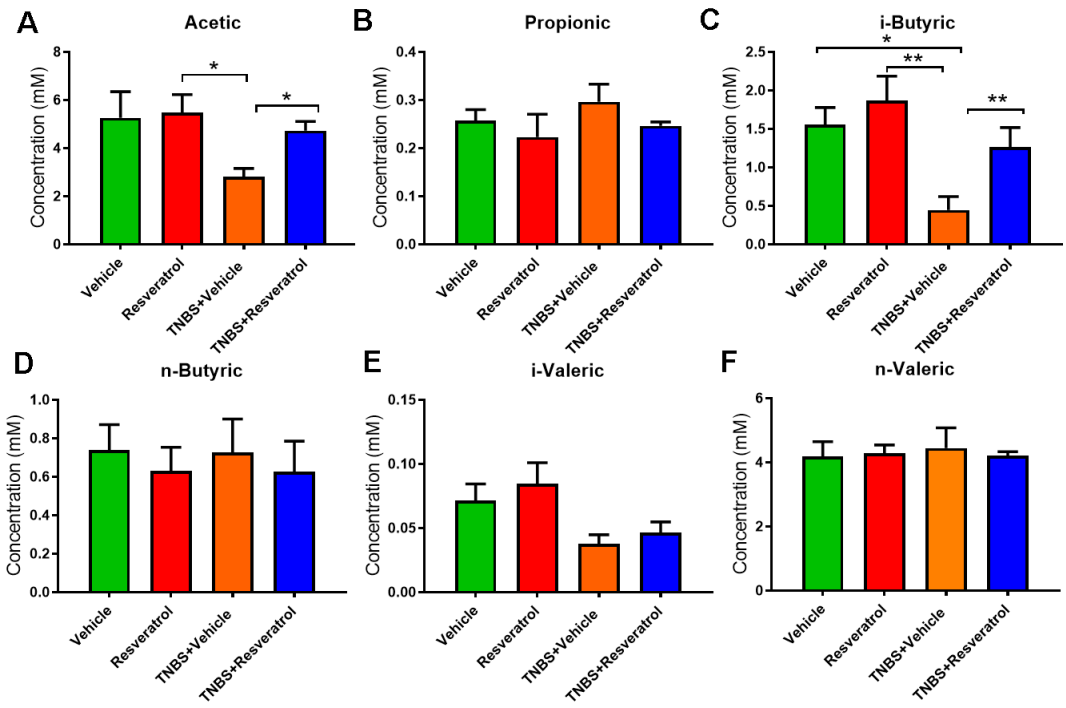

Figure 2.10 Resveratrol treatment alters SCFA production in TNBS colitis. The study was designed as described in Figure 2.2 legend. SCFA were isolated from cecal contents of experimental groups through acidification using metaphosphoric acid. GC-FID analysis was performed to determine the concentrations of acetic (A), propionic (B), i-butyric (C), n-buytric (D), i-valeric (E), and n-valeric (F) acids. SCFAs were identified using standard compounds purchased from Sigma-Aldrich. Representative data from two independent experiments with 5 mice in each group is depicted. Significance (p-value: *<0.05, **<0.01, ***<0.005, ****<0.001) was determined using one-way ANOVA followed by Tukey's post-hoc multiple comparisons test.

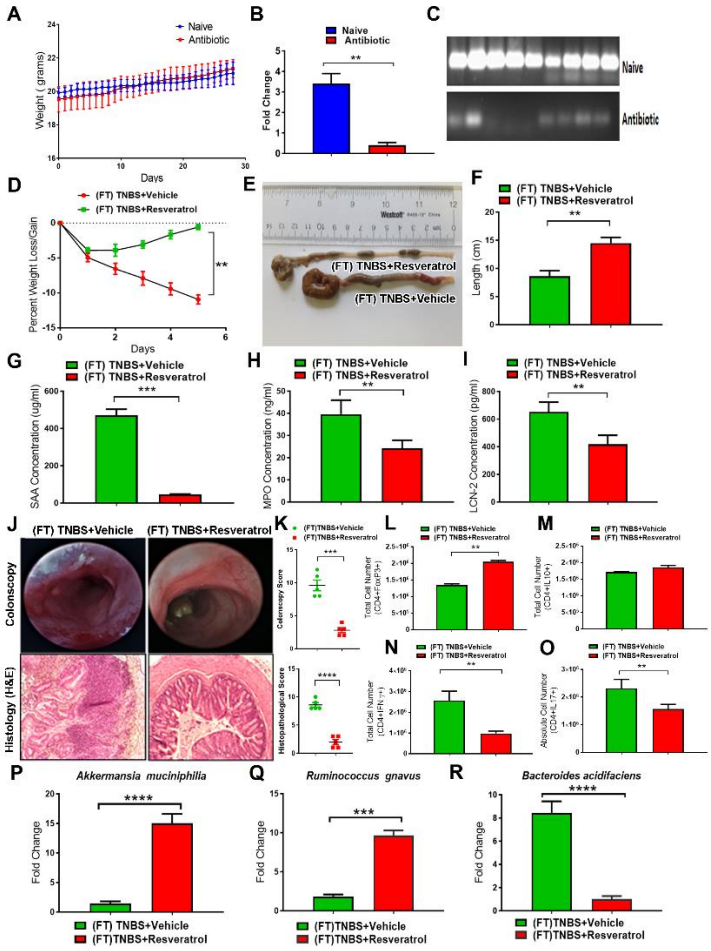

Figure 2.11 Transfer of resveratrol-treated fecal contents leads to amelioration of colitis. Female Balb/c mice were treated for 4 weeks with streptomycin and ampicillin (1g/L) prior to being injected intrarectally with 1mg of TNBS to induce colitis. Antibiotic-treated mice were weighed (A) and PCR performed on colonic flush samples to determine abundance of bacteria in the gut compared to naïve mice (B-C). These mice received fecal transfer (FT) from either colitis disease groups, (FT) TNBS+Vehicle, or from TNBS+Resveratrol-treatment groups, (FT) TNBS+RES. The percent weight loss (D) was determined over the course of the study. Colon lengths were measured upon sacrifice (E-F). Serum biomarkers for SAA (G), MPO (H), LCN2 (I) were detected using ELISA kits. Endoscopic images (J, top panel) and H&E stains of colons (J, bottom panel) are depicted (n=5 per group). Colonoscopy scores (K, top) and histological scores (K, bottom) are provided. Cells were isolated from mesenteric lymph nodes of experimental groups and absolute cell numbers from fecal transfer experiments were determined for CD4+FOXP3+ (L), CD4+IL10+ (M), CD4+IL17+ (N) and CD4+IFNγ+ (O). PCR validation from colonic flushes was performed after fecal transfer to confirm alterations in Akkermansia muciphila (P) Ruminococcus gnavus (Q) and Bacteroides acidifaciens (R), using delta-delta CT method with comparison to Vehicle controls. Each group had 10 recipient mice in this experiment and significance (p-value: *<0.05, **<0.01, ***<0.005, ****<0.001) was determined using one-way ANOVA followed by Tukey's post-hoc multiple comparisons test.

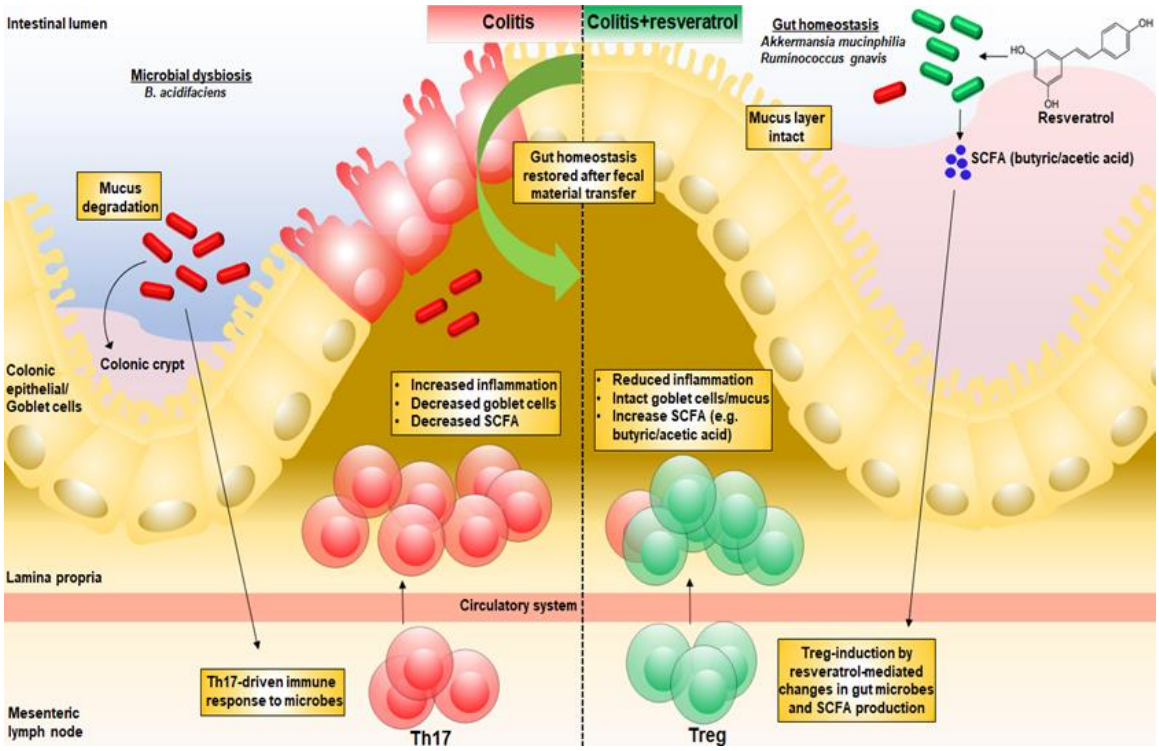

Figure 2.12 Graphical Abstract. TNBS-induced colitis results in microbial dysbiosis, with increased abundance of Bacteroides acidifaciens. However, treatment with resveratrol prevents this colitis-associated gut microbial shift, leading to increased abundance of bacteria such as Akkermansia muciphila and Ruminococcus gnavus, and production of SCFA butyrate. Increased presence of Akkermansia muciphila, Ruminococcus gnavus, and butyrate shifts the CD4+ T helper response from Th17 to anti-inflammatory Tregs. Fecal transfer of resveratrol-treated mice confirms these alterations in the immune response were the result of changes in the gut microbial profile mediated by resveratrol.

CHAPTER 3

RESVERATROL ATTENUATES MURINE AOM-DSS INDUCED COLORECTAL CANCER BY PROMOTING BUTYRATE PRODUCTION AND INDUCING ANTI-INFLAMMATORY T CELLS VIA ALTERATIONS IN THE GUT MICROBIOME AND SUPPRESSION OF HDACS

3.1 ABSTRACT

Inflammatory bowel disease (IBD) is known to significantly increase the risk for development of colorectal cancer (CRC), thereby suggesting that inflammation and cancer development are closely intertwined. Thus, it is likely that agents that suppress inflammation in the colon may prevent the onset of cancer. In the current study, we investigated the effect of resveratrol, a stilbenoid, in inflammation-induced murine model of CRC using a combination of azoxymethane (AOM) and dextran sodium sulphate (DSS) and tested the role of microbiota in preventing inflammation-driven CRC. Resveratrol treatment caused an increase in the levels of anti-inflammatory CD4+FOXP3+ and CD4+IL10+ cells while decreasing proinflammatory such as Th1 and Th17 cells, as well as attenuated development of CRC in AOM/DSS mice. Examination of colonic contents showed that resveratrol altered the gut microbiome and increased levels of the short chain fatty acid (SCFA), butryate. Fecal transfer from resveratrol-treated AOM/DSS mice resulted in attenuation of CRC and suppression of inflammation as evidenced by alterations in T cell subsets. Moreover, supplementation of butyrate in CRC resulted in similar alterations in microbial profile. *In vivo* and *In vitro* data also revealed both RES and BUT were capable of inhibiting histone deacetylases (HDACs),

which correlated with Treg induction. Interestingly, analysis of TCGA datasets of CRC patients, also revealed that increased expression of Treg-specific transcription factor FoxP3 or anti-inflammatory IL-10 resulted in an increase in 5-year survival of patients with CRC. Together, these data suggest that resveratrol-mediated shift in T cells from pro-inflammatory to anti-inflammatory phenotype, in AOM/DSS model, may result from alterations in gut microbiome and increased butyrate production leading to attenuation of inflammation-driven CRC.

3.2 INTRODUCTION

The current study was undertaken to investigate alterations in the gut microbiome by resveratrol during CRC. We show that in the AOM/DSS CRC murine model, resveratrol was able to alter the gut microbiome profile and increase microbial-production of short-chain fatty acid (SCFA), butyrate, to promote an anti-inflammatory T cell response (Treg and CD4+IL-10) which decreased disease severity and tumor development in the colon. Additionally, fecal transfer of resveratrol-treated fecal material and butyrate supplementation experiments showed that modulation of gut microbiota and suppression of histone deacetylases (HDACs) were key mechanisms through which resveratrol, through butyrate-dependent mechanisms, was able to regulate the immune response and prevent CRC development. Lastly, we show that in the human CRC population, increased expression of Treg-associated genes (FoxP3 and IL-10) correlates with increased survival rates, thereby providing additional proof of the role of anti-inflammatory environment in CRC suppression.

3.3 MATERIALS AND METHODS

Animals. Female C57BL/6 mice (aged 6-8 weeks) were purchased from Jackson Laboratories (Bar Harbor, ME) and all mice were housed at the AAALAC-accredited animal facility at the University of South Carolina, School of Medicine (Columbia, SC). All procedures were performed according to NIH guidelines under protocols approved by the Institutional Animal Care and Use Committee (IACUC).

Induction of AOM/DSS CRC in mice and treatment(s). To test the efficacy of treatment in AOM/DSS-induced CRC model, AOM was purchased from Sigma-Aldrich (St. Louis, MO), and administered one time via intraperitoneal (i.p.) injection into C57BL/6 mice at a dose of 10 mg/kg at day zero, followed by three cycles of 2% DSS (Chem-Impex International, Wood Dale, IL) as previously described (Cui et al., 2010). For treatment groups, resveratrol (Sigma-Aldrich) was administered by oral gavage at 100 mg/kg suspended in 100 µl of water, as previously reported by us (Singh et al., 2010). The regimen for resveratrol consisted of administering this compound 24 hours prior to the injection of AOM, followed by daily treatment throughout the duration of the experiment (10 weeks). Control groups consisted of naïve mice receiving either normal water or 100 mg/kg resveratrol. For butyrate supplementation experiments, sodium butyrate (BUT) from Sigma-Aldrich was given to mice at 200 mg/kg dissolved in water using the same regimen (days and controls) as resveratrol for 10 weeks.

Procedures for evaluating CRC disease severity. During AOM/DSS induced CRC, mice were weighed daily after AOM injection. Animals were euthanized at the experimental endpoint (10 weeks after AOM injection) for further evaluation of clinical signs to include counting the number and size of tumors in the colon highlighted by 1% Alcian blue dye and measured by a ruler or digital caliper. Colonoscopies were

performed weekly to experimental groups using a Karl Storz (Tuttlingen, Germany) Tele Pack Vet X LED endoscope and scored the following way: 0 = normal colon, 1 = presence of blood and tissue sloughing, 2 = presence of 1-2 colonic polyps, 3 = 3-5 colonic polyps present, 4 = 5-10 colonic polyps present, 5 = <10 polyps present in the colon. Colon, mesenteric lymph node (MLN), spleen, and blood were collected from euthanized mice for further evaluation. Colons were cleaned by saline wash and sectioned for histological analysis. Colon sections (tumor and normal adjacent tissue) were fixed with 4% paraformaldehyde and embedded in paraffin, cut into 5µm sections, deparaffinized in xylene, serially diluted in decreasing concentrations of ethanol, and stained with hematoxylin-eosin (H&E) and Periodic Acid Schiff (PAS) staining kits (Sigma-Aldrich). Images of stained sections were taken using a Biotek (Winooski, VT) Cytation 5 with digital wide field microscopy capabilities.

Cellular phenotyping by flow cytometry. Cells from MLN, spleen, and blood were isolated from experimental groups and lysed with RBC lysis buffer (Sigma-Aldrich) before being filtered and stained with appropriate antibodies for cellular phenotyping using flow cytometry. All cells were pre-blocked with Fc receptor, washed with FACS staining buffer (PBS with 2% fetal bovine serum), and stained with commercially-available antibodies (Biolegend, San Diego, CA) as follows: FITC- anti-CD3, PE-anti-CD8, and PE-CY7-anti-CD4 to identify T cells; FITC-anti-Gr1 and PE-anti-CD11b to identify myeloid-derived suppressor cells (MDSCs). For phenotyping of T cell subsets, intracellular (Intracellular Staining Permeabilization Wash Buffer) and intranuclear (True-Nuclear Transcription Factor Buffer Set) staining kits (Biolegend) were used by way of manufactures instructions. Permeabilized cells were stained with PE-Cy7-anti-

CD4, PE-anti-Foxp3, FITC-anti-IL10, PE-anti-IFNγ, and/or FITC-anti-IL17 (Biolegend). Flow cytometry data were analyzed using a CXP FC500 flow cytometry (Beckman Coulter, Brea, CA).

***In vitro* treatment of activated splenocytes with resveratrol or BUT**. For *in vitro* experiments treated with resveratrol or BUT, whole splenocytes were excised from 8-10 week old C57BL/6 mice and single cell suspensions were cultured in anti-CD3-coated (.5µg/ml) 96-well plates at 1 $x10^6$ cells/mL density in complete RPMI media for 24 hours at 37°C, 5% CO_2. Cultured cells were then activated with soluble anti-CD28 (2µg/ml) in the presence or absence of resveratrol (5, 10, or 25 µM) or BUT (1mM, 5mM, or 10mM) for 24 hours (37°C, 5% CO_2). *In vitro* doses of resveratrol were based on previous reports from our lab (Singh et al., 2007). The range of doses for BUT was determined using information gathered from other publications (Kespohl et al., 2017; Salimi et al., 2017).

16S rRNA gut microbiota profiling, Phylogenetic Investigation of Communities by Reconstruction of Unobserved States (PiCRUSt), and SCFA analysis. 16S rRNA gut microbial profiling and SCFA quantification were done as previously described in our lab (Chitrala et al., 2017). Briefly, colonic contents were collected immediately after euthanasia and gathered in 2 ml eppendorf tubes while under anaerobic conditions and stored at −80 °C for downstream analysis purposes. For 16S rRNA sequencing, genomic DNA was extracted from 100 mg of colonic flush contents by using the QIAamp DNA Stool Mini Kit (Qiagen, Valencia, CA) according to instructions from the manufacturer. DNA libraries were prepped by amplification of the 16S rRNA V3-V4 hypervariable region with added Illumina adapter overhang nucleotide

sequences and sequencing with Illumina (San Diego, CA) MiSeq platform. Sequenced reads were than analyzed using Nephele (https://nephele.niaid.nih.gov), an open-source analysis tool provided by the National Institute of Allergy and Infectious Diseases (NIAID) Office of Cyber Infrastructure and Computational Biology (OCICB) in Bethesda, MD (Weber et al., 2018). For microbial profiling, QIIME FASTQ paired end with chimera removal, open reference, and SILVA rRNA database project (Silva_99) options were used. For PiCRUSt data, a closed reference against the Greengenes database (Greengene_99) option was used. Operational taxonomic unit (OTU) tables generated from Nephele were further subjected to Linear Discrimination Analysis Effect Size (LEfSe) provided by the Huttenhower group (https://huttenhower.sph.harvard.edu/galaxy/) (Segata et al., 2011). For quantification of SCFAs present in colonic flushes, HP 5890 gas chromatograph configured with flame-ionization detectors (GC-FID) was performed as previously described (Chitrala et al., 2017; Zhao et al., 2006). SCFA detection by GC-FID was quantified using Varian MS Workstation (version 6.9.2.) software and concentrations were calculated by using standards for the detectable SCFAs.

Fecal transfer (FT) experiments. For FT experiments, colonic contents were collected immediately after euthanasia, gathered in 2 ml eppendorf tubes while under anaerobic conditions, and placed in 30% glycerol solution prior to inoculation into recipient mice. Before FT inoculation, recipient mice were treated with 1g/L of streptomycin and penicillin dissolved in water and orally gavaged at 100 µl total volume daily for four weeks to deplete endogenous gut microbiota. Depletion of microbiota was validated by PCR analysis using the universal 16S rRNA Eubacteria primer. AOM/DSS

CRC induction was performed as previously described in recipient mice. 48 hours after the last treatment with the antibiotic cocktail, recipient mice were given fecal material collected from the following groups: Naïve, Resveratrol-treated only, AOM, and AOM+Resveratrol. FT treatments were given via oral gavage every even days for a total of 35 days. Body weight and other clinical parameters described previously were also performed for the FT experiments to include weekly colonoscopies, 1% Alcian blue staining for quantification of colonic tumors, colon histology (H&E and PAS stains), and flow cytometry for analysis of T cell subsets.

Quantitative Real-Time PCR (qRT-PCR) for bacterial species validation and HDAC expression. For validation of bacteria identified by 16S rRNA analysis, qRT-PCR was used with primers designed to identify the 16s rRNA subunit of significantly altered bacterial species. DNA was extracted from colonic samples using the QIAamp DNA Stool Mini Kit (Qiagen) as previously described. For HDAC expression data, RNA was extracted from single cell suspensions of MLN *(in vivo*) or cultured splenocytes (*in vitro*) using RNeasy Mini kits (Qiagen) followed by conversion to cDNA using iScript synthesis kit (Bio-Rad). PCR amplification was performed using QuantiFast (bacteria) or QuantiTech (HDAC) SYBR Green PCR kits from Qiagen, and reactions were performed on a CFX96 qPCR system from Bio-Rad (Hercules, CA). Primers were designed by Intergrated DNA Technologies (Coralville, IA). Sequences for all primers are included in Table 3.1.

Correlation of gene expression with survival in CRC patient data sets. The correlation of gene expression pattern with survival of human patients with CRC was performed using the TCGA datasets for colorectal cancer from The Cancer genome Atlas

maintained at TCGA (https://cancergenome.nih.gov/). TCGA examines the genome-wide expression, copy number variations, methylation status and mutations in an immense number of samples with a primary advantage such as i) each patient sample is accompanied with a comprehensive clinico-pathological data ii) a huge portion of the samples with integrated molecular profiles iii) number of matched normals for tumor samples iv) generation of data using latest and widely measured standard molecular profiling technologies (Bacolod et al., 2015). Survival analysis for the TCGA datasets were performed using the Kaplan-Meier survival curves which is defined as the probability of survival in a given length of time while considering time in many small intervals (Goel et al., 2010). It mainly involves the calculation of the probability of occurrence of an event at a certain point of time.

Statistical analysis and data availability. GraphPad Prism software (San Diego, CA) was used for all statistical analysis unless otherwise stated. Experiments were repeated at least three times to confirm reproducibility. For statistical differences, one-way ANOVA and Tukey's post-hoc comparison test was used unless otherwise noted in the text. Significance was determined to have a p value of ≤ 0.05 (*), 0.01 (**), 0.005 (***), or 0.001 (****). Raw sequencing data (FASTq files) were uploaded to the NCBI Sequence Read Archive (SRA).

3.4 RESULTS

Resveratrol attenuates AOM-induced CRC by preventing early onset of inflammation and decreasing tumor burden

To study the effects of resveratrol on CRC in the context of studying host immune response and microbiome, we used the well-characterized AOM/DSS CRC murine

model. For these studies, experimental groups consisted of naïve mice (Naïve), naïve mice treated with only resveratrol (Resveratrol), AOM/DSS disease mice with no treatment (AOM), and AOM/DSS disease mice treated with resveratrol (AOM+Reservatrol). Inducing CRC by AOM resulted in a significant decrease in body weight (~20%) compared to controls (naïve or resveratrol-treated only), but treatment of CRC mice with resveratrol reduced this disease-associated weight loss and resulted in ~8% weight gain by the end of the study (Figure 3.1A). In addition, the administration of AOM resulted in decreased survival of mice (~75%) by the end of the study, whereas CRC mice treated with resveratrol resulted in 100% survival (Figure 3.1B). Resveratrol treatment also was able to reduce tumor burden in AOM-induced CRC mice as assessed during the experimental endpoint (10 weeks), as AOM-treated mice developed at least 10 or more tumor polyps along the colon, whereas AOM+Reservatrol mice had little to no tumors polyps present (Figure 3.1C-D). In order to monitor the first signs of inflammation and tumor development during disease and treatment, colonoscopies were performed weekly among experimental groups. In AOM mice, inflammation development, which was characterized by the presence of bloody lesions and tissue sloughing along the colon, developed around week 3 of the disease model, but AOM+Resveratrol mice maintained more normal appearing colons (Figure 3.2). The presence of tumors was seen in AOM mice by week 5 and continued developing to week 9, but CRC mice treated with resveratrol showed a marked decrease in colonic tumor development (Figure 3.1E-F; Figure 3.2). Colon histology reinforced these observations as AOM colons showed loss of normal mucosal architecture and abnormal tissue growth with standard H&E staining which was not apparent in AOM+Resveratrol colon sections

which more closely resembled controls (Figure 3.1G). PAS staining on fixed colon sections was also performed as a way to access mucin production and goblet cell formation (Agawa et al., 1988). Mice challenged with AOM showed a high reduction in the number of goblet cells and presence of mucus compared to controls, but these observations were greatly reversed in colon sections excised from AOM+Resveratrol groups (Figure 3.1H). Collectively, these data demonstrated that resveratrol treatment attenuated tumor development in the AOM CRC model, perhaps by way of preventing early signs of inflammation caused by multiple cycles of DSS, as shown in week 3 of the colonoscopy images.

Resveratrol treatment reduces inflammatory T cell subsets while increasing anti-inflammatory T cells in AOM-induced CRC

In order to examine immune cell alterations during disease and treatment, cells were isolated from the MLN, spleen, and blood of all experimental groups and phenotyped using flow cytometry (Figures 3.3-3.6). In the MLN, expression of T cell marker (CD3+), along with T helper (CD3+CD4+) and cytotoxic T cell (CD3+CD8+), were significantly decreased in AOM mice compared to controls, and restoration of these T cell phenotypes occurred in the AOM+Resveratrol groups (Figure 3.1I). These data suggested that activated T cells in AOM group were leaving MLN and going to the colon while resveratrol reversed this. Similar observations were seen in both the spleen (Figure 3.4) and the blood (Figure 3.5). Going further in phenotyping the CD4+ subsets, intracellular/intranuclear staining was performed to identify the effect of resveratrol inflammatory (IFNγ- and IL17-producing) cells) and to anti-inflammatory (FOXP3+ Tregs and IL10-producing) CD4+ T cell populations. The data collected from the MLN

showed that there was a significant increase in both anti-inflammatory CD4+FOXP3+ (Fig. 1J) and CD4+IL10+ (Figure 3.1K) cells population in AOM mice treated with resveratrol when compared with AOM disease mice. However, proinflammatory T cell subsets, such as Th17 (Figure 3.1L) and Th1 (CD4+IFNγ+) (Figure 3.1M) were significantly higher in AOM mice compared to the controls, but treatment with resveratrol was able to effectively reduce these inflammatory T cell phenotypes. This shift in the proinflammatory to anti-inflammatory T cell subsets after resveratrol treatment was also observed in the spleen (Figure 3.5). Lastly, as MDSCs are known to increase in the CRC human population and are thought to be a potential immunotherapy target (Sun et al., 2012), data collected from the spleen and blood revealed that MDSCs were significantly increased in the AOM disease state, but were effectively reduced by treatment with resveratrol (Figure 3.6). Together, these data suggested that resveratrol promoted an anti-inflammatory T cell response in the AOM CRC model.

Alterations in gut microbiota and SCFA composition in AOM-DSS colorectal induced mice treated with resveratrol

In order to determine if resveratrol-mediated alterations in inflammation is associated with changes in gut microbiome, we first analyzed the gut microbiota from all experimental groups by using 16S rRNA V3-V4 sequencing technique for microbial profiling. From colonic fecal matter, we isolated genomic DNA and performed pyrosequencing with Illumina MiSeq platform. Nephele analysis output showed that the alpha diversity, represented as chao1, was slightly enriched in the AOM and AOM+Resveratrol groups compared to controls (Figure 3.7A). In terms of beta diversity, depicted as a principle component analysis (PCA) plot, samples clustered within their

own respective groups, with resveratrol-treated groups showing more similar diversity compared to naïve controls, and the AOM disease group clustering further away from all other experimental groups (Figure 3.7B). 16s rRNA sequencing analysis from Nephele allowed sample reads to be classified into OTUs from the phylum to the species level (Figures. 3.8-3.12), and divergent microbial composition among the experimental groups was apparent starting even at the phylum level. At this taxa level, *Verrucomicrobia*, *Tenericutes*, and *TM7* were found to be significantly reduced in abundance within AOM groups compared to the controls, whereas levels of these phyla were restored or increased in AOM+Resveratrol mice (Figure 3.8). AOM mice also had a slight increase in *Firmicutes* compared to the other groups, and an even more significant increase in *Proteobacteria*, which were reduced to normal levels in the AOM+Resveratrol the treatment group (Figure 3.8). At class level, *Verrumcomicrobiae*, *Mollicutes*, *TM7-3*, and *Alphaproteobacteria* were decreased in AOM mice, but found to be restored in most cases after treating mice with resveratrol (Figure 3.9). *Deltaproteobacteria* and *Bacilli* were increased in AOM, and while *Deltaproteobacteria* levels were reduced to control levels the in AOM+Resveratrol groups; in *Bacilli*, AOM+Resveratrol had the most of this class (Figure 3.9). Within the order level, *Verrucomicrobiales*, A*naeroplasmales*, and *CW040* showed significant reduction in abundance in the disease state when compared to the treatment group, while *Clostridiales*, *Turicibacterales*, and *Desulfovibrionales* showed significant increases in abundance in AOM mice compared to controls, and in AOM+Resveratrol group, these were reduced except for *Turicibaterales* (Figure 3.10). In a continuing trend, some bacteria at the family level, including *Verrucomicrobiaceae*, *Dehalobacteriaceae*, *Anaeroplasmataceae*, *F16*, *Lachnospiraceae*, *Mogibacteriaceae*

and *Closteridiaceae* showed a decrease in AOM groups but an increase in the AOM+Resveratrol group, whereas *Desulfovibrionaceae* increased during the untreated disease state, but reduced to control levels in AOM+resveratrol group (Figure 3.11). Lastly, at genus level *Ruminococcus*, *Akkermansia*, *Dehalobacterium*, *Anerostipes*, *Anaeroplasma*, *Blautia*, and *Clostridium* were reduced in AOM mice compared to controls but were restored or increased significantly after treatment with resveratrol (Figure 3.12), whereas, *Oscillospira* and *Desulfovibrio* increased in AOM, but were significantly reduced in AOM+Resveratrol groups (Figure 3.12). As several bacteria were altered in the disease and treated states, LEfSe analysis, which is a useful tool to determine potential bacterial biomarkers among experimental groups (Segata et al., 2011), was used to highlight the more relevant significant differences in the microbial community. From this analysis, it was found that among the species detected by 16S rRNA sequencing, *Ruminococcus gnavus*, *Akkermansia muciniphillia*, and *Mucispirillum schaedleri* were among the potential biomarkers in the AOM+Resveratrol treatment group (Figure 3.7C-D). As shown in Figure 3.7E, all of these species were significantly reduced in AOM mice, but were increased after treatment with resveratrol, and we validated these finding using PCR (Figure 3.7F).

In addition to microbial profiling, we investigated the resulting changes in the microbial community altered bacterial-related metabolism, as PiCRUSt allows evaluation of bacterial function to be performed with 16S rRNA data (Langille et al., 2013). Using combined PiCRUSt (via Nephele) and LEfSe analyses, it was shown that there were marked changes in microbial functions amongst the experimental groups particularly after treatment with resveratrol, which included those that were connected to CRC (e.g.

P53 signaling) (Slattery et al., 2018), and those involved in generation of Tregs (e.g. TGF-β signaling) (Becker et al., 2018) (Figure 3.13). Lastly, we determined if changes in SCFA production, metabolite produced by gut flora in the host organism (Marchix et al., 2018), could be seen in response to these changes in the gut microbiome composition triggered by treatment of CRC with resveratrol. Examination of colonic contents showed that n-buytric and i-butyric acid concentrations were significantly reduced in the AOM groups compared to controls. However, AOM group treated with resveratrol restored or increased the levels of these SCFAs (Figure 3.7G). Among the other detectable SCFAs, propionic acid, i-valeric acid, and n-valeric acid showed no significant changes among the experimental groups (Figure 3.7G). Together, these studies demonstrated that treatment of CRC-induced mice with resveratrol leads to significant changes in both the gut microbial profile and function.

Fecal transfer from resveratrol-treated groups attenuates AOM/DSS-induced CRC and alters the T cell-specific immune response:

In order to determine whether or not resveratrol-induced alterations in the gut microbiome were contributing to the altered immune response in CRC, we performed fecal transfer (FT) experiments. After receiving antibiotics to deplete the existing gut microbiome, AOM-induced CRC recipient mice were inoculated with feces from either Naïve, Resveratrol, AOM, or AOM+Resveratrol groups. Mice inoculated with fecal material from disease controls, referred to as AOM(FT), showed gradual decrease in body weight throughout the study compared to controls, whereas AOM+Resveratrol(FT) mice recovered and gained weight by the end of 10 weeks (Figure 3.14A). AOM+Resveratrol(FT) mice also showed increased survival when compared to

AOM(FT) mice (Figure 3.14B), along with decreased incidence of tumor development in the colon (Figure 3.14C-D). In addition, weekly colonoscopy examination (Figure 3.15) showed increased ulceration and sloughing in portions of the colon in mice fed disease-derived feces, however, mice that were given FT from resveratrol-treated groups showed a reduced presence of polyps and abnormal colonic tissue growths at the end of the study (Figure 3.14E-F). Histological examination by H&E stains revealed AOM(FT) colon tissues had abnormal growth and damage to the mucosal layer, whereas AOM+Resveratrol tissues resembled that of control colons (Figure 3.14G). PAS stains also showed that AOM(FT) recipients had decreased mucus production and goblet cells, and just as with treatment with resveratrol in the AOM disease state, AOM+Resveratrol(FT) colon tissues had restored intestinal architecture with normal mucus present and distribution of goblet cells (Figure 3.14H). Together, these FT experiments demonstrated that the clinical benefits provided by resveratrol against AOM-induced CRC can be attributed, at least in part, to changes in gut microbiota. Next, we tested if the changes in the gut microbiota induced by resveratrol also resulted in changes in inflammation.

As in the previous experiment, flow cytometry analysis was performed in the FT experiments and collected data showed in the MLNs (Figure 3.16) of AOM(FT) mice, a marked decrease in both T helper (Figure 3.14I) and cytotoxic T cells (Figure 3.14J), whereas AOM+Resveratrol(FT) mice had increased numbers of these cells present in the tissue. Going further in phenotyping the CD4+ T helper phenotypes, AOM mice showed significant decreases in anti-inflammatory Tregs (Figure 3.14K) and CD4+IL10-producing cells (Figure 3.14L), which were significantly increased in all resveratrol-

treated groups. On the other hand, proinflammatory Th17 (Figure 3.14M) and IL17-producing CD4+ T cells (Figure 3.14N) were found to be significantly higher in AOM(FT) recipients compared to the other FT groups, and while AOM+Resveratrol(FT) recipients had decreased Th17 phenotype, this group was not able to decrease Th1 (CD4+IFNγ+) cells. In order to confirm the transfer of feces resembled our previous sequencing data, PCR validation was performed showing a similar microbial profile for significantly altered species *Ruminococcus gnavus* and *Akkermansia muciniphilia*, which were decreased in AOM(FT) and increased in the AOM+Resveratrol(FT) group (Figure 3.14O). Collectively, these data demonstrated that the alterations of microbiome by resveratrol were directly modulating the T cell immune response in AOM-induced CRC, particularly in increasing anti-inflammatory subsets (Tregs and CD4+IL-10-producers), while decreasing proinflammatory types (Th17 and Th1).

Butyrate supplementation attenuates AOM/DSS-induced CRC and promotes an anti-inflammatory T cell response similar to resveratrol:

In the current study, one of the distinct outcomes gathered regarding resveratrol-mediated alterations in the gut microbiome was the increase in SCFA butyrate, which is known to have anti-inflammatory properties (Sitkin and Pokrotnieks, 2018; van der Beek et al., 2017). To test its role further, supplementation with sodium butyrate (BUT) was given in lieu of resveratrol to determine the potential effects of increased levels of this SCFA produced in the AOM-induced CRC model. To address this, experimental groups were designed to mimic the previous experiments with the exception of substituting resveratrol with BUT, and these groups included: Naive alone, BUT alone, AOM, and AOM+BUT. As expected, AOM mice had significant decrease in body weight (~20%)

compared to controls, but like AOM+Resveratrol groups from the previous experiments, AOM+BUT mice had significant reduction in weight loss over time (Figure 3.17A). Additionally, while the AOM group had a decrease in overall percent survival, AOM+BUT mice showed 100% survival after 10 weeks (Figure 3.17B). Similar to AOM+Resveratrol mice, AOM+BUT mice had decreased or nonexistent colonic tumors (Figure 3.17C-D). Colonoscopic examination at 5 different time points (weeks 0,3,5,7 and 9) during the experiment gave a clear picture of the development of CRC-associated lesions and tissue sloughing after AOM injection, but AOM+BUT groups showed marked decrease in tissue disruption (Figure 3.17E-F, Figure 3.18). Histological examination of formalin-fixed colon tissues stained with H&E was also performed on experimental groups, which clearly showed in AOM colons there was a loss of mucosal, submucosal, and serosa architecture, which was not seen in AOM+BUT (Figure 3.17G). PAS staining showed that AOM+BUT colons were also able to maintain significant amount of mucus presence and number of goblet cells which were lost in AOM tissue sections (Figure 3.17H). Supplementation with butyrate was thus able to attenuate the clinical parameters of AOM-induced CRC much like resveratrol, so it was reasonable to examine whether or not increased butyrate was able to alter the T cell repertoire.

Just as with resveratrol treatment, flow cytometric analysis of the MLN (Figure 3.19) showed expression of T cells in general, CD4+ T helper, and CD8+ cytotoxic T cells increased in AOM+BUT groups after being depleted in number in AOM-induced CRC (Figure 3.17I). AOM+BUT groups also had increased numbers in anti-inflammatory Tregs (Fig. 4K) and CD4+IL-10 cells (Figure 3.17L) when compared to AOM mice which had much lower number of these cells than the control groups.

Alternatively, inflammatory Th17 (Figure 3.17M) and Th1 cells (Figure 3.17N), were much lower in AOM+BUT mice when compared to the AOM disease controls, in addition to anti-inflammatory CD4+FOXP3+ and CD4+IL10+ populations in both mesenteric lymph node and blood. A similar shift from proinflammatory Th17/Th1 to anti-inflammatory Tregs/IL-10 was seen after treatment with BUT in the spleen (Figure 3.20). Collectively, these data showed that butyrate supplementation reduces the inflammatory T cell response much in the same manner as resveratrol, suggesting that increased production of this SCFA by resveratrol is another mechanism through which this natural compound may be effective against AOM-induced CRC.

Supplementation of butyrate alters the microbial profile in AOM-induced CRC with similarities to resveratrol treatment:

As resveratrol-mediated increases in colonic butyrate could also lead to alterations in the microbiome in addition to promoting anti-inflammatory T cell phenotypes, 16S rRNA microbial sequencing was performed on experimental groups in the butyrate supplementation experiments. Alpha diversity indicated that compared to the naïve group, all other experimental groups (BUT, AOM, AOM+BUT) had lower overall diversity within the samples (Figure 3.21A). Beta diversity or PCA clustering in the butyrate supplementation experiments mimicked closely what was seen in the resveratrol treatment experiments, with all experimental samples clustering within their own groups tightly, but the AOM group being the most divergent (Figure 3.21B). OTU abundances were calculated from the phylum to the genus level (Figure 3.22-3.25) as previously done. Several significant differences were seen at taxa levels with butyrate supplementation, however, for the current report and in context in explaining resveratrol-

mediated mechanisms, only those with changes similar to the resveratrol treatment experiments are highlighted. For example, BUT-treated groups were able to restore or increase bacteria at the phyla *Verrucomicrobia* and *Tenericutes*, which were significantly reduced in the AOM group, while butyrate supplementation decreased *Proteobacteria* which rose in AOM-induced CRC (Figure 3.22). At the class level, AOM+BUT mice had increased *Verrucomicrobiae*, *Mollicutes*, and *TM7-3* which were significantly reduced in AOM disease mice, and the AOM-increased *Deltaproteobacteria* were reduced after butyrate supplementation (Figure 3.23). At the order level, butyrate supplementation increased *Verrucomicrobiales*, A*naeroplasmales*, and *CW040* much like resveratrol did after being decreased in AOM groups, whereas *Desulfovibrionales* increased during AOM disease, but was reduced in the AOM+BUT samples (Figure 3.24). At the family level, *Verrucomicrobiaceae*, *Anaeroplasmataceae*, *Closteridiaceae*, *Mogibacteriaceae*, and *F16* were all reduced in AOM mice compared to controls as previously shown, however, AOM+BUT increased levels of these gut microbials, whereas the increase seen in families in AOM samples (*Desulfovibrionaceae*) were reduced after supplementation with butyrate (Figure 3.25). At the genus level and closely mimicking resveratrol treatment experiments, *Ruminococcus*, *Akkermansia*, *Anerostipes*, *Anaeroplasma*, and *Clostridium* were reduced in AOM mice compared to controls but were restored or increased significantly after butyrate supplementation, whereas *Desulfovibrio* increased in AOM, but was significantly reduced in AOM+BUT groups (Figure 3.26). LeFSe analysis was then performed to determine which bacterial species had the highest LDA score among the experimental groups (Figure 3.21C-D), and combined with OTU abundance data, *Ruminicoccus gnavus* and *Akkermansia muciniphilia* (Fig 3.21E) were

found to be restored by butyrate after depletion in AOM-induced CRC, which was validated with PCR (Figure 3.21F). Take altogether, these data suggested that resveratrol-mediated alterations in the gut microbiome and shifting to anti-inflammatory T cell phenotype in AOM-induced CRC can be explained, at least in part, by the ability of resveratrol to increase levels of butyrate in the gut microenvironment.

Resveratrol and BUT inhibit HDACs *in vivo* and *in vitro*

The increase in colonic butyrate production in resveratrol-treated CRC mice was interesting given the fact that previous reports show butyrate not only increases Treg production (Arpaia et al., 2013; Vieira et al., 2019), but the HDAC inhibiting activities of this SCFA have been implicated as a key mechanism in which it exerts anti-inflammatory and anti-cancer properties (Martin-Gallausiaux et al., 2018; Sethi et al., 2018; Silva et al., 2018), including in colorectal cancer models (Zhang et al., 2016b). With is in mind, studies were performed to examine the ability of resveratrol and BUT to suppress HDACs *in vitro* and in the CRC *in vivo* model and how this correlated with increased Treg production. For *in vitro* studies, resveratrol increased Tregs in activated splenocytes in a dose-dependent manner (Figure 3.27, Figure 3.28A). BUT significantly increased Tregs at the higher doses (5 and 10mM) when treating activated cells in the same manner (Figure 3.27, Figure 3.28B). Following these observations, the expression of class I (HDAC I; HDACs 1, 2, 3, and 8) and class II HDACs (HDAC II; HDACs 4, 5, 6, 7, 9, and 10) were examined in cultures with the most significantly increased Treg expression (25μM for resveratrol and 5mM for BUT). Resveratrol in the *in vitro* cultured system was able to significantly reduce expression of all HDAC I (Figure 3.28C), but interestingly decreased only selective HDAC II, specifically not being able to reduce HDAC 6, 9, and

10 (Figure 3.28D). BUT, being a well-known HDAC inhibitor, was able to reduce expression of all HDACs, regardless of specific classes (Figure 3.28E-F). Lastly, the expression of HDAC I and II was evaluated in *in vivo* CRC experiments given treatment with either resveratrol or BUT. Interestingly, similar results were seen. For HDAC I, resveratrol treatment compared to either naïve controls or CRC disease mice resulted in decreased expression (Figure 3.28G). While HDAC II were all decreased upon treatment with resveratrol compared to naïve controls, once again, select HDACs (HDAC 6, 9, and 10) were not inhibited by resveratrol compared to AOM disease controls (Figure 3.28H). However, supplementation experiments with BUT resulted in overall decreased HDAC expression for HDAC I and HDAC II (Figure 3.28I-J). Altogether, this data suggests that while increased butyrate can lead to inhibition of HDACs, which correlates to increased Treg expansion, resveratrol is able to at least in part reduce select HDAC expression itself, independent of butyrate.

Increased expression of anti-inflammatory T cell markers results in increased survival in human CRC patients:

Lastly, as the current study was able to show that resveratrol modulated the gut microbiome to increase anti-inflammatory T cell subsets (Treg and IL-10-producers) while decreasing proinflammatory Th17/Th1 types, we examined whether there was any correlation between gene expression of T cell-specific makers in CRC patients with survival. Looking at the TCGA datasets of CRC patients, it was shown that increased expression of Treg-specific transcription factor FoxP3 (Figure 3.29A) or anti-inflammatory IL-10 (Figure 3.29B) resulted in an increase in CRC 5-year patient survival. High expression of TGF-β, known to influence the development of Tregs, also

correlated with increased overall survival in the patient population (Figure 3.29C). However, high expression of Th-17 associated IL-17 cytokine was just the opposite, as it resulted in decreased patient survival, while patients with lower expression of IL-17 had increased survival over time (Figure 3.29D). While expression of Th-17 transcription factor RORγt was shown to have no difference in CRC patient survival over a 5-year period (Figure 3.29E), expansion past 5 years showed that high expression of this transcription factor was capable of bringing down overall CRC patient survival (Figure 3.29F). Just as in the AOM-induced mouse model in the current study, IFNγ expression, associated with Th1 cells, didn't seem to have much effect on CRC patient survival (Figure 3.29G), but in the context of Th1-specific transcription factor (Tbx21), high expression of this gene did appear to decrease the expected overall CRC patient survival. The results in the current study are promising given that T cell differentiation altered by resveratrol towards anti-inflammatory phenotype, via modulation of the gut microbiome, appears to have significant impact in overall human CRC patient survival.

3.5 DISCUSSION

Published reports with resveratrol date back to the late 1970s, and since then research has shown that this natural plant polyphenol has therapeutic properties ranging from anti-inflammatory (Koushki et al., 2018), anti-oxidant (Samsamikor et al., 2016; Singh et al., 2011a), anti-depressant (de Oliveira et al., 2018; Finnell et al., 2017), anti-atherogenic (Riccioni et al., 2015), anti-aging (Li et al., 2017), as well as anti-cancer (Guan et al., 2012; Ko et al., 2017; Singh et al., 2011b). Our lab has published extensively on the anti-inflammatory properties of resveratrol in various disease models, showing often how the effects of this compound are AhR-dependent (Alghetaa et al.,

2018; Chen et al., 2015b; Rieder et al., 2012; Singh et al., 2007; Singh et al., 2010). Activation of AhR by known ligands, such as resveratrol, has been shown by us as well as others to have significant impact on T cell development and phenotype (Busbee et al., 2013; Ehrlich et al., 2018). For example, we have shown that activation of AhR by dietary indoles in a delayed-type hypersensitivity (DTH) model is essential for shifting the T cell response from a proinflammatory Th17 to an anti-inflammatory Treg phenotype (Singh et al., 2016). This is important in regards to CRC as studies have shown that high expression of Tregs in CRC patients indicate a more favorable prognosis (Hu et al., 2017; Xu et al., 2017), whereas increased Th17 has been linked to CRC pathogenicity and tumor development (Bedoui et al., 2018; Lee et al., 2017; Yan et al., 2018). The current report reinforces this notion, as gene expression data of CRC patients seemed to indicate that high expression of anti-inflammatory T cell factors (FoxP3, IL-10) improved patient survival, whereas proinflammatory makers linked to Th17 and Th1 phenotypes decreased overall survival in the patient population. It is important to note that in the context of cancer, the exact role of Tregs/Th17 is not so clear, as other reports indicate that Tregs promote cancer development, whereas inflammatory Th17 cells prevent tumor invasion and metastasis (Amicarella et al., 2017; Timperi et al., 2016; Zhuo et al., 2015). Reports seem to indicate that the role these T cell phenotypes in cancer largely depends on the type of cancer along with the stage of disease severity, as well as whether the cancer is driven by chronic inflammation, which could explain the conflicted reports. For CRC, which is linked to chronic inflammation in the colon, an anti-inflammatory response may be more favorable, at least in terms of the early stages of the disease. This could explain why our lab as well as others have shown resveratrol as an

effective preventative treatment in CRC animal models (Altamemi et al., 2014; Cui et al., 2010; Huderson et al., 2018; Lee et al., 2018), which is in part due to the ability of this compound to shift from a proinflammatory T cell response to anti-inflammatory one. While the ability of resveratrol to illicit this type of immune response has been well-characterized, the significance of this report is in the fact that resveratrol-mediated modulation of the gut microbiome seems to be an important mechanism in promoting this T cell shift.

A recent report by Wong et al. showed that inoculation with feces from CRC patients in germ-free or conventional mice resulted in an increase in colonic tumor development, proinflammatory markers, and Th17 phenotype (Wong et al., 2017). These findings are interesting because in addition to promoting the idea of Th17 as CRC-inducing in nature as discussed already, this report showed that microbiota plays an important role in CRC development and progression. Prior to and since this report, it has been well-established that the complex interaction between microbiota and the host immunity play major roles in CRC pathogenicity (Chen, 2018; Yang et al., 2018b). For example, several bacteria, such as *Helicobacter pylori*, *Streptococcus bovis*, *Bacteroides fragilis*, and *Clostridium septicum* have been known to be major contributors to CRC development (de Almeida et al., 2018). Even shifts in certain phylum, such as increases in *Proteobacteria*, have been associated with CRC malignancy (Mori et al., 2018). Thus, it would stand to reason that therapeutics directed at combating CRC disease would also be able to modulate the gut microbiome to promote more beneficial effects.

Previous reports have shown that resveratrol was capable of altering the gut microbiome in other disease models (Etxeberria et al., 2015; Qiao et al., 2014). In line

with the current study, researchers found that resveratrol was able to increase bacteria such as *Verrucomicrobia* and *Akkermansia muciniphila*, while decreasing *Bacteroides*, *Dysgonomonas*, and *Turicibacter* in a hypertension model with high-fructose diet (Tain et al., 2018). Additionally, in an obesity model it was found that resveratrol treatment increased *Akkermansia* and *Ruminococcaceae*, which were shown to alleviate the clinical effects associated with a high-fat diet (Zhao et al., 2017). Interestingly enough, studies found that *Ruminococcus gnavus* was in fact reduced in CRC patients when compared to controls (Chen et al., 2012), and that *Akkermansia muciniphilia* was associated with increased response to chemotherapy in CRC patients (Cani, 2018). The current study showed that these species were decreased in AOM-induced CRC, which correlates well with human CRC patients, but more importantly, resveratrol was able to restore or increase these bacteria. This could further explain why resveratrol is such an effective therapeutic in CRC models, as it seems to increase the presence of bacteria lost or decreased during CRC development and progression. These particular bacteria appear to possess properties essential for controlling and preventing tumor development in the gastrointestinal system.

Alterations in the microbial profile were not the only interesting aspect obtained from the current studies, but rather it was significant to find that resveratrol-mediated alterations in the gut microbiome promoted SCFA, butyrate, production as well. Butyrate has been shown to act in an anti-inflammatory manner in various disease models. For example, supplementation with sodium butyrate was capable of attenuating diabetes-associated inflammation (Xu et al., 2018), as well as inflammation linked to high-fat-diet-induced non-alcoholic fatty liver disease (Sun et al., 2018). Oral administration of

butyrate was also shown to reduce microbial-associated gastrointestinal inflammation and liver disease in Gulf War illness by mechanisms such as decreasing inflammatory-mediated toll-like receptor (TLR) activation (Seth et al., 2018). In the context of CRC specifically, decreases in butyrate production are linked to CRC development (Chen and Vitetta, 2018), and it was shown that butyrate inhibited aberrant epigenetic modifications in CRC cells by upregulating α-ketoglutarate, which is important in mediating DNA methylation (Sun and Zhu, 2018). A more recent report closely linked to the current one showed that a mix of SCFA (butyrate, acetate, and propionate) was protective against AOM-induced CRC and was able to suppress key inflammatory cytokines such as IL-6 and inducing apoptosis in tumor-associated epithelial cells (Tian et al., 2018). However, in our studies, we focused solely on butyrate supplementation and showed that this SCFA could alter T cells in CRC specifically by shifting from inflammatory Th1/Th2 to anti-inflammatory Treg/IL-10-producers. One of the key mechanisms butyrate has been shown to promote an anti-inflammatory response is through inhibition of HDACs(Patnala et al., 2017; Zhang et al., 2016a), even in the case of promoting Treg production specifically in CRC (Zhang et al., 2016b). Interestingly though, the results in the current report seemed to suggest that resveratrol alone was promoting HDAC inhibition, independent of butyrate, and this correlated with induction of Tregs. However, it is important to note that resveratrol treatment in CRC resulted in increased colonic butyrate levels, and the T cell subsets were examined in the gut-specific draining lymph node (MLN). Therefore, the relationship between resveratrol modulation of the gut microbiome, increased butyrate, HDAC expression, and Treg expansion needs to be

further analyzed at the local site, in this case the colon, to further understand the interplay related to these mechanisms.

Combined with the findings discussed above, the current study is able to provide new and exciting insights into how resveratrol has the potential to be a strong preventive agent against CRC. As the gut microbiota is now known to be important in disease progression and development, the fact that resveratrol can modulate this microenvironment in such a way as to induce a beneficial T cell immune response proven to help CRC patients is important, and through FT experiments, this resveratrol-mediated mechanism linked to microbiome-modulation appears more conclusive now. In addition, to our knowledge, this is the first report to confirm this and also provide evidence that resveratrol modulates the microbiome to increase butyrate production. Our studies also suggest that resveratrol and other dietary AhR ligands may constitute preventive modalities in the fight against CRC and potentially other types of inflammatory diseases linked to microbial dysbiosis.

Table 3.1. Primer Sequences

Primer	Forward	Reverse
Ruminococcus gnavus	AGAGGGATGTCAAGACCAGGTA	TACTAGGTGTCGGGTGGAAAAG
Akkermansia muciniphila	GTATCTAATCCCTTTCGCTCCC	GACTAGAGTAATGGAGGGGGAA
Mucispirillum schaedleri	CACATGCAAGTCAGGGAGAAA	CAGGTCTCCCCAACTTTTCCTA
HDAC 1	CCGCATGACTCACAATTTGCT	TCTGGGCGAATAGAACGCAGG
HDAC 2	TACAACAGATCGCGTGATGAC	TCCCTTTCCAGCACCAATATC
HDAC 3	GAAATGTTGCCCGGTGTTGGA	TGAGTTCTGATTCTCGATGCG
HDAC 4	AACTTCTTCCCAGGAAGTGGA	TGCGATAGGCATAACCACCGT
HDAC 5	TGGACTGGGATATTCACCATG	AGAGCCTGGAAAGAAGTTCCC
HDAC 6	ATTGCTGCTTTCCTGCACATC	AATCAACTTGCCTCCTGCCAA
HDAC 7	GCTGAAGAATGGCTTTGCTGT	AATGAGGATCTTGCTGGCTTT
HDAC 8	AGTGCCTGATTGACGGGAAGT	CGGTCAAATTTCCGTCGCAAT
HDAC 9	AGGATGATGATGCCTGTGGTG	GCCTGGTCAAATTCTGGTGCT
HDAC 10	AGCAGAAATATGGGCTGAAGA	AGAAGCTTCCATGCTCATAGC

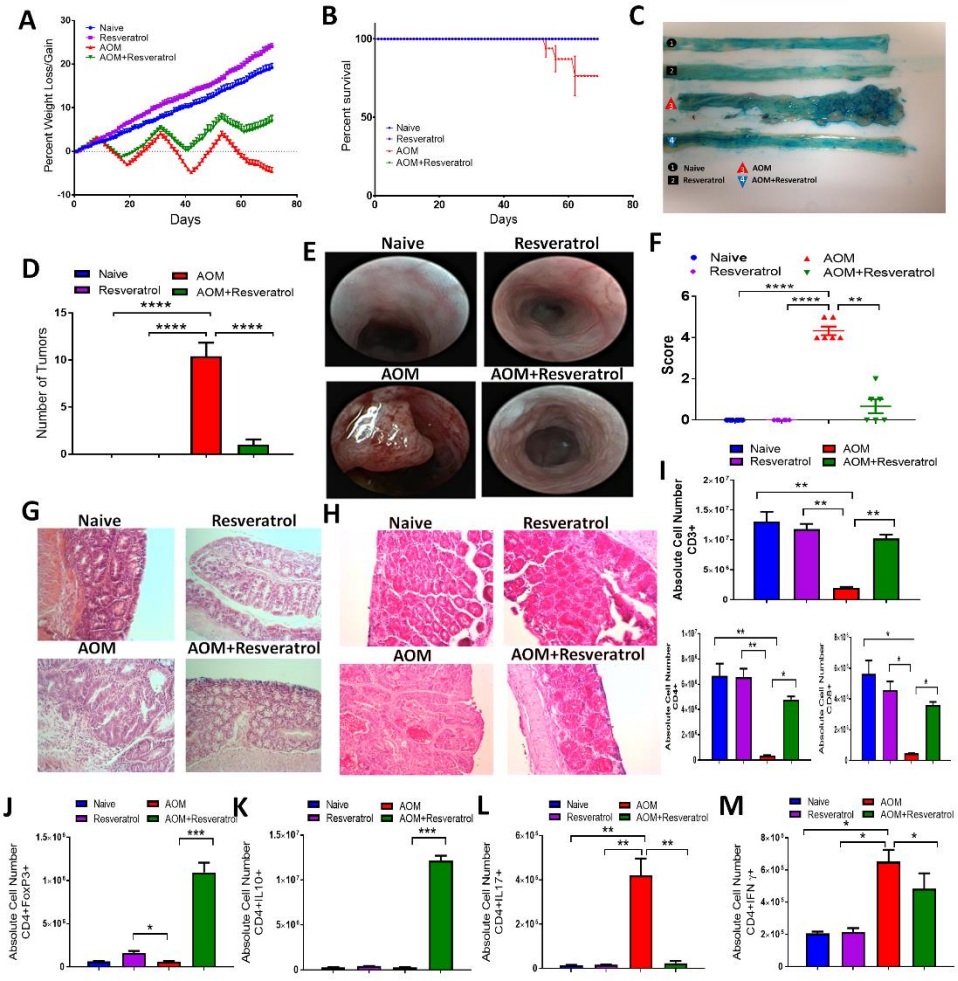

Figure 3.1 Treatment with resveratrol reduces clinical symptoms and alters T cell phenotype in AOM-induced CRC model. C57BL/6 mice were injected intraperitoneal with 10 mg of AOM followed by 3 cycles of 2% DSS, to induce CRC. Experimental groups consisted of: Naïve (n=6), Resveratrol (n=6), AOM (n=6), and AOM+Resveratrol (n=6). Clinical parameters consisted of percent weight loss (A) and survival (B), (C) Representative colons stained with 1% Alcian blue, (D) Bar graph depicting number of tumors counted in each experimental group, (E) Representative colonoscopic images from experimental groups, (F) Bar graph depicting scores after examination of tumor polyps detected during colonoscopies, (G) Representative colon sections stained with H&E; scale bar = 100 µM at 40x objective, (H) Representative colon sections with PAS staining; scale bar = 100 µM at 40x objective, (I) Bar graphs depicting absolute cell numbers in MLN for all T cells (CD3+), T helper (CD3+CD4+), and cytotoxic (CD3+CD8+) T cells. (J-M) Bar graphs depicting absolute cell numbers in MLN for Tregs (J), Th cells producing IL-10 (K), Th17 (L), and Th1 (M) cells. Significance (p-value: *<0.05, **<0.01, ***<0.005, ****<0.001) was determined by using one-way ANOVA and post-hoc Tukey's test for bar/dot graphs, Mann-Whitney test for weight data, and log rank test for survival curve. Data are representative of at least 3 independent experiments.

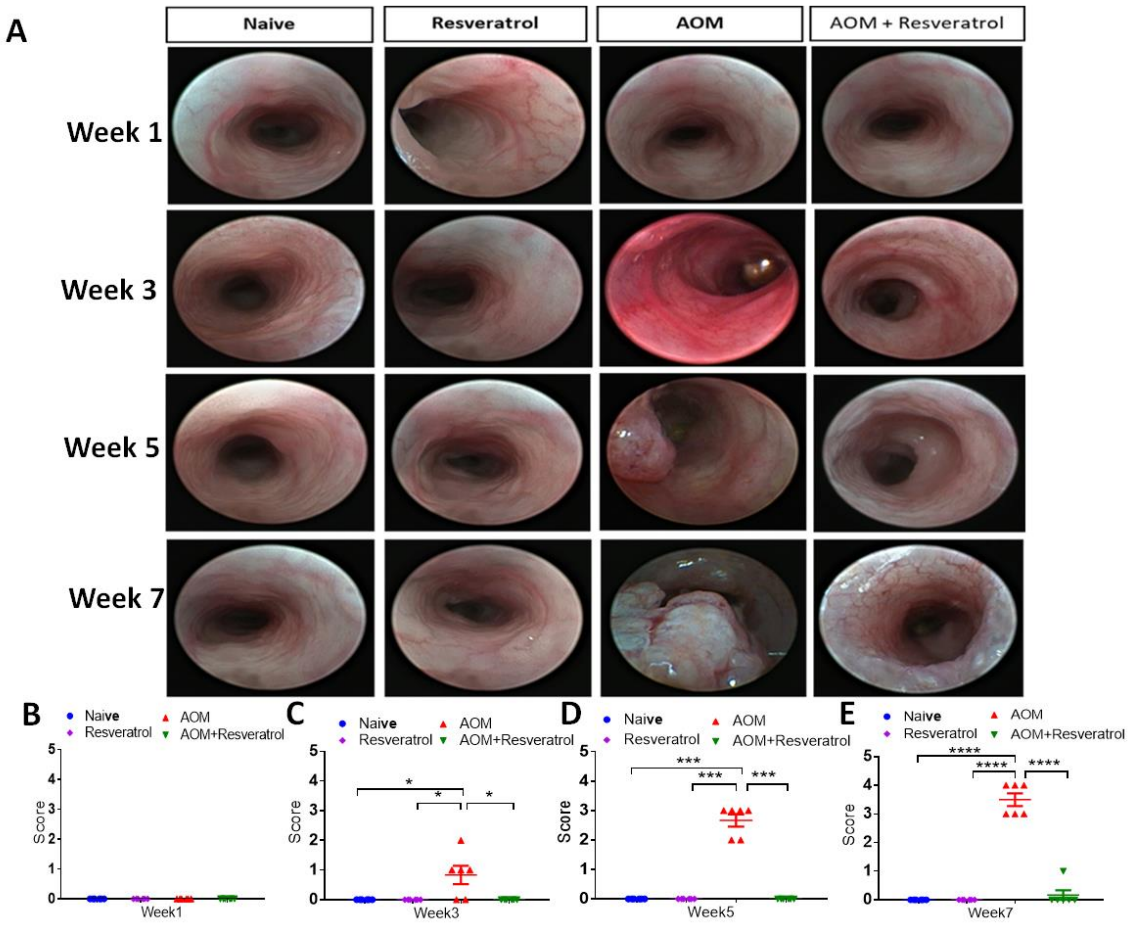

Figure 3.2 Weekly colonoscopy images in AOM-induced CRC treated with resveratrol. Induction of AOM CRC and treatment with resveratrol were performed as described in Figure 3.1 legend. (A) Representative colonoscopies are shown from experimental groups which included Naïve (n=6), Resveratrol (n=6), AOM (n=6), AOM+Resveratrol (n=6) at weeks 1, 3, 5, and 7. Bar graphs depict colonoscopy scores (described in Materials and Methods) for experimental groups at week 1(B), week 3 (C), week 5 (D), and week 7 (E). Significance (p-value: *<0.05, **<0.01, ***<0.005, ****<0.001) was determined by using one-way ANOVA followed by Tukey's post-hoc multiple comparisons test for depicted bar graphs.

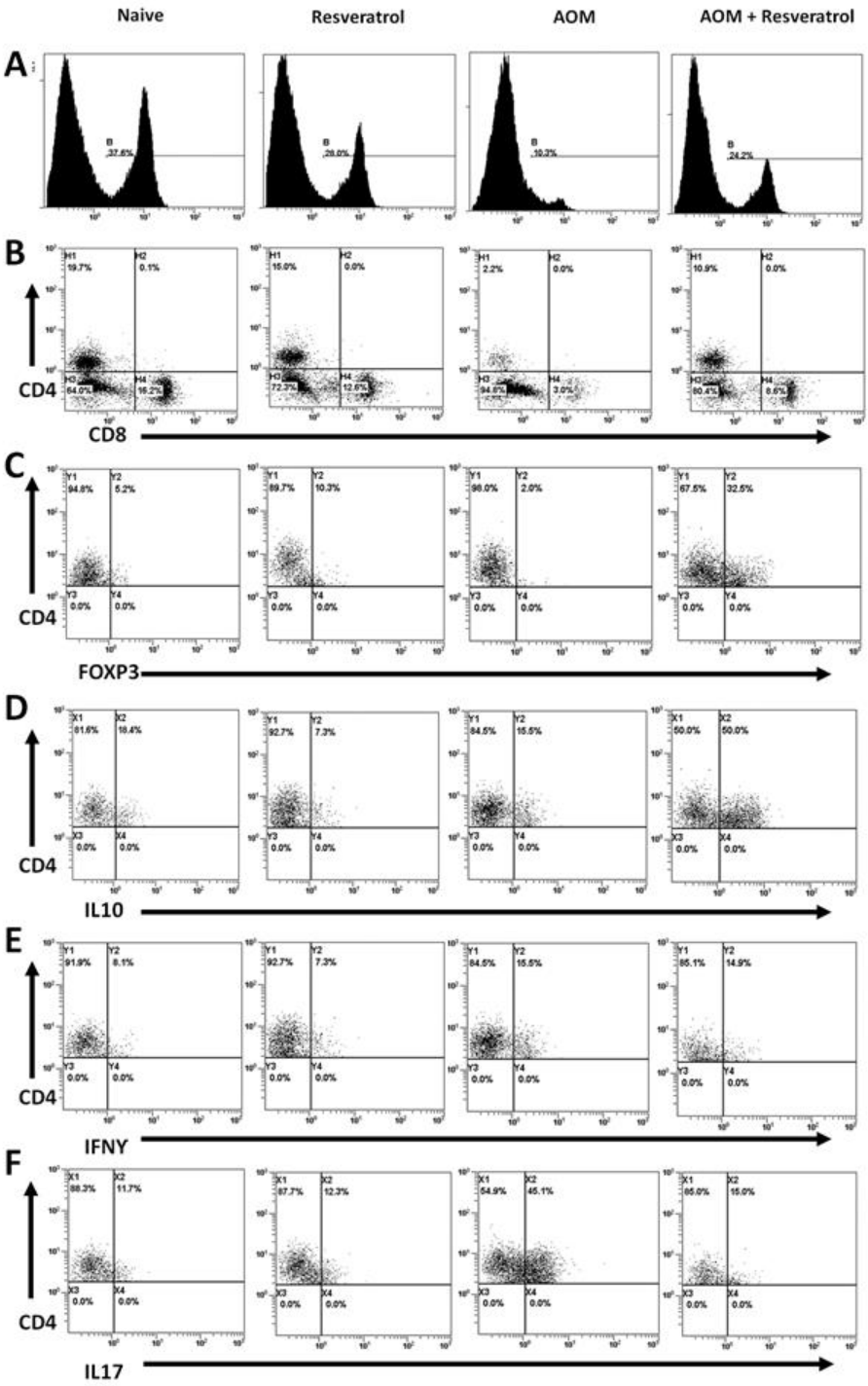

Figure 3.3 T cell phenotyping in MLN of AOM-induced CRC mice treated with resveratrol. Induction of AOM CRC and treatment with resveratrol was performed as described in Figure 3.1 legend. Representative flow cytometry histograms and dot plots are depicted for the following T cell subsets: CD3+ (A), CD3+CD4+CD8+ (B), CD4+FOXP3+ (C), CD4+IL10+ (D) and CD4+IFNγ+ (E), and CD4+IL-17+ (F). For Figures C-F, cells were gated on CD4+ population. Data are representative of at least 3 independent experiments.

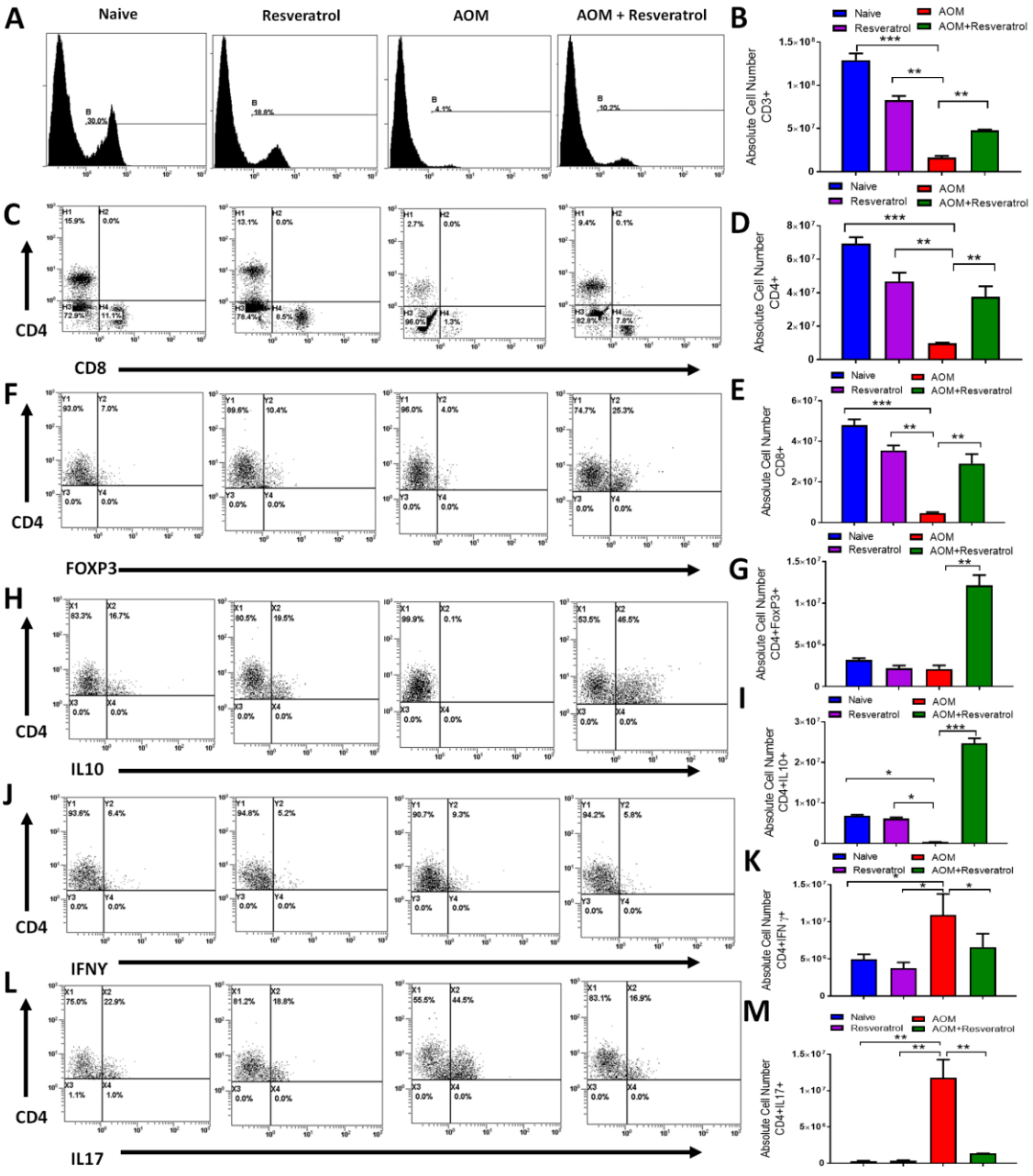

Figure 3.4 T cell phenotyping in spleen of AOM-induced CRC mice treated with resveratrol. Induction of AOM CRC and treatment with resveratrol was performed as described in Figure 3.1 legend. Flow cytometry dot plots and quantitative bar graphs depicting absolute cell numbers are shown respectively for the following T cell subsets: CD3+ (A-B), CD4+ or CD8+ cells (C-E), CD4+FOXP3+ (F-G), CD4+IL10+ (H-I) and CD4+IFNγ+ (J-K), and CD4+IL-17+ (L-M) expressing cells. For Figures F-M, cells were gated on CD4+ population. Each experimental group had at least 5 mice included, and significance (p-value: *<0.05, **<0.01, ***<0.005, ****<0.001) was determined for absolute cell numbers by using one-way ANOVA followed by Tukey's post-hoc multiple comparisons test. Data are representative of at least 3 independent experiments.

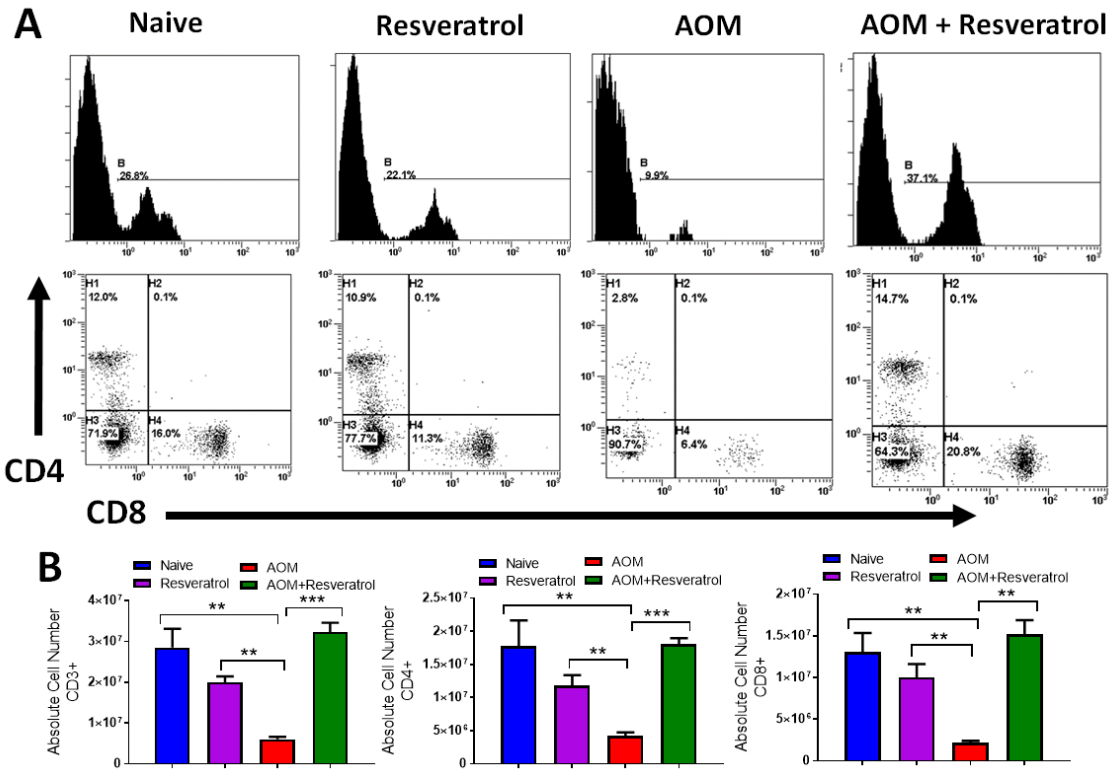

Figure 3.5 T cell phenotyping in blood of AOM-induced CRC mice treated with resveratrol. Induction of AOM CRC and treatment with resveratrol was performed as described in Figure 3.1 legend. (A) Representative flow cytometry plots are depicted showing CD3+ histogram (top) and CD4+/CD8+ dot plots (bottom) from experimental groups. (B) Bar graphs showing absolute cell numbers for the following T cell subsets respectively: CD3+, CD3+CD4+ (T helper), and CD3+CD8+ (cytotoxic T cells). Significance (p-value: *<0.05, **<0.01, ***<0.005, ****<0.001) was determined by using one-way ANOVA followed by Tukey's post-hoc multiple comparisons test in bar graphs. Experiments are representative of at least 3 independent experiments.

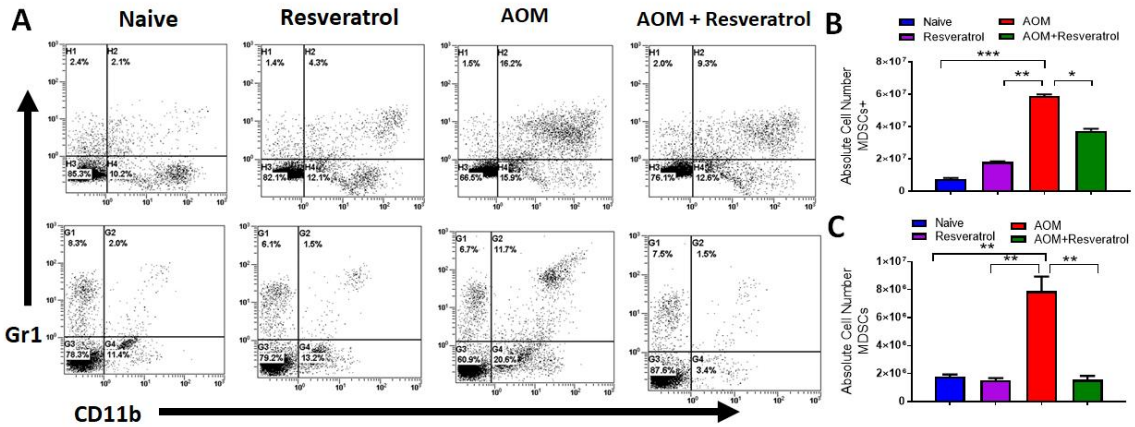

Figure 3.6 MDSCs in the spleen and blood of AOM-induced CRC mice treated with resveratrol. Induction of AOM CRC and treatment with resveratrol was performed as described in Figure 3.1 legend. (A) Representative flow cytometry dot plots are depicted showing MDSCs (CD11b+GR1+) in the spleen (top) and blood (bottom) from experimental groups. (B) Bar graphs showing absolute cell numbers for MDSCs in the spleen. (C) Bar graphs showing absolute cell numbers for MDSCs in the blood. Significance (p-value: *<0.05, **<0.01, ***<0.005, ****<0.001) was determined by using one-way ANOVA followed by Tukey's post-hoc multiple comparisons test in bar graphs. Experiments are representative of at least 3 independent experiments.

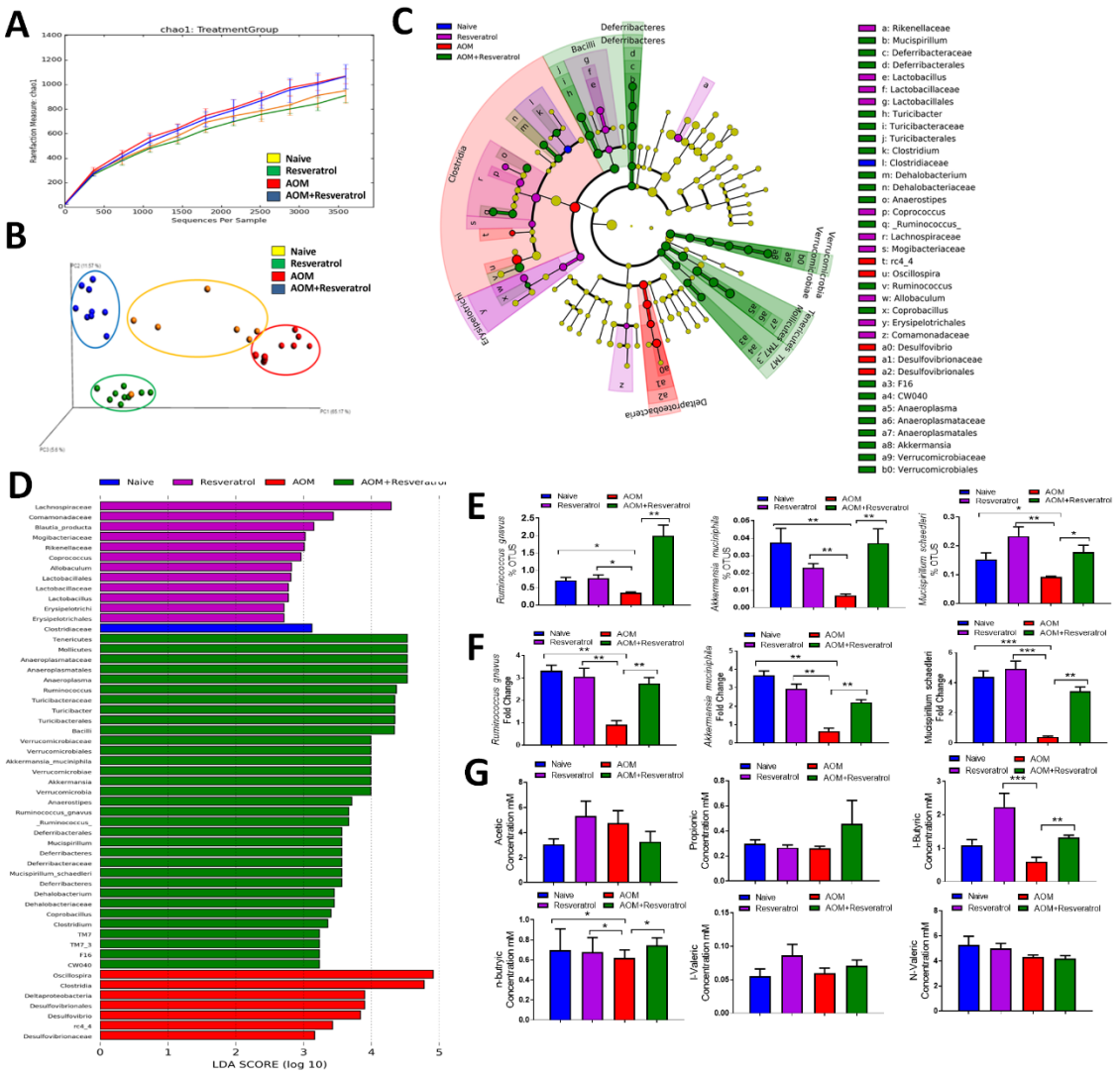

Figure 3.7 16S rRNA sequencing analysis during AOM-induced CRC treated with resveratrol. The study was designed as described in Figure 3.1 legend. Gut microbiome samples were collected from experimental groups by performing colonic flushes in experimental groups, which were: Naïve (n=7), Resveratrol (n=9), AOM (n=10), and AOM+Resveratrol (n=9). Nephele analysis (nephele.niaid.nih.gov) was used to generate charts for chao1 alpha diversity (A) and PCA beta diversity (B). LeFSe analysis of the Nephele OTU output files generated the cladogram (C) and LDA score bar graph (D). (E) OTU percent abundances are shown in bar graphs for the species *Ruminococcus gnavus*, *Akkermansia muciniphila*, and *Mucispirillums schaedleri*. (F) PCR validation of *Ruminococcus gnavus*, *Akkermansia muciniphila*, and *Mucispirillums schaedleri*. (G) Bar graphs representing concentration of SCFAs acetic acid, propionic acid, i-butyric acid, n-butyric acid, i-valeric acid, and n-valeric acid. Significance (p-value: *<0.05, **<0.01, ***<0.005, ****<0.001) was determined by using one-way ANOVA followed by Tukey's post-hoc multiple comparisons test for depicted bar graphs. Experiments are representative of 3 independent experiments.

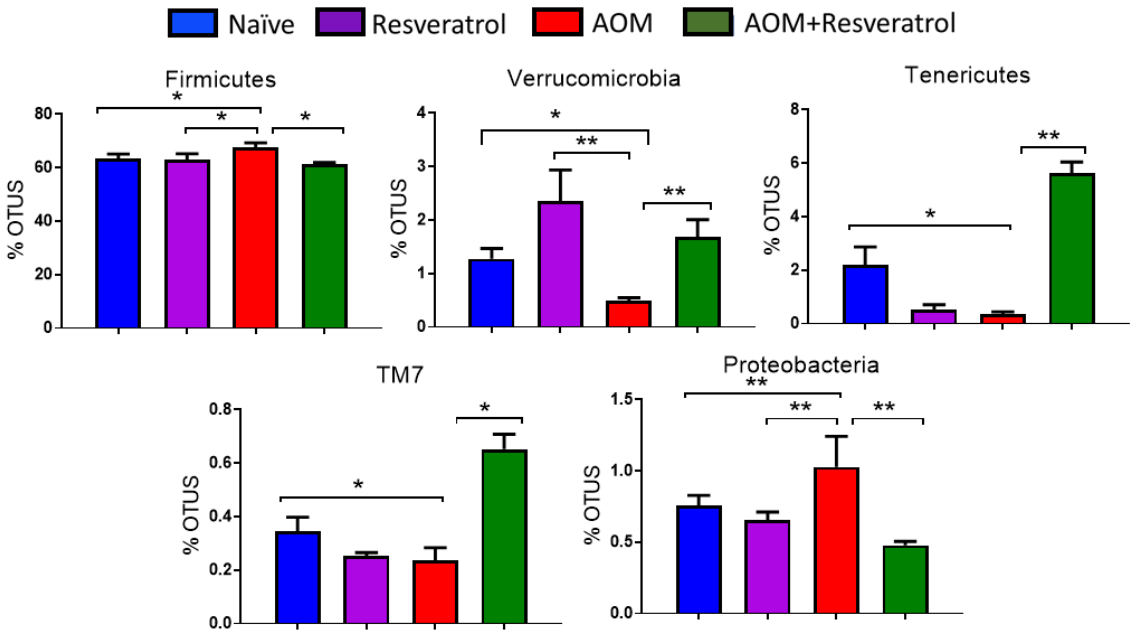

Figure 3.8 Significantly altered bacteria in AOM-induced CRC sample treated with resveratrol at the phylum level. Induction of AOM CRC and treatment with resveratrol was performed as described in Figure 3.1 legend, and 16S rRNA sequencing was performed as described in Figure 3.7 legend. Significance (p-value: *<0.05, **<0.01, ***<0.005, ****<0.001) was determined by using one-way ANOVA followed by Tukey's post-hoc multiple comparisons test in bar graphs. Experiments are representative of at least 3 independent experiments.

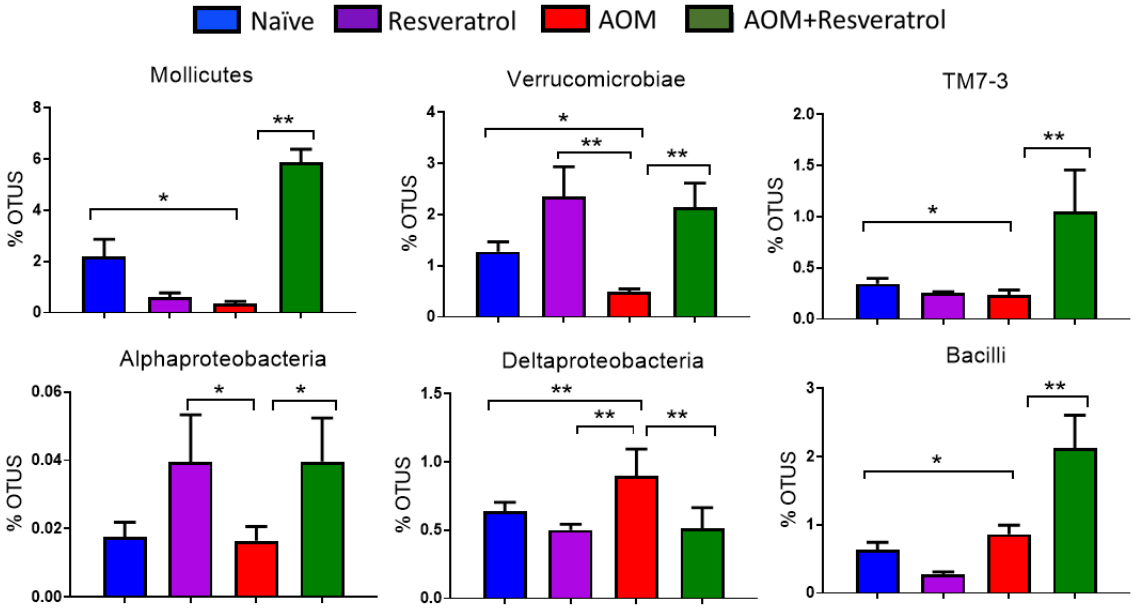

Figure 3.9 Significantly altered bacteria in AOM-induced CRC sample treated with resveratrol at the class level. Induction of AOM CRC and treatment with resveratrol was performed as described in Figure 3.1 legend, and 16S rRNA sequencing was performed as described in Figure 3.7 legend. Significance (p-value: *<0.05, **<0.01, ***<0.005, ****<0.001) was determined by using one-way ANOVA followed by Tukey's post-hoc multiple comparisons test in bar graphs. Experiments are representative of at least 3 independent experiments.

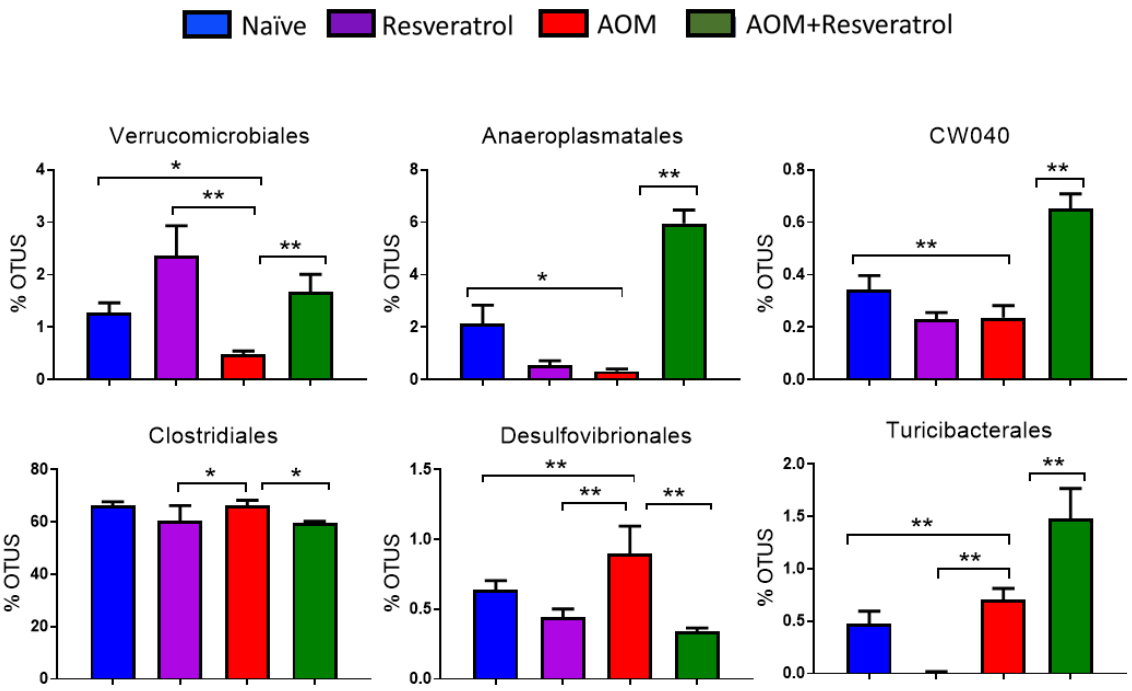

Figure 3.10 Significantly altered bacteria in AOM-induced CRC sample treated with resveratrol at the order level. Induction of AOM CRC and treatment with resveratrol was performed as described in Figure 3.1 legend, and 16S rRNA sequencing was performed as described in Figure 3.7 legend. Significance (p-value: *<0.05, **<0.01, ***<0.005, ****<0.001) was determined by using one-way ANOVA followed by Tukey's post-hoc multiple comparisons test in bar graphs. Experiments are representative of at least 3 independent experiments.

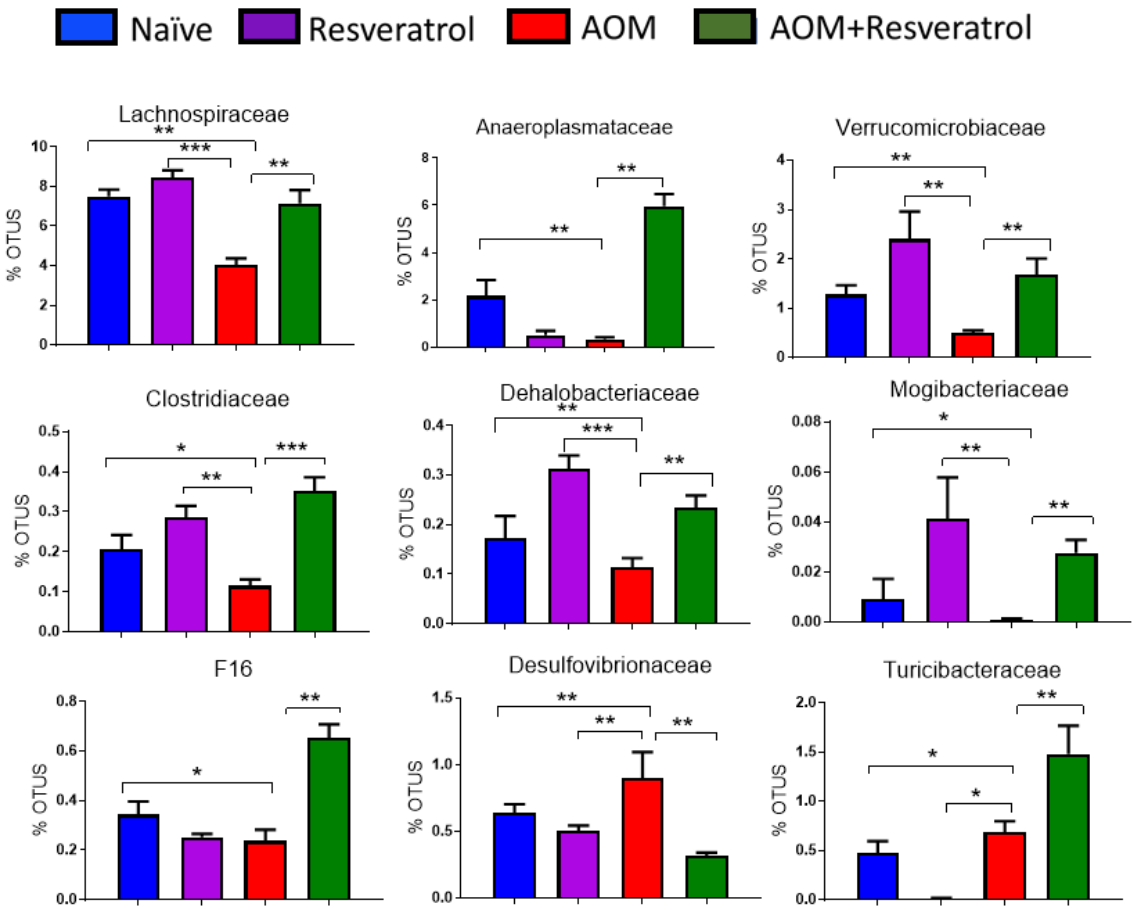

Figure 3.11 Significantly altered bacteria in AOM-induced CRC sample treated with resveratrol at the family level. Induction of AOM CRC and treatment with resveratrol was performed as described in Figure 3.1 legend, and 16S rRNA sequencing was performed as described in Figure 3.7 legend. Significance (p-value: *<0.05, **<0.01, ***<0.005, ****<0.001) was determined by using one-way ANOVA followed by Tukey's post-hoc multiple comparisons test in bar graphs. Experiments are representative of at least 3 independent experiments.

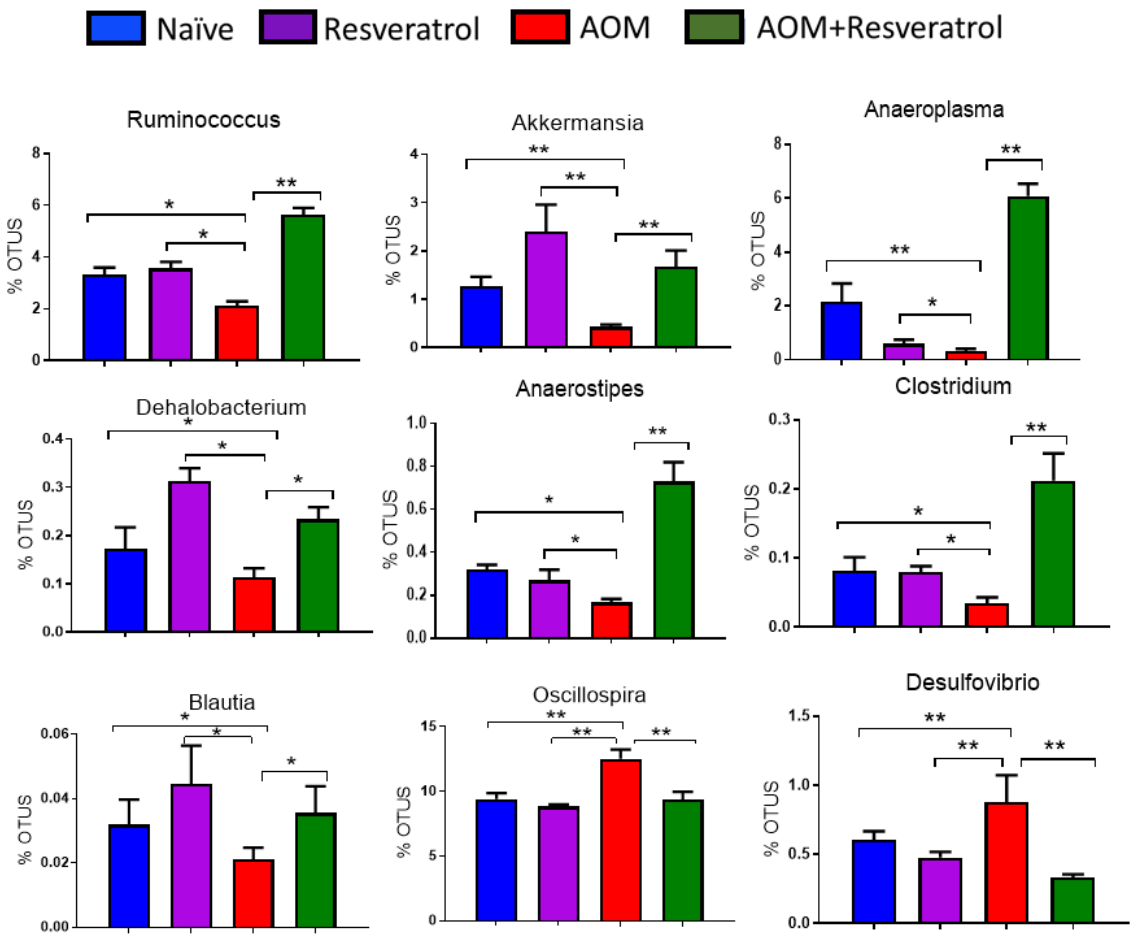

Figure 3.12 Significantly altered bacteria in AOM-induced CRC sample treated with resveratrol at the genus level. Induction of AOM CRC and treatment with resveratrol was performed as described in Figure 3.1 legend, and 16S rRNA sequencing was performed as described in Figure 3.7 legend. Significance (p-value: *<0.05, **<0.01, ***<0.005, ****<0.001) was determined by using one-way ANOVA followed by Tukey's post-hoc multiple comparisons test in bar graphs. Experiments are representative of at least 3 independent experiments.

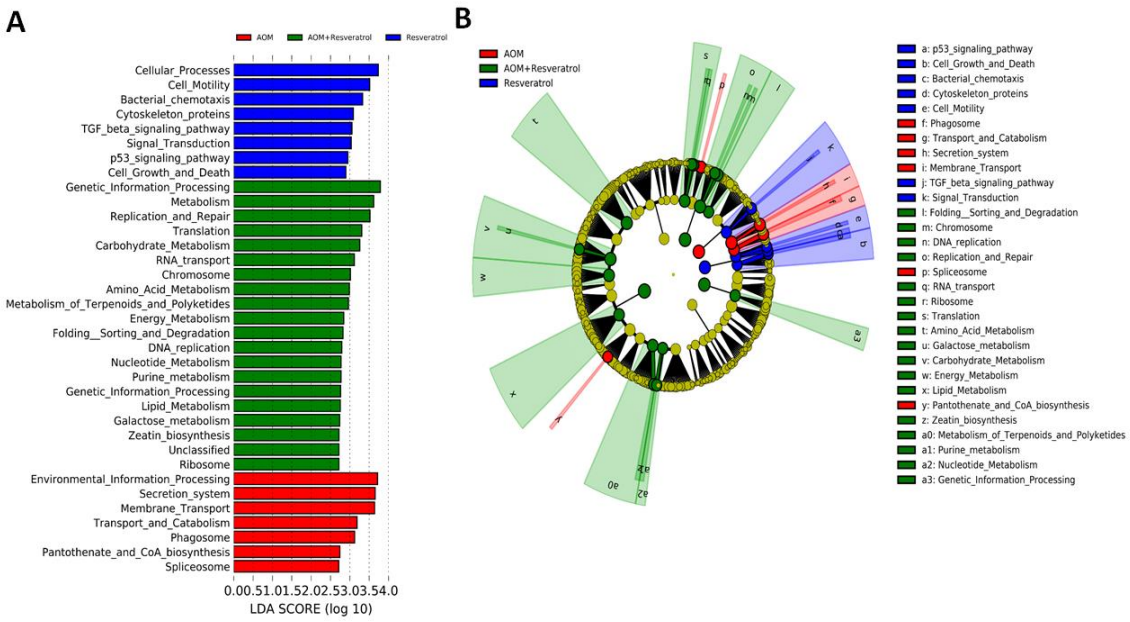

Figure 3.13 LefSe analysis of Nephele-generated PiCRUSt data investigating bacterial function based on 16S rRNA sequencing. To study functional changes within the microbial samples collected, Nephele-based was performed using the PiCRUSt option, which requires a closed reference against the Greengenes database (Greengene_99) at taxa levels 2 and 3 for KEGG annotations of the uploaded dataset. LefSe was performed using the OTU table generated from the Nephele output analysis software as described in Materials and Methods.

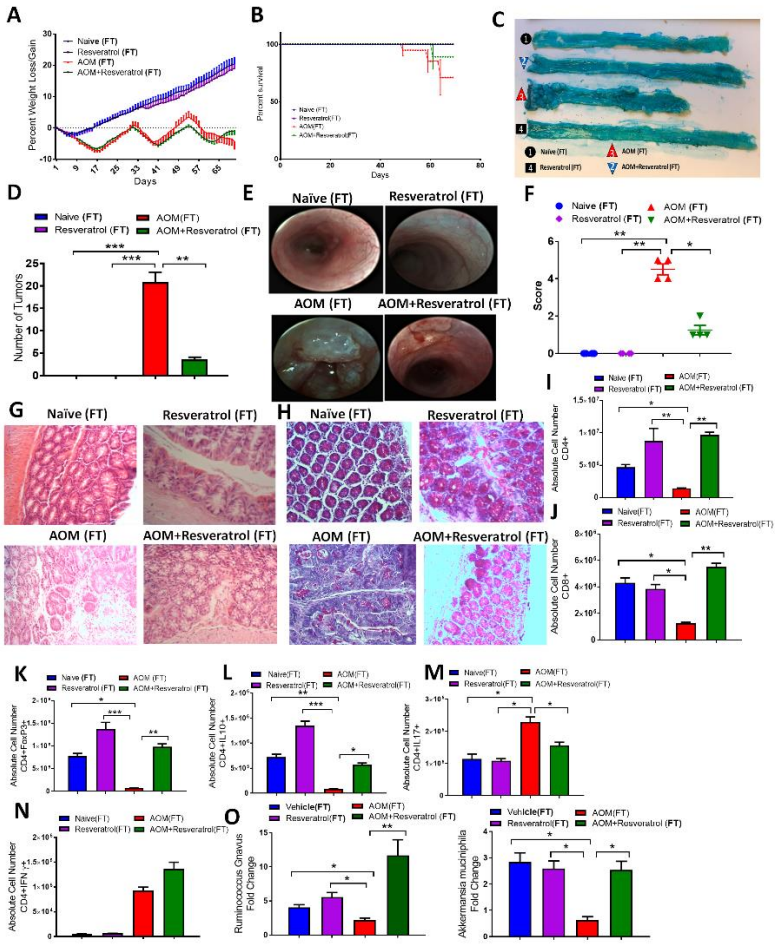

Figure 3.14 Results from FT experiments in AOM-induced CRC model. Antibiotic-treated C57BL/6 mice were injected i.p. with 10 mg of AOM to induce colorectal cancer followed by 3 cycles of 2% DSS. Fecal material was inoculated into recipient mice from the following donors: Naïve (n=4), Resveratrol (n=4), AOM (n=4), and AOM+Resveratrol (n=4). Clinical parameters consisted of percent weight loss (A) and survival (B), both which were found to have significant differences in AOM(FT) vs. AOM+Resveratrol(FT) groups. (C) Representative colons stained with 1% Alcian blue. (D) Bar graph depicting number of tumors counted in each experimental group. (E) Representative colonoscope images from experimental groups. (F) Bar graph depicting scores after examination of tumor polyps detected during colonoscopies. (G) Representative colon sections stained with H&E; scale bar = 100 µM at 40x objective. (H) Representative colon sections which underwent PAS staining; scale bar = 100 µM at 40x objective. (I-J) Bar graphs depicting absolute cell numbers in MLN for general T cells T helper (I), and cytotoxic (J) T cells. (K-N) Bar graphs depicting absolute cell numbers in MLN for Tregs (K), Th cells producing IL-10 (L), Th17 (M), and Th1 (N) cells. (O) PCR validation for the bacterial species *Ruminococcus gnavus* and *Akkermansia muciniphila*. Significance (p-value: *<0.05, **<0.01, ***<0.005, ****<0.001) was determined by using one-way ANOVA and post-hoc Tukey's test for bar/dot graphs, Mann-Whitney test for weight data, and log rank test for survival curve. Data are representative of at least 3 independent experiments.

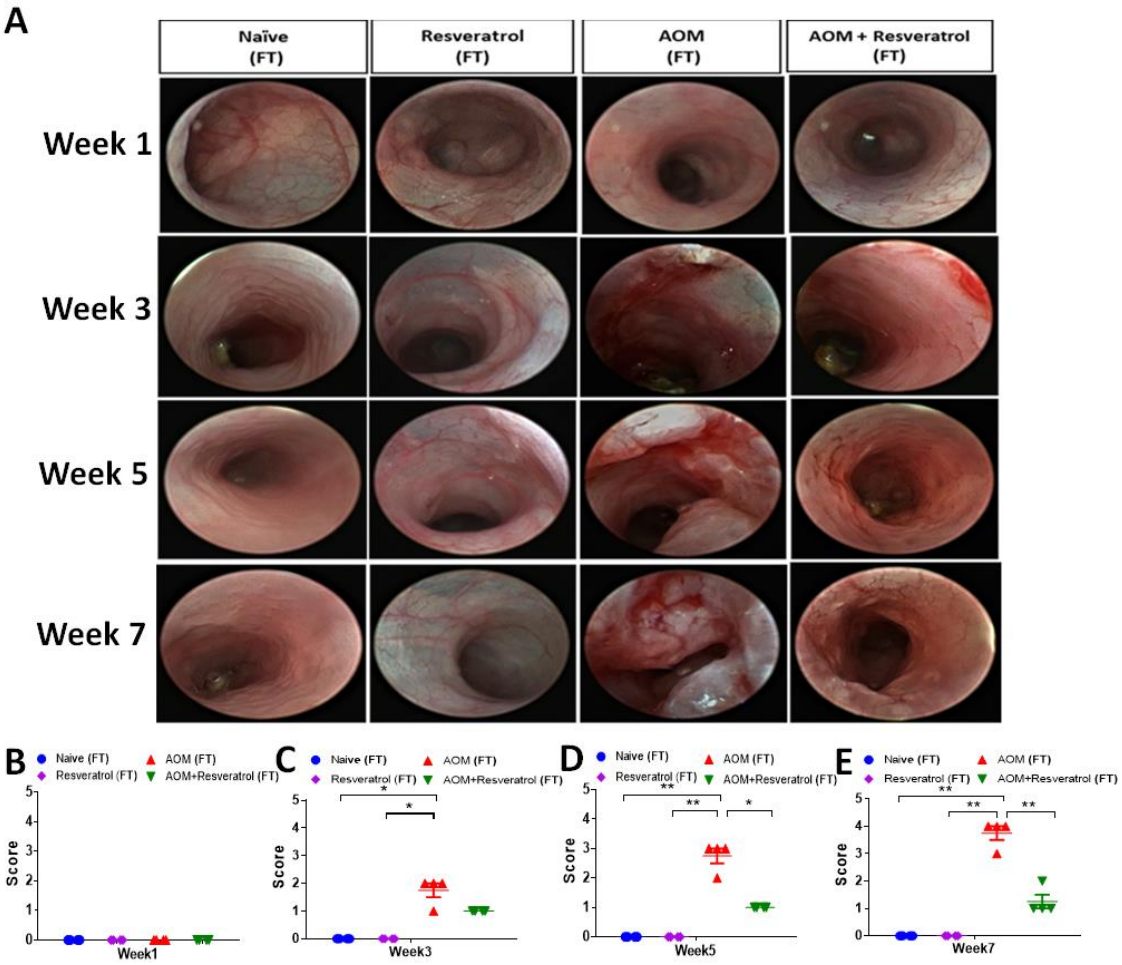

Figure 3.15 Weekly colonoscopy images in FT experiments. Induction of AOM CRC and FT were performed as described in Figure 3.14 legend. (A) Representative colonoscopies are shown from experimental groups which included Naïve(FT) (n=4), Resveratrol(FT) (n=4), AOM(FT) (n=4), AOM+Resveratrol(FT) (n=4) at weeks 1, 3, 5, and 7. Bar graphs depict colonoscopy scores (described in Materials and Methods) for experimental groups at week 1(B), week 3 (C), week 5 (D), and week 7 (E). Significance (p-value: *<0.05, **<0.01, ***<0.005, ****<0.001) was determined by using one-way ANOVA followed by Tukey's post-hoc multiple comparisons test for depicted bar graphs.

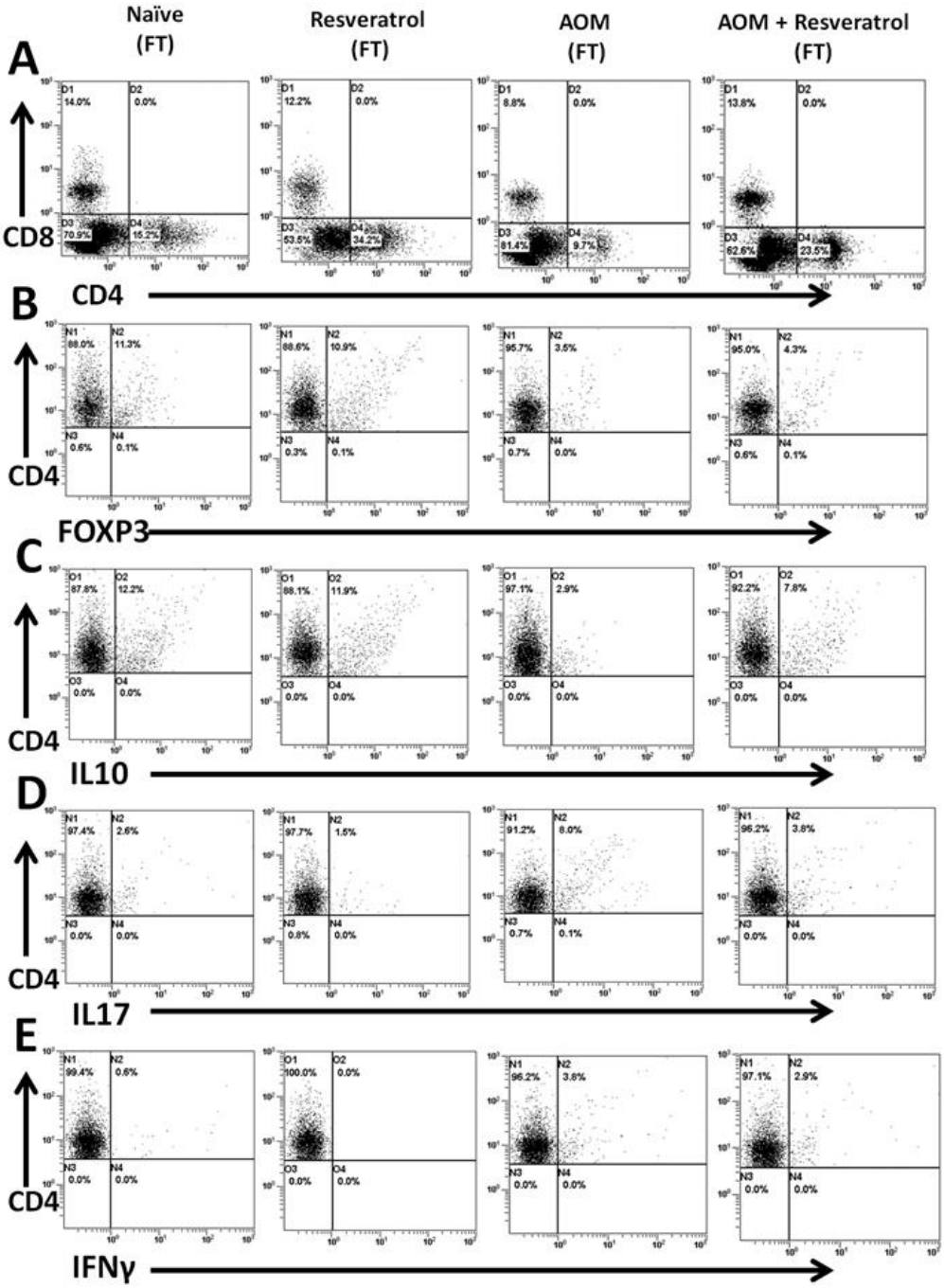

Figure 3.16 T cell phenotyping in MLN of FT experiments. Induction of AOM CRC and FT were performed as described in Figure 3.14 legend. Representative flow cytometry dot plots are depicted for the following T cell subsets: CD3+CD4+CD8+ (A), CD4+FOXP3+ (B), CD4+IL10+ (C) and CD4+IFNγ+ (D), and CD4+IL-17+ (E). For Figures B-E, cells were gated on CD4+ population. Data are representative of at least 3 independent experiments.

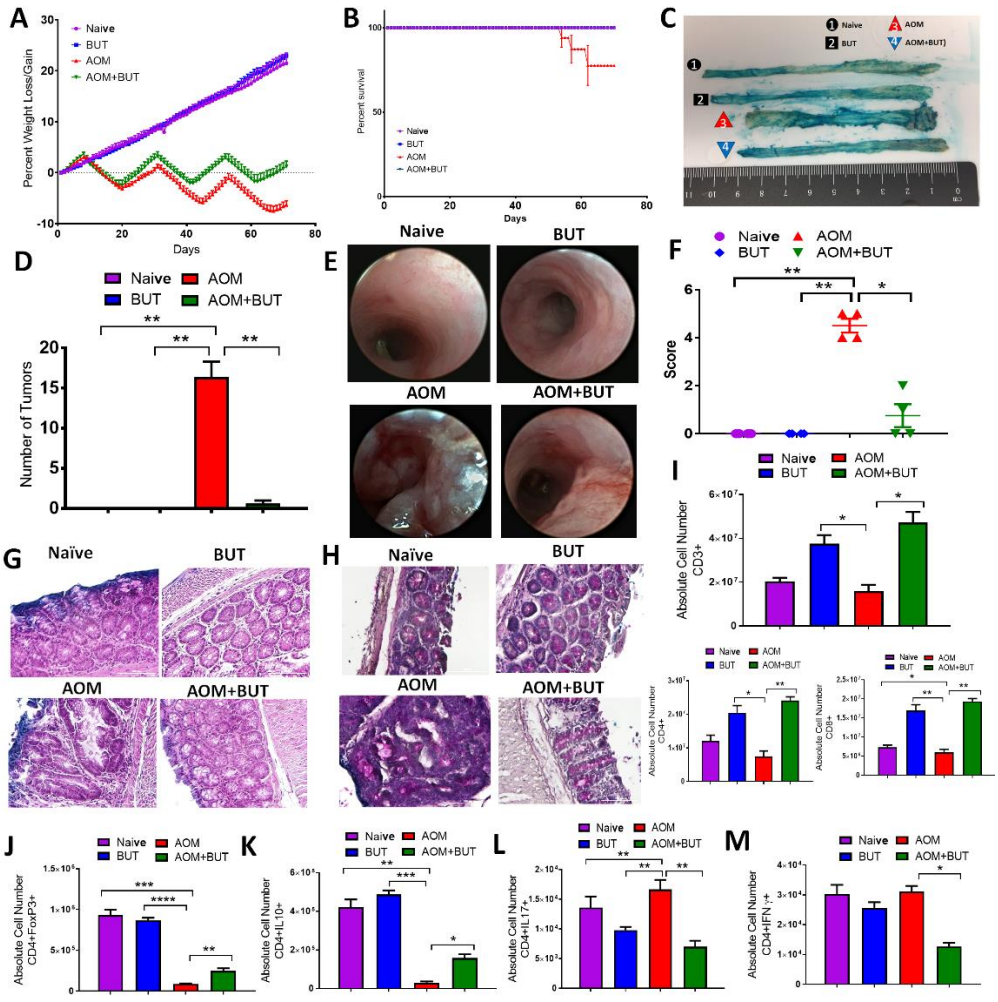

Figure 3.17 Treatment with sodium butyrate (BUT) reduces clinical symptoms and alters T cell phenotype in AOM-induced CRC model. Female C57BL/6 mice were injected intraperitoneal with 10 mg of AOM to induce colorectal cancer followed by 3 cycles of 2% DSS. Experimental groups consisted of: Naïve (n=4), BUT (n=4), AOM (n=4), and AOM+BUT (n=4). Clinical parameters consisted of percent weight loss (A) and survival (B), both of which were found to have significant differences in AOM vs. AOM+Resveratrol groups. (C) Representative colons stained with 1% Alcian blue. (D) Bar graph depicting number of tumors counted in each experimental group. (E) Representative colonoscopic images from experimental groups. (F) Bar graph depicting scores after examination of tumor polyps detected during colonoscopies. (G) Representative colon sections stained with H&E; scale bar = 100 µM at 40x objective. (H) Representative colon sections which underwent PAS staining; scale bar = 100 µM at 40x objective. (I) Bar graphs depicting absolute cell numbers in MLN for general T cells (CD3+), T helper (CD3+CD4+), and cytotoxic (CD3+CD8+) T cells. (J-M) Bar graphs depicting absolute cell numbers in MLN for Tregs (J), Th cells producing IL-10 (K), Th17 (L), and Th1 (M) cells. Significance (p-value: *<0.05, **<0.01, ***<0.005, ****<0.001) was determined by using one-way ANOVA and post-hoc Tukey's test for bar/dot graphs, Mann-Whitney test for weight data, and log rank test for survival curve. Data are representative of at least 3 independent experiments.

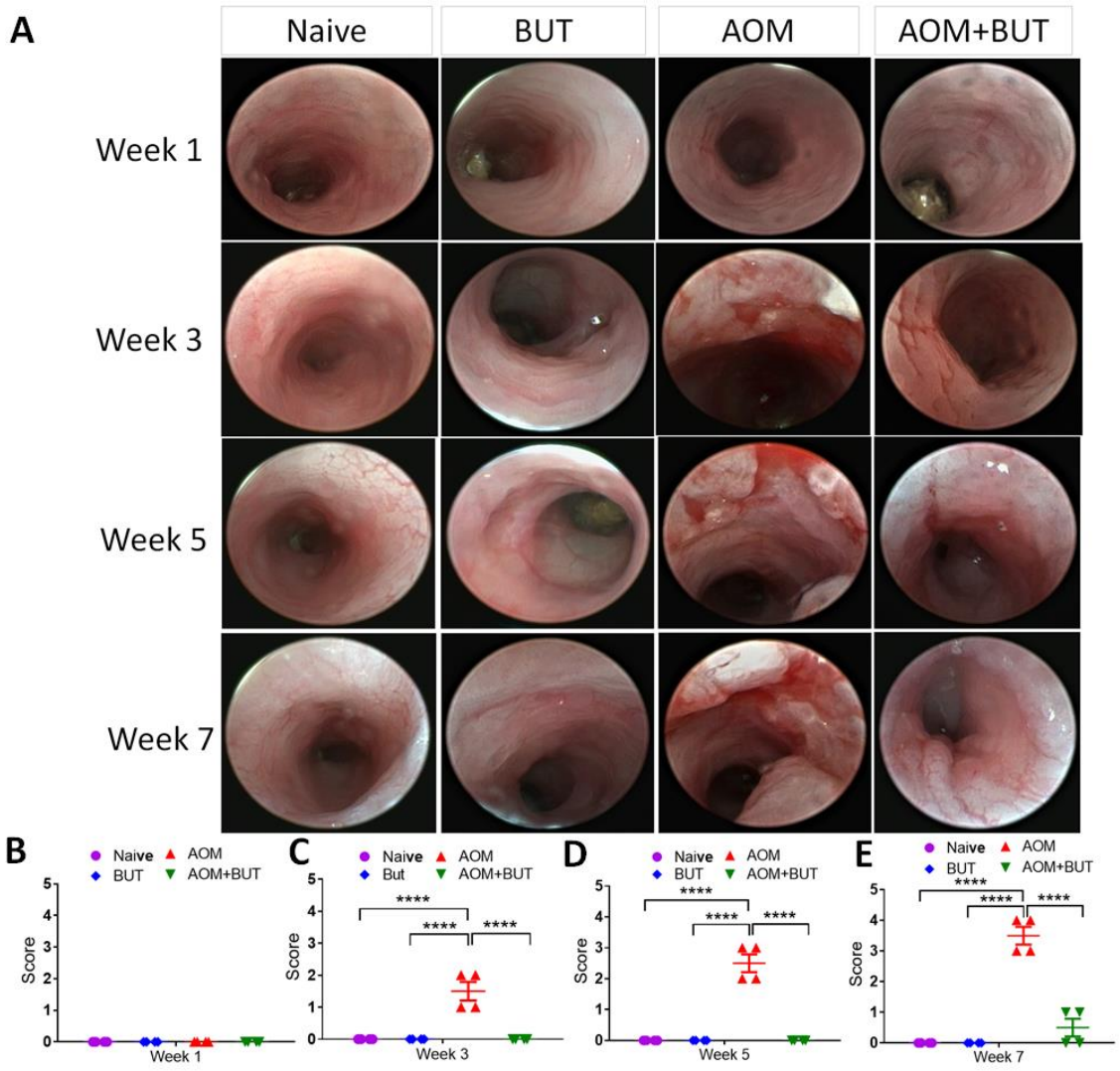

Figure 3.18 Weekly colonoscopy images in AOM-induced CRC treated with BUT. Induction of AOM CRC and treatment with resveratrol was performed as described in Figure 3.17 legend. (A) Representative colonoscopies are shown from experimental groups which included Naïve (n=4), BUT (n=4), AOM (n=4), AOM+BUT (n=4) at weeks 1, 3, 5, and 7. Bar graphs depict colonoscopy scores (described in Materials and Methods) for experimental groups at week 1(B), week 3 (C), week 5 (D), and week 7 (E). Significance (p-value: *<0.05, **<0.01, ***<0.005, ****<0.001) was determined by using one-way ANOVA followed by Tukey's post-hoc multiple comparisons test for depicted bar graphs.

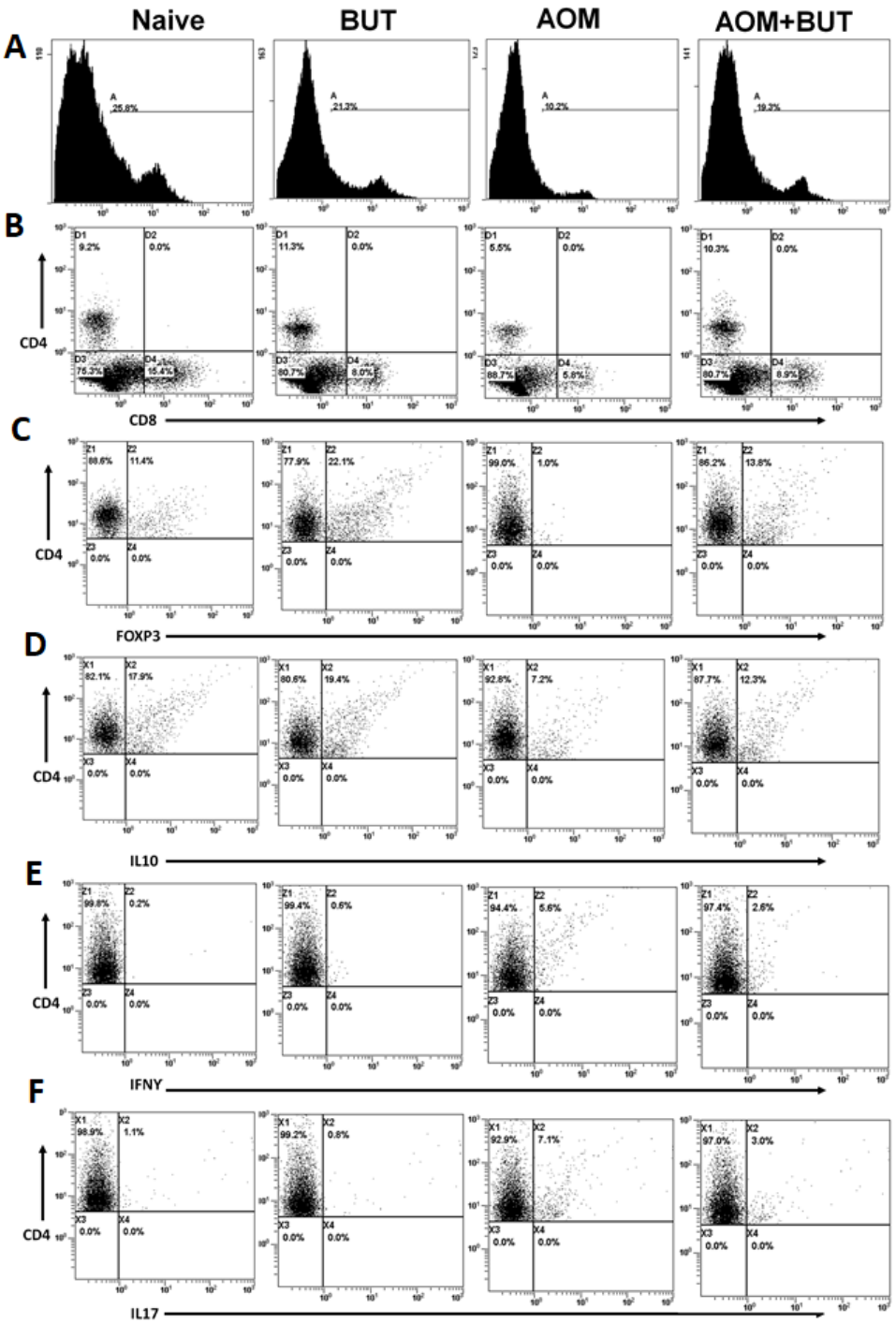

Figure 3.19 T cell phenotyping in MLN of AOM-induced CRC mice treated with BUT. Induction of AOM CRC and treatment with resveratrol was performed as described in Figure 3.17legend. Representative flow cytometry histograms and dot plots are depicted for the following T cell subsets: CD3+ (A), CD3+CD4+CD8+ (B), CD4+FOXP3+ (C), CD4+IL10+ (D) and CD4+IFNγ+ (E), and CD4+IL-17+ (F). For Figures C-F, cells were gated on CD4+ population. Data are representative of at least 3 independent experiments.

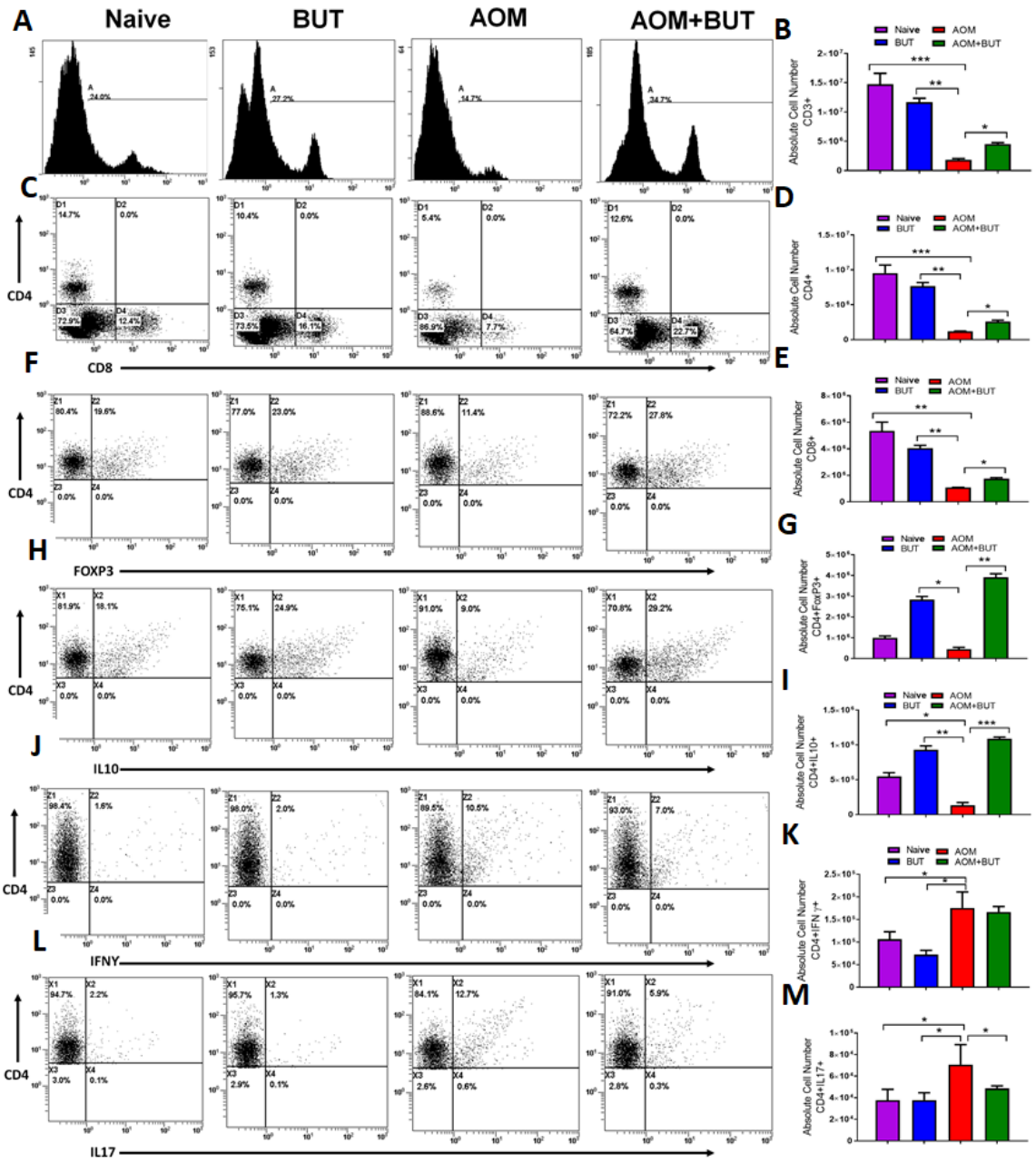

Figure 3.20 T cell phenotyping in spleen of AOM-induced CRC mice treated with BUT. Induction of AOM CRC and treatment with resveratrol was performed as described in Figure 3.17 legend. Flow cytometry dot plots and quantitative bar graphs depicting absolute cell numbers are shown respectively for the following T cell subsets: CD3+ (A-B), CD4+ or CD8+ cells (C-E), CD4+FOXP3+ (F-G), CD4+IL10+ (H-I) and CD4+IFNγ+ (J-K), and CD4+IL-17+ (L-M) expressing cells. For Figures F-M, cells were gated on CD4+ population. Each experimental group had at least 5 mice included, and significance (p-value: *<0.05, **<0.01, ***<0.005, ****<0.001) was determined for absolute cell numbers by using one-way ANOVA followed by Tukey's post-hoc multiple comparisons test. Data are representative of at least 3 independent experiments.

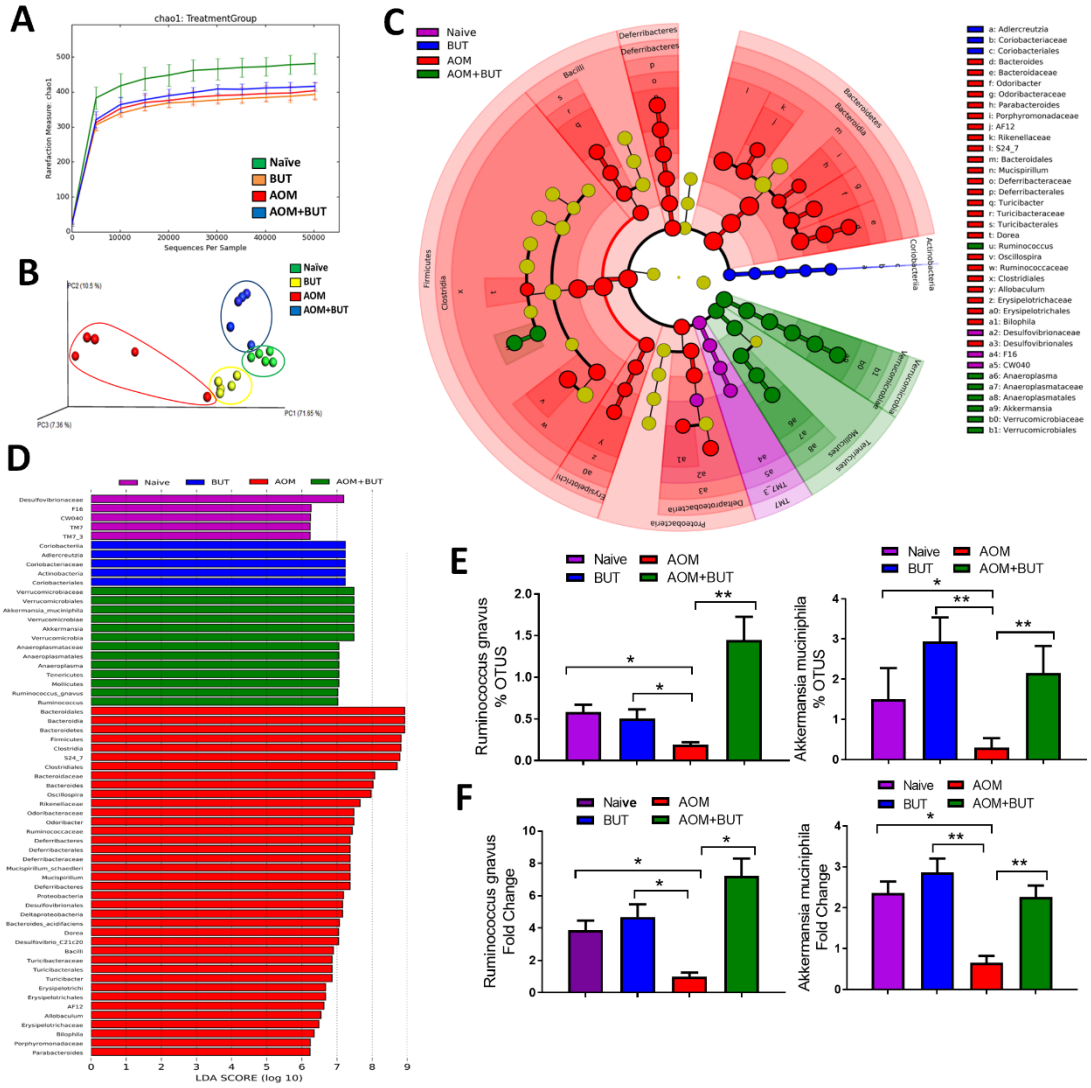

Figure 3.21 16S rRNA sequencing analysis during AOM-induced CRC treated with BUT. AOM induction and treatment with BUT were performed as described in Figure 3.17 legend. Gut microbiota samples were collected from experimental groups by performing colonic flushes in experimental groups, which were: Naïve (n=5), BUT (n=5), AOM (n=5), and AOM+BUT (n=5). Nephele analysis (nephele.niaid.nih.gov) was used to generate charts for chao1 alpha diversity (A) and PCA beta diversity (B). LeFSe analysis of the Nephele OTU output files generated the cladogram (C) and LDA score bar graph (D). (E) OTU percent abundances are shown in bar graphs for the species *Ruminococcus gnavus* and *Akkermansia muciniphila*. (F) PCR validation of *Ruminococcus gnavus* and *Akkermansia muciniphila.* Significance (p-value: *<0.05, **<0.01, ***<0.005, ****<0.001) was determined by using one-way ANOVA followed by Tukey's post-hoc multiple comparisons test for depicted bar graphs. Experiments are representative of 3 independent experiments.

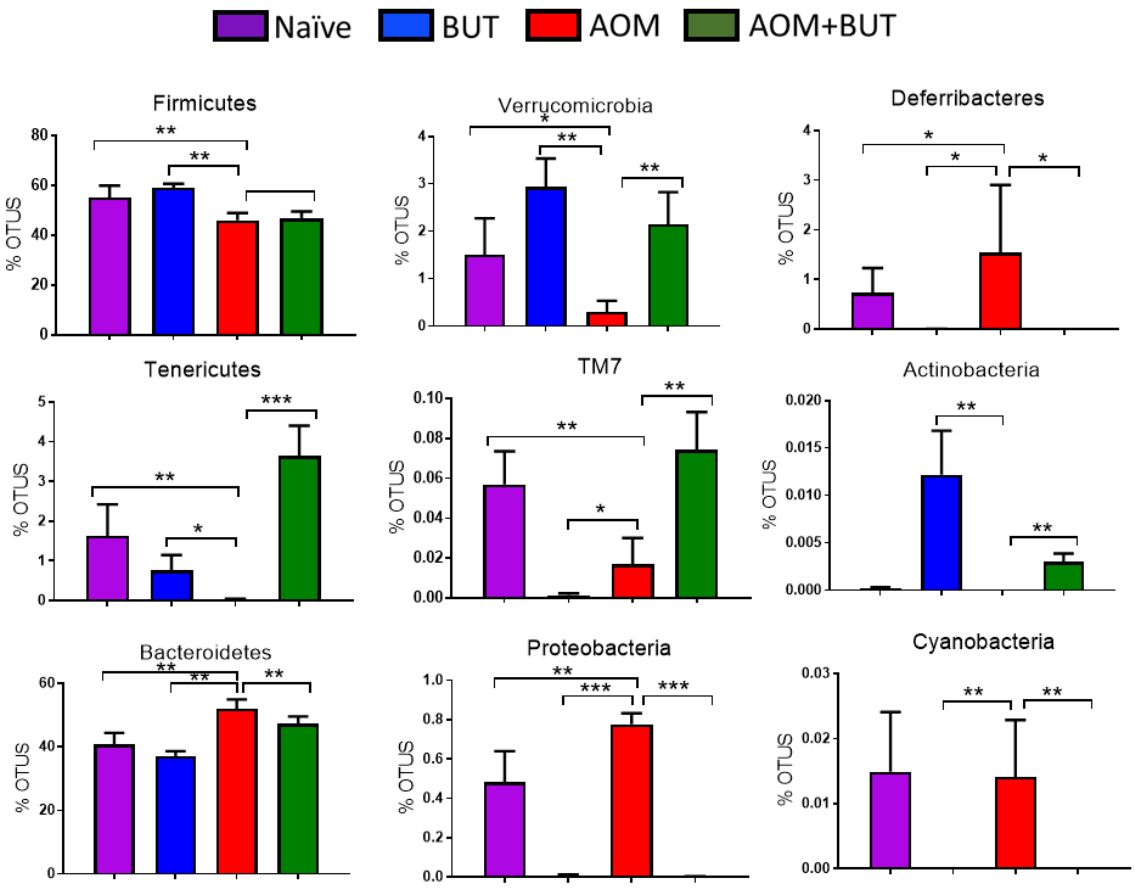

Figure 3.22 Significantly altered bacteria in AOM-induced CRC sample treated with BUT at the phylum level. Induction of AOM CRC and treatment with resveratrol was performed as described in Figure 3.17 legend, and 16S rRNA sequencing was performed as described in Figure 3.21 legend. Significance (p-value: *<0.05, **<0.01, ***<0.005, ****<0.001) was determined by using one-way ANOVA followed by Tukey's post-hoc multiple comparisons test in bar graphs. Experiments are representative of at least 3 independent experiments.

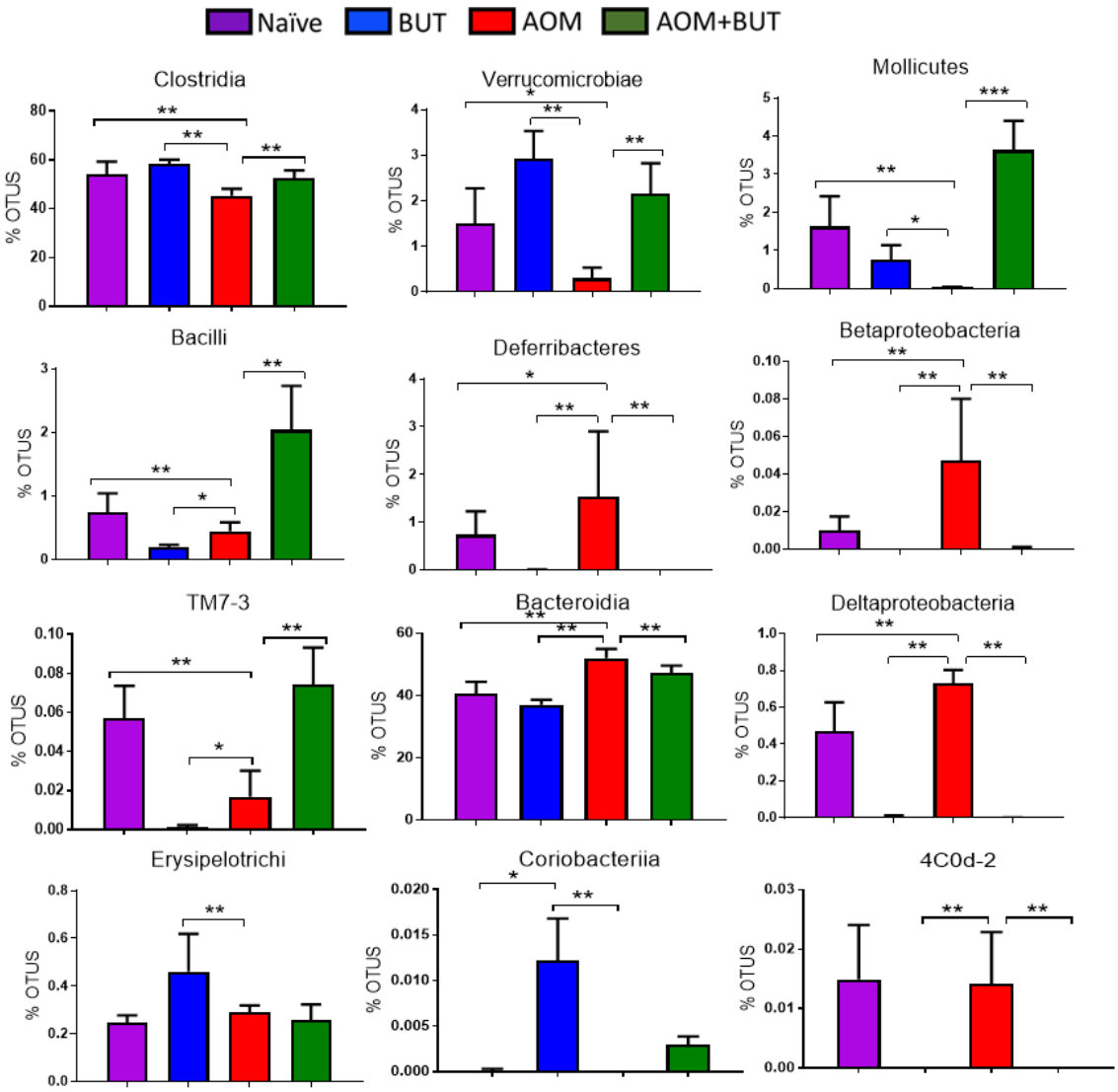

Figure 3.23 Significantly altered bacteria in AOM-induced CRC sample treated with BUT at the class level. Induction of AOM CRC and treatment with resveratrol was performed as described in Figure 3.17legend, and 16S rRNA sequencing was performed as described in Figure 3.21 legend. Significance (p-value: *<0.05, **<0.01, ***<0.005, ****<0.001) was determined by using one-way ANOVA followed by Tukey's post-hoc multiple comparisons test in bar graphs. Experiments are representative of at least 3 independent experiments.

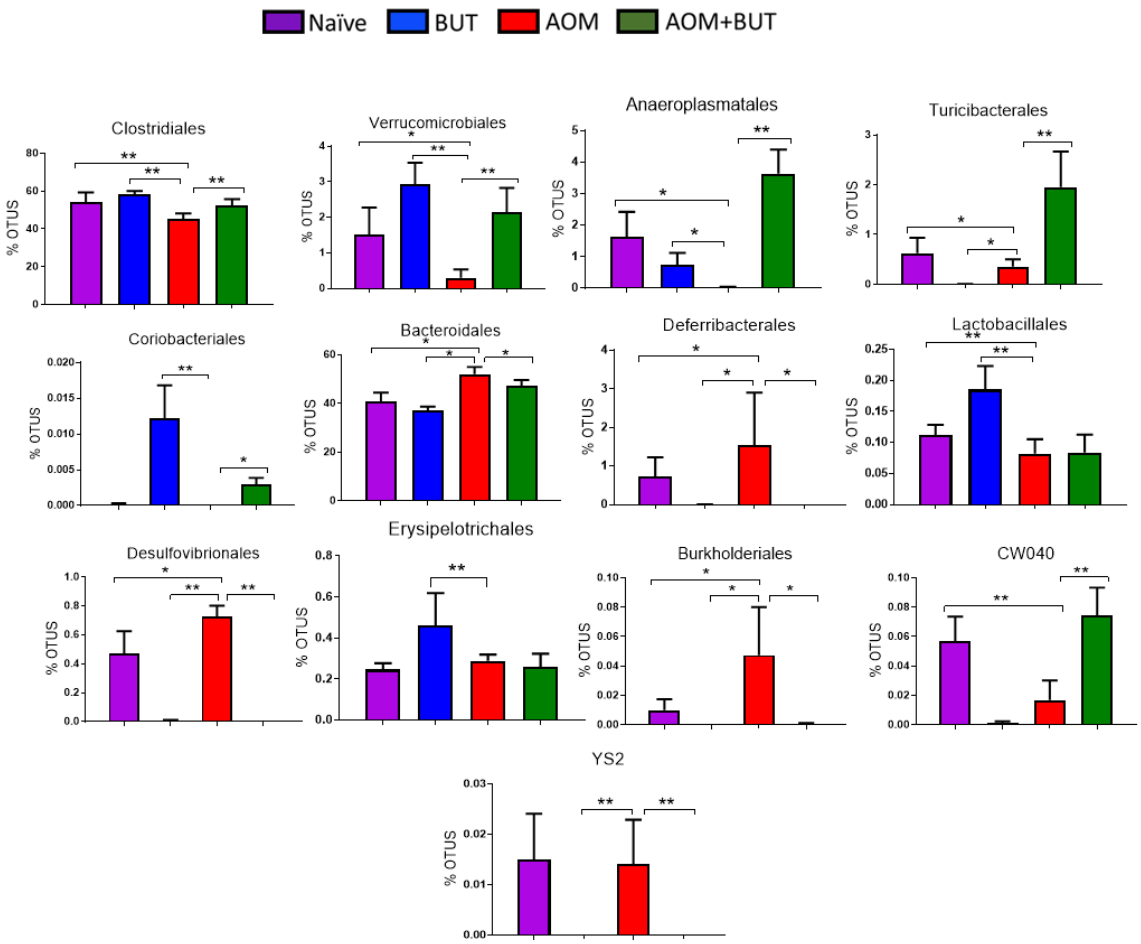

Figure 3.24 Significantly altered bacteria in AOM-induced CRC sample treated with BUT at the order level. Induction of AOM CRC and treatment with resveratrol was performed as described in Figure 3.17 legend, and 16S rRNA sequencing was performed as described in Figure 3.21 legend. Significance (p-value: *<0.05, **<0.01, ***<0.005, ****<0.001) was determined by using one-way ANOVA followed by Tukey's post-hoc multiple comparisons test in bar graphs. Experiments are representative of at least 3 independent experiments.

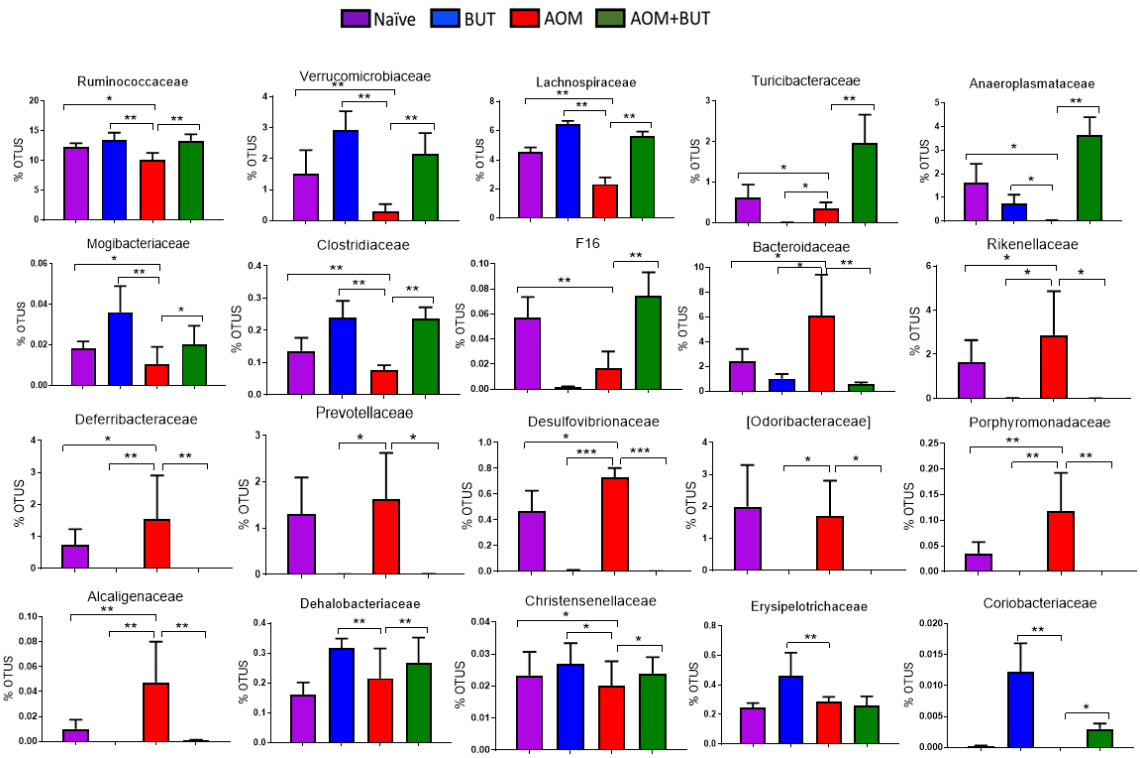

Figure 3.25 Significantly altered bacteria in AOM-induced CRC sample treated with BUT at the family level. Induction of AOM CRC and treatment with resveratrol was performed as described in Figure 3.17 legend, and 16S rRNA sequencing was performed as described in Figure 3.21 legend. Significance (p-value: *<0.05, **<0.01, ***<0.005, ****<0.001) was determined by using one-way ANOVA followed by Tukey's post-hoc multiple comparisons test in bar graphs. Experiments are representative of at least 3 independent experiments.

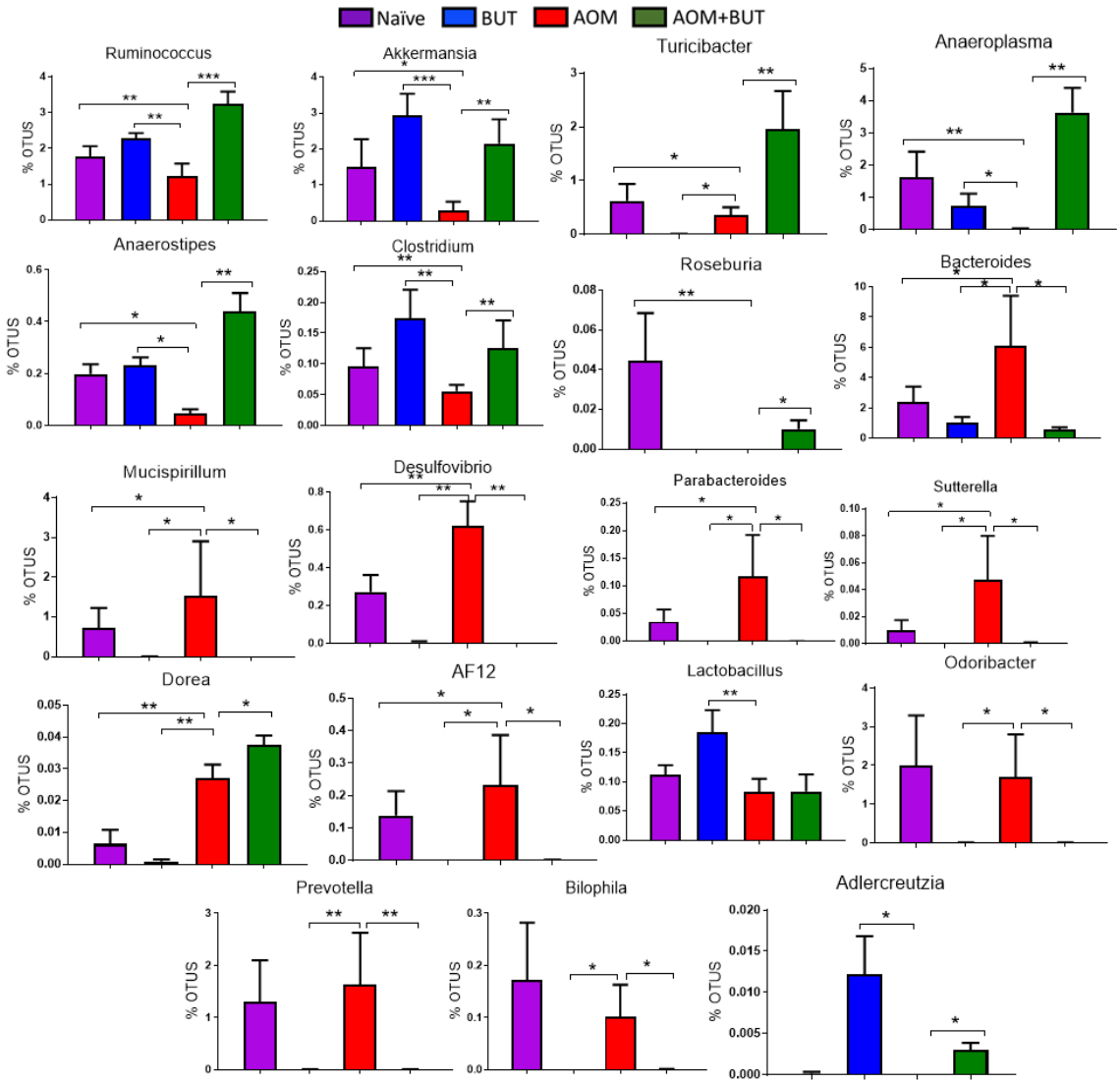

Figure 3.26 Significantly altered bacteria in AOM-induced CRC sample treated with BUT at the genus level. Induction of AOM CRC and treatment with resveratrol was performed as described in Figure 3.17 legend, and 16S rRNA sequencing was performed as described in Figure 3.21 legend. Significance (p-value: *<0.05, **<0.01, ***<0.005, ****<0.001) was determined by using one-way ANOVA followed by Tukey's post-hoc multiple comparisons test in bar graphs. Experiments are representative of at least 3 independent experiments.

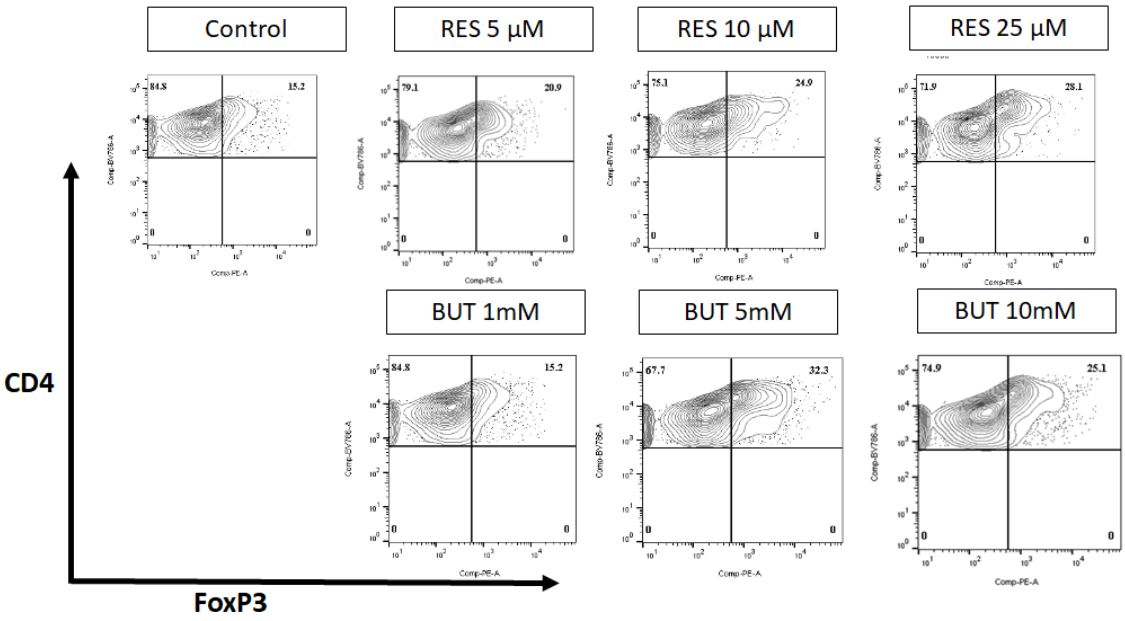

Figure 3.27 Resveratrol and BUT dose-dependently increase Tregs *in vitro*. Whole splenocytes (seeded at 1 x 10^6 cells/ml) from 8-10 week old C57BL/6 mice were activated using CD3 (.5µg/ml) and CD28 (2µg/ml) in the absence or presence of appropriate vehicle control, resveratrol (5, 10, or 25µM), or BUT (1, 5, or 10mM). After 24 hours, cells were fixed and stained with antibodies to identify percentages of Tregs (CD4+FoxP3+). Plots are representative flow dot plots for vehicle control and the various doses of RES and BUT gated on the CD4 population. A total of 3 independent wells (n=3) were used for each group and the data is representative of 2 independent experiments.

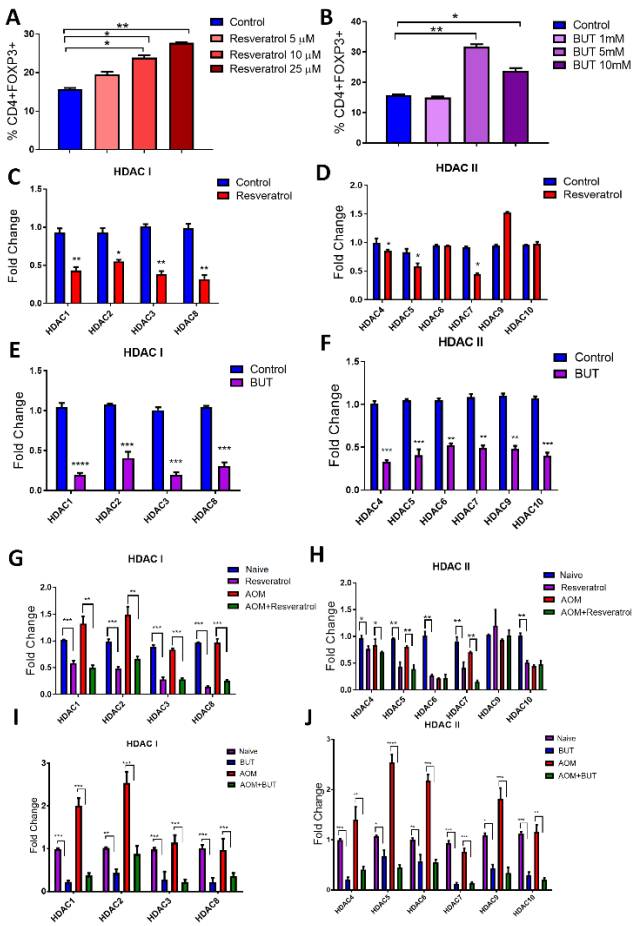

Figure 3.28 Treatment with Resveratrol and BUT leads to HDAC suppression. Whole splenocytes (seeded at 1 x 10^6 cells/ml) from 8-10 week old C57BL/6 mice were activated using CD3 (.5μg/ml) and CD28 (2μg/ml) in the absence or presence of appropriate vehicle control, resveratrol (5, 10, or 25μM), or BUT (1, 5, or 10mM). Tregs were identified by flow cytometry as represented in Figure 3.27. (A) Treg percentages after treatment with various doses of resveratrol. (B) Treg percentages after treatment with varying doses of BUT. Fold change expression as assessed by PCR for HDAC I (C) and HDAC II (D) after treatment with resveratrol (25μM). Fold change expression as assessed by PCR for HDAC I (E) and HDAC II (F) after treatment with BUT (5mM). Expression of HDAC I (G) and HDAC II (H) was evaluated from MLNs isolated from experimental groups (Naive, Resveratrol, AOM, and AOM+Resveratrol). Expression of HDAC I (I) and HDAC II (J) was evaluated from MLNs isolated from experimental groups (Naive, BUT, AOM, and AOM+BUT). For *in vitro* experiments, each group consisted of 3 wells (n=3), and the data are representative of 2 independent experiments. For *in vivo* experiments, each group consisted of 5 mice (n=5), and the data is representative of at least 3 independent experiments.Significance (p-value: *<0.05, **<0.01, ***<0.005, ****<0.001) was determined by using one-way ANOVA followed by Tukey's post-hoc multiple comparisons test for depicted bar graphs.

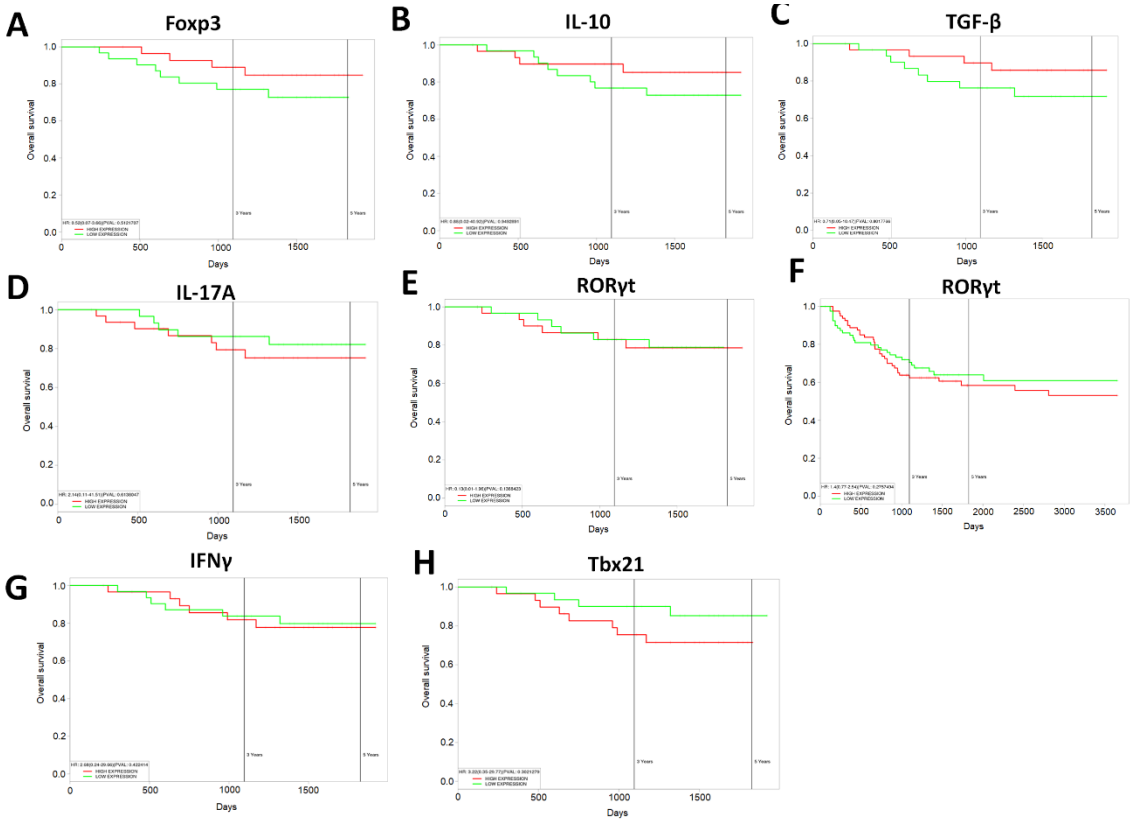

Figure 3.29 Human CRC patient survival correlated with gene expression. TCGA datasets for colorectal cancer from The Cancer genome Atlas maintained at (TCGA, https://cancergenome.nih.gov/) were used to correlate gene expression with patient survival over a 5-year period or more. Correlations to patient survival were performed based on the following gene expressions: (A) FoxP3, (B) IL-10, (C) TGF-β, (D) IL-17A, (E) ROR-γt, (F) ROR-γt (past five year interval), (G) IFN-γ, and (H) Tbx21. Kaplan-Meier survival curves, defined as the probability of survival in a given length of time while considering time in many small intervals, were used to generate survival curves plots.

CHAPTER 4

RESVERATROL DOWNREGULATES MIR-31 TO PROMOTE CD4+FOXP3+ T REGULATORY CELLS DURING PREVENTION OF TNBS-INDUCED COLITIS

4.1 ABSTRACT

Colitis, an inflammatory bowel disease, is associated with aberrant regulation of the colonic mucosal immune system. Resveratrol, a natural plant product, has been found to exert anti-inflammatory properties and attenuate the development of murine colitis. In the current study, we examined the role of microRNA (miR) in the ability of resveratrol to suppress colonic inflammation. Resveratrol treatment of mice bearing TNBS-induced colitis improved the overall clinical scores by reversing weight loss and colitis-associated pathogenesis. Flow cytometric analysis of the mesenteric lymph nodes (MLNs) demonstrated that resveratrol reduced colitis-associated induction of inflammatory T cells (Th17 and Th1) while increasing CD4+Foxp3+ regulatory T cells (Tregs) and IL-10-producing CD4+ T cells. miR microarray analysis and PCR validation from CD4+ cells isolated from MLN showed that treatment with resveratrol decreased the expression of several miRs (miR-31, Let7a, miR-132) that targeted cytokines and transcription factors involved in anti-inflammatory T cell responses (Foxp3 and TGF-β). Transfection studies with FoxP3-targeting miR-31 mimic or inhibitors confirmed that this miR directly regulated the expression of Foxp3. Analysis of data from human patients with ulcerative colitis (UC) revealed that miR-31 expression was significantly increased when compared to controls and additionally, this miR was highly induced in UC colon biopsies that

exhibited colon cancer-associated neoplastic lesions. Together, the current study demonstrates resveratrol-mediated attenuation of colitis may be regulated by miR-31 through induction of Foxp3+ Tregs and that miR-31 may serve as a therapeutic target for human colitis.

4.2 INTRODUCTION

Previously, we have shown that treatment with resveratrol, a natural product found in a variety of plant products (Busbee et al., 2013), is able to lessen disease burden in chemical (dextran sodium sulfate, DSS) and genetic (IL-10 knockout) models of colitis (Singh et al., 2010; Singh et al., 2012), as well as colitis-associated colon cancers (Altamemi et al., 2014; Cui et al., 2010). A current review by Nunes et al. highlights findings from our lab as well as others showing the effectiveness of resveratrol in ameliorating or preventing animal models of colitis (Nunes et al., 2018). One of the key findings from our previous report in the colitis-associated tumorigenesis model was that resveratrol was able to regulate several microRNAs (miRs) that modulated inflammatory genes and factors (Altamemi et al., 2014). This was a significant finding because miRs, small non-coding RNA molecules that target and regulate gene transcripts (Guo et al., 2018), were found to be important in both the development and progression of colitis, particularly in terms of regulating inflammation, serving as disease biomarkers, and responding to therapies (Feng et al., 2018; Lopetuso et al., 2018; Minacapelli et al., 2019; Morilla et al., 2018; Schonauen et al., 2018; Singh et al., 2014a). The importance of miRs in regulating colitis was highlighted in our previous report showing that deficiency in only one miR (miR-155) was able to protect mice from developing severe colitis

symptoms by a reduction in the inflammatory T helper (Th) type responses (Singh et al., 2014a).

In the current report, we investigated the effectiveness of resveratrol treatment in another mouse model of chemically-induced colitis, using 2,4,6-Trinitrobenzenesulfonic acid solution (TNBS), which is known to activate inflammatory T cells. We found that resveratrol treatment attenuated severe disease development, resulting in a shift from a pro-inflammatory Th17 phenotype to a more anti-inflammatory T cell response characterized by increased regulatory T cells (Tregs) and those producing IL-10. Microarray analysis of miR profiles in T cells revealed several miRs (e.g. miR-31, Let-7a, and miR-132) that target anti-inflammatory T cell factors were downregulated by resveratrol. In this study we further analyzed the role of miR-31, which was found to target Treg transcription factor FoxP3. These findings were even more interesting after analysis of human UC colitis patients revealed this patient population had significantly higher expression of miR-31 in disease-associated tissues. Altogether, the study highlights that miR-31 is a potential target for prevention of colitis and possibly CRC.

4.3 MATERIALS AND METHODS

Animals. Female mice (BALB/c) aged 8-10 weeks were obtained from Jackson Laboratories (Bar Harbor, ME) and housed at the University of South Carolina, School of Medicine (Columbia, SC) AAALAC-accredited animal facility. All mice were housed in specific pathogen (SPF) free conditions in rooms with controlled temperature, ventilation, and normal light/dark cycles. All procedures performed on mice followed National Institutes of Health (NIH) guidelines under protocols approved by the Institutional Animal Care and Use Committee (IACUC).

Induction of colitis and treatment with resveratrol. Colitis was induced in experimental mice as previously described (Elson et al., 1996). Briefly, TNBS purchased from Sigma-Aldrich (MO, USA) was administered by intrarectal injection using a 38 mm catheter into lightly anesthetized (5% isoflurane) at a concentration of 1 mg TNBS dissolved in 0.1 ml of ethanol (50%). Mice were keep upright for 30 seconds following injection to ensure proper dispersion of the chemical into the colon area. Vehicle control mice were given an injection of 0.1 ml of ethanol (50%) without TNBS to negate any inflammatory or adverse effects caused by the alcohol. Resveratrol, purchased from Sigma-Aldrich, was given 24 hours prior to TNBS injection and given daily until completion of the experiment (5 days) by using a 30 mm oral gavage needle at a dose of 100 mg/kg in 0.1ml of vehicle (1% carboxymethyl cellulose, CMC). In the current study, the following experimental groups were used: Control mice (Vehicle) were given 50% ethanol intrarectal administration and daily oral gavage of vehicle (1% CMC); Naïve mice given treatment (Resveratrol) were given intrarectal administration of 50% ethanol and daily oral gavage of 100 mg/kg of the resveratrol. Disease controls (TNBS+Veh) were given 1mg intrarectal administration of TNBS and daily oral gavage of vehicle (1% CMC). Treatment groups (TNBS+Res) were given 1mg intrarectal administration of TNBS and daily oral gavage of resveratrol (100 mg/kg).

Assessment of disease parameters. To assess disease, experimental mice were weighed daily through the entirety of the experiment (5-6 days). Colonoscopies were performed to evaluate extent of damage (ulcerations and bleeding) to the colons prior to the end of the experiment (day 3). At the study endpoint, mice were euthanized by overdose of isoflurane. Excised colons were measured for length and proximal colons

sections (1cm) were collected for histology. 10% formalin fixed tissues were stained with hematoxylin and eosin (H&E) to assess colonic damage caused by TNBS administration. To assess T cell response to disease and treatment, flow cytometry was performed on single cell suspensions isolated from MLNs and stained using antibodies for the following T cell and T cell subsets: overall T cells (CD3+), T helper cells (CD4+), cytotoxic T cells (CD8+), Tregs (CD4+FoxP3+), IL-10 producing cells (CD4+IL-10+), Th17 cells (CD4+IL-17+), and Th1 cells (CD4+IFNγ+). All antibodies used in these studies were purchased from BioLegend (CA, USA). For transcription factor staining, True-Nuclear Transcription Factor Buffer set from BioLegend was used as per instructions from the manufacturer.

Analysis of miRNA. MicroRNA arrays were performed on RNA isolated from cells collected from the MLN of experimental mice as previously described (Miranda et al., 2018). Each sample consisted of a pool of 5 biological replicates. For each miRNA microarray, FlashTag Biotin HSR RNA Labeling kit from Affymetrix (Thermo Fisher Scientific, MA, USA) was used and tagged samples were later hybridized to the Affymetrix miRNA 4.0 chip. Chips were scanned with an Affymetrix GCS 3000 system. For transcriptome microarrays, 100ng total RNA was used as starting material. RNA was prepared for hybridization by using the Affymetrix GeneChip WT PLUS Reagent Kit according to protocol from the manufacturer. Affymetrix Expression Console Version software was used to evaluate quality control of the samples, as well as initial analysis of the microarray data to include principal component analysis, heatmaps depicting raw signal expression, log2 fold change (FC) calculations, and direct comparisons among the experimental groups. Ingenuity Pathway Analysis (IPA, http://www.ingenuity.com/) was

used to generate miRNA-gene target pathways based on differentially regulated miRNA profiles, which was determined to be a greater than ±2 log2 fold change between two different experimental groups. miR validation studies were performed by first preparing complimentary DNA (cDNA) from isolated RNA samples using the miScript II RT kit (Qiagen, MD, USA) followed by quantitative real time PCR (qRT-PCR) using a CFX Connect Real Time System (Bio-Rad, PA, USA). PCR reactions were performed using mouse-specific miR primers purchased from Qiagen. Primers included mmu-miR-31-5p (MI0000579), mmu-Let-7a (MIMAT0004620), and mmu-miR-132-3p (MIMAT0000144). Expression levels were normalized to Snord96a (MS00033733) levels. Fold changes were calculated using the $2^{-\Delta\Delta CT}$ method.

Transfection experiments with miR-31-5p mimic or inhibitor and target gene quantification. Transfection experiments were carried out as previously described (Alghetaa et al., 2018; Busbee et al., 2015). Excised MLNs from naïve BALB/c were prepared in a single cell suspension before culturing in complete RPMI 1640 media supplemented with heat inactivated 10% fetal bovine serum, 10mM L-glutamine, 10mM HEPES, 50µM β-mercaptoethanol, and 100µg/ml penicillin/streptomycin. MLN cells were seeded (2×10^5 cells per well) in a 24-well plate and activated with 1 µg/ml of bacterial toxin staphylococcal enterotoxin B (SEB) purchased from Toxin Technologies Inc. (FL, USA). Cells were then transfected with either 20nM of synthetic mmu-miR-31–5p mimic (AGGCAAGAUGCUGGCAUAGCUG) or anti-mmu-miR-31–5p (AGGCAAGAUGCUGGCAUAGCUG) using HiPerfect Transfection Reagent from Qiagen for 24 hours. Expression levels for miR-31 and transcriptional factor FoxP3 (forward: CCCATCCCCAGGAGTCTTG; reverse: ACCATGACTAGGGGCACTGTA)

were determined using qRT-PCR. For FoxP3, expression levels were normalized to β actin (forward: GGCTGTATTCCCCTCCG; reverse: CCAGTTGGTAACAATGCCATGT).

Dataset for human colitis patient population. Data on human miR-31 expression levels was obtained from the National Center for Biotechnology Information (NCBI) Gene Expression Omnibus (GEO) repository. The human dataset used was GEO accession GSE68306 provided by Huang et al. and published elsewhere (Pekow et al., 2017). The data set consisted of colon tissue biopsies from normal healthy controls (n=16) and ulcerative colitis (UC) patients (n=29). For UC patients, samples consisted of three distinct tissue biopsy types: UC associated with neoplastic tissues (n=11), UC patients without neoplasia (n=9), and non-dysplastic UC mucosa adjacent to a neoplastic lesion (n=9). For the current report, analysis was performed using two different comparisons. First, expression of miR-31 in healthy tissue samples (n=16) was compared to UC patients (n=29). Second, miR-31 expression from healthy controls (n=16) was compared to colonic tissues from UC patients associated with neoplasia (n=11). Raw expression values were obtained from the provided online dataset and based on NanoString nCounter v1.7.0 platform performed on RNA isolated from formalin-fixed paraffin embedded tissue samples.

Statistical Analysis. GraphPad Prism software (CA, USA) was used for most of the statistical analysis depicted in the current report unless otherwise noted. For *in vivo* colitis experiments, at least 5 mice were used per experimental group. For *in vitro* assays, all experiments were performed in triplicate. For statistical differences, significance (p

value of ≤ 0.05) was determined using one-way ANOVA followed by Tukey's post-hoc multiple comparisons test unless otherwise stated.

4.4 RESULTS

Treatment with resveratrol reduces severity of TNBS-induced colitis

In the current study, we investigated the efficiency of resveratrol to prevent a chemically-induced murine colitis model using TNBS. To investigate prevention of disease by this natural compound, treatment groups were given resveratrol 24 hours prior to induction of disease by TNBS, followed by daily oral administrations of the treatment. As shown, colitis mice (TNBS+Veh) had significant weight loss (~15%) during the course of the study compared to control groups (Vehicle or Resveratrol), but colitis mice pre-treated with resveratrol (TNBS+Res) had significantly decreased incidence of weight loss (Fig. 1A-B). Another hallmark of many colitis models is the shortening of the colon after disease induction. The colons from TNBS mice were significantly shorter while TNBS+Res mice had similar colon lengths when compared to controls (Fig. 1C-D). Colonoscopies performed during the peak of disease (day 3) revealed that while TNBS mice had typical disease-associated features such as ulcerations and bleeding compared to normal colons, colons of TNBS+Res mice had reduced presence of these classical clinical parameters (Fig. 1E). Histological evaluation corroborated with these observations from colonoscopies as there were significant signs of tissue damage (e.g. cellular infiltration, loss of normal colonic tissue architecture) in TNBS mouse colons compared to controls, and this damage was not present or reduced in colons from TNBS+Res mice (Fig. 1F). These observations together demonstrated that resveratrol treatment effectively prevented TNBS-induced colitis.

Treatment of TNBS-induced colitis mice with resveratrol results in a shift from a pro-inflammatory to anti-inflammatory T helper response in MLN

To investigate if this effect of resveratrol was due to reduction in pro-inflammatory T helper responses (IL-17) while inducing anti-inflammatory types (Tregs and IL-10 production), MLNs from the TNBS experimental groups were evaluated to determine T cell distribution during disease and treatment. The T cell subsets evaluated included all T cells (Fig. 2A), T helper and cytotoxic T cells (Fig. 2B), Tregs (Fig. 2C), IL-10 T helper cells (Fig. 2D), and Th17 cells (Fig. 2E). Based on percentages obtained from flow cytometry phenotyping (Figs. 2A-E), absolute cell numbers were assessed in MLNs from all experimental groups. Overall T cells (Fig. 3A), including CD4+ T helper (Fig. 3B) and CD8+ cytotoxic (Fig. 3C), were significantly increased in TNBS+Veh mice compared to the other experimental groups, and TNBS+Res mice reduced these subsets to the levels seen in normal controls. Despite an overall increase in CD4+ T cells, there was a decrease in the anti-inflammatory Treg (Fig. 3D) and IL-10-producing (Fig. 2E) cells during TNBS induction, while colitis mice treated with resveratrol had significantly higher numbers of these anti-inflammatory subsets compared to controls. A significant proportion of the CD4+ T cell subsets in TNBS+Veh mice appeared to be pro-inflammatory Th17 cells (Fig. 3F), and treatment with resveratrol during the disease state showed ablation of the increase in this T cell subset, comparable to control levels. Taken altogether, treatment with resveratrol appeared to prevent colitis-associated increases in pro-inflammatory Th17 cells, likely through the induction of anti-inflammatory subsets such as Tregs and CD4+ IL-10-producing cells.

Resveratrol treatment downregulates miRs that target Treg transcription factor FoxP3 and other anti-inflammatory T cell-associated factors

Next, we investigated if miRs regulated the anti-inflammatory properties of resveratrol. To that end, we investigated the miR profile of cells from the MLN. Principal component analysis (PCA) from pooled samples from all experimental groups showed that the miR profiles of controls (Vehicle and Resveratrol) were most similar with opposite deviations occurring when compared to TNBS+Veh and TNBS+Res groups (Fig. 4A). Direct comparisons among two groups at a time, with the significance criteria set to a ±2-fold change, revealed the greatest difference was among the TNBS+Veh vs. TNBS+Res groups (Fig. 4B). Comparison of these two groups showed 260 total miRs (out of 3195 probed) were significantly altered, with TNBS+Res downregulating 198 and upregulating 62 compared to TNBS+Veh (Fig. 4C). A heatmap showing raw expression of these 260 significantly altered miRs for all experimental groups is depicted in Fig. 3D. IPA analysis of these 260 significantly altered miRs revealed several were downregulated in the TNBS+Res group that targeted key anti-inflammatory T cell components such as FoxP3 (miR-31-5p, miR-182-5p, miR-210-3p), IL-10 (miR-146-a-5p and miR-27a-5p), TGFβ2/3 (miR132-3p, miR-1999a-5p, miR193a-3p, miR-148a-3p, let-7a-3p, miR-29b-3p), and several SMAD proteins (miR-330-5p, miR-139-3p, miR-30c-1-3p*, miR-16-5p*, miR-27a-3p) (Fig. 5). Among these miRs targeting key anti-inflammatory T cell factors, miR-31, predicted to target FoxP3, was the most significantly downregulated (-6.790 fold change) when comparing TNBS+Res vs TNBS+Veh groups (Fig. 5). Thus, the microarray data suggested that treatment with

resveratrol was able to downregulate miRs that normally targeted anti-inflammatory gene expression and components.

Resveratrol downregulates FoxP3-targeting miR-31 which is highly upregulated in human colitis patients

As miR-31 was the most significantly downregulated miR indicated in targeting anti-inflammatory T cell response and factors, PCR was performed to validate the microarray results. Results showed that miR-31 was significantly increased in the MLN of TNBS+Veh mice compared to the control groups, whereas TNBS mice treated with resveratrol had decreased expression of this miRNA (Fig. 6A). Validation was also performed on other miRs highlighted in Fig. 5 to include let-7a (Fig. 6B) and miR-132 (Fig. 6C). As with miR-31, results showed these miRs were increased in the disease state (TNBS+Veh), but treatment with resveratrol (TNBS+Res) prevented their disease-associated upregulation. Next, alignment analysis was performed to determine the potential of FoxP3 being a target. miR-31 was found to have three potential binding sites on the 3'-untranslated region (UTR) of the FoxP3 transcript, two of which had highly-probable miR-target mRNA interactions as predicted by mirSVR and PhastCons scores (Fig. 6D). Transfection experiments were performed to determine if alterations in this miR affected FoxP3 expression by giving SEB-activated T cells from the MLN either mock (just transfection reagent), miR-31-mimic, or miR-31-inhibitor. PCR validation of miR-31 expression showed the transfection was successful (Fig. 6E), and the results indicated that when miR-31 was upregulated (miR-mimic), expression of FoxP3 transcript was downregulated (Fig. 6F). On the contrary, if miR-31 was inhibited, as in the case of treatment with resveratrol, then FoxP3 expression was increased. Collectively,

these data showed that FoxP3 expression was altered by miR-31, a diseased-associated miR that resveratrol treatment prevented from becoming upregulated. Lastly, as the TNBS-induced model indicated FoxP3-targeting miR-31 was a potential target in this murine model of colitis, human studies looking at miR expression in colon biopsies of UC patients was investigated to determine any applicable correlation between this animal model and the human patient population. As shown, miR-31 was found to be significantly increased in patients with UC when compared to controls (Fig. 6G). Interestingly enough, this upregulation of miR-31 was found to be even more significant in UC colon biopsies that developed colon cancer-associated neoplastic lesions when compared to healthy controls (Fig. 6H). These data provided a link with observed miR-31 upregulation in the mouse model of colitis and human UC patient population, which resveratrol was able to prevent, effectively inhibiting miR-31 from targeting anti-inflammatory FoxP3-mediated response.

4.5 DISCUSSION

Previous studies have shown resveratrol is capable of preventing or at least reducing symptoms associated with animal models of colitis by a variety of different mechanisms. For example, in our earliest reports in the DSS-induced model of colitis, we showed resveratrol upregulated silent mating type information regulation-1 (SIRT-1) and downregulating nuclear transcription factor-kappaB (NF-κB) in immune cells (Singh et al., 2010). In a more recent report by Zhang et al., researchers confirmed our results that resveratrol treatment in the DSS model upregulated SIRT-1 in addition to mechanistic target of rapamycin (mTOR), while also downregulating other pro-inflammatory factors (e.g. autophagy-related 12, Beclin-1, and microtubule-associated protein light chain 3 II)

(Zhang et al., 2019). As in this report, Yao et al. showed resveratrol effectively regulated Treg/Th17 signaling during DSS-induced colitis via modulating hypoxia inducible factor (HIF)-1α/mammalian target of rapamycin (mTOR) signaling pathways (Yao et al., 2015). In another chemically-induced colitis model in rats using oxazolone, resveratrol treatment was shown to exert anti-inflammatory and pro-apoptotic properties by inhibiting myeloperoxidase (MPO) and sphingosine kinase 1 (SphK1) (Abdin, 2013). In fact, the success of resveratrol treatment in animal models of colitis translates even into the human patient population. A double-blinded, placebo-controlled pilot study in UC patients has shown that supplementation of 500mg/kg of resveratrol for 6 weeks appears to improve quality of life and partially reduce disease severity in this patient population, thought to be due to the ability of this natural product to reduce oxidative stress (Samsami-Kor et al., 2015; Samsamikor et al., 2016). In addition to the growing number of studies identifying resveratrol as a potential preventative and therapeutic against colitis and even CRC, there are a number of reports linking dysregulation in miRs possible mechanisms which drive disease development and progression.

As early as a decade ago, reports highlighted the differential expression of certain miRs in patients with colitis (UC and CD) and CRC (Ahmed et al., 2009; Takagi et al., 2010; Wu et al., 2008). In one of the earliest animal model reports, Chen et al. identified miR-155 was altered in activated CD4+ cells from TNBS-induced colitis mice (Chen et al., 2010), which supported our previous report showing miR-155 deficient mice had protection against colitis induction (Singh et al., 2014a). Since these early reports, the role of miR dysregulation in colitis is becoming more established from both a potential diagnostic tool to areas of therapeutic intervention. For example, a recent published

report suggest that serum levels of miR-146-5p are a better diagnostic tool to evaluate UC and CD severity than the standard C-reactive protein levels (Chen et al., 2019). miR-449a was suggested to be a possible predictor of colitis-associated CRC progression (Feng et al., 2018). Going beyond just diagnostic and biomarkers of disease, miRs are being looked as potential promoters and inhibitors of colitis as well. miR-590-5p, via inhibition of Yes-associated protein 1 (YAP), was shown to reduce intestinal inflammation in both colon cancer cells and mouse models of colitis with significant correlations in intestinal tissues from CD patients (Yu et al., 2018). An antagomir for miR-148a was reported to be a potentially effective drug treatment in amelioration of colitis because of its ability to selectively deplete the pro-inflammatory Th1 response without interrupting other protective immunological function during chronic colitis (Maschmeyer et al., 2018). The current report advances previous studies on miRs by demonstrating that miR-31 is a potential therapeutic target in colitis and CRC prevention.

The current study identifies the miR-31/FoxP3 axis as a means to prevent colitis development, showing this miR was significantly upregulated in the TNBS-induced murine model of colitis as well as documented in a dataset of UC colitis patients. In 2011, researchers reported that miR-31 was found to be highly dysregulated in epithelial cells from chronically inflamed mouse colons and APC(Min/+) tumors (Necela et al., 2011), and in that same year a report described how miR-31 increase correlated with chronic inflammation in IBD developing into neoplasia (Olaru et al., 2011). However, while many reports identify miR-31 as being abnormally high in colitis patients and animal models of colitis, the exact role of this miR in disease progression and development is somewhat controversial.

Liu et al. found that colon epithelial-specific deletion of miR-31 resulted in a more severe form of colitis-associated colorectal cancer than wild-type counterparts (Liu et al., 2017), and another report suggested that overexpression of miR-31 in UC targeted and regulated the pro-inflammatory IL-13 signaling (Gwiggner et al., 2018). These reports align with other studies suggesting miR-31 is important in protecting against colitis by way of engaging mucosal healing processes during inflammatory events within the colon (Tian et al., 2019; Whiteoak et al., 2018). It is important to note that such findings do not necessarily contradict our data suggesting resveratrol-mediated targeting of miR-31 assists in prevention of colitis. Such reports indicated miR-31 seemed to be protective in epithelial cells, whereas our report shows that in CD4+ immune cells, downregulating miR-31 helps initiate a potential anti-inflammatory Treg response. Thus, while upregulation of miR-31 in colonic epithelial cells might serve a protective role, in immune cells it has the potential to promote inflammation by reducing Treg development. This highlights the need to better understand through additional research how regulating miRs in different cell types might have varying consequences. Nevertheless, the current study provides evidence for additional pathways through which resveratrol offers a highly valuable preventative and therapeutic properties against colitis and possibly colitis-associated CRC.

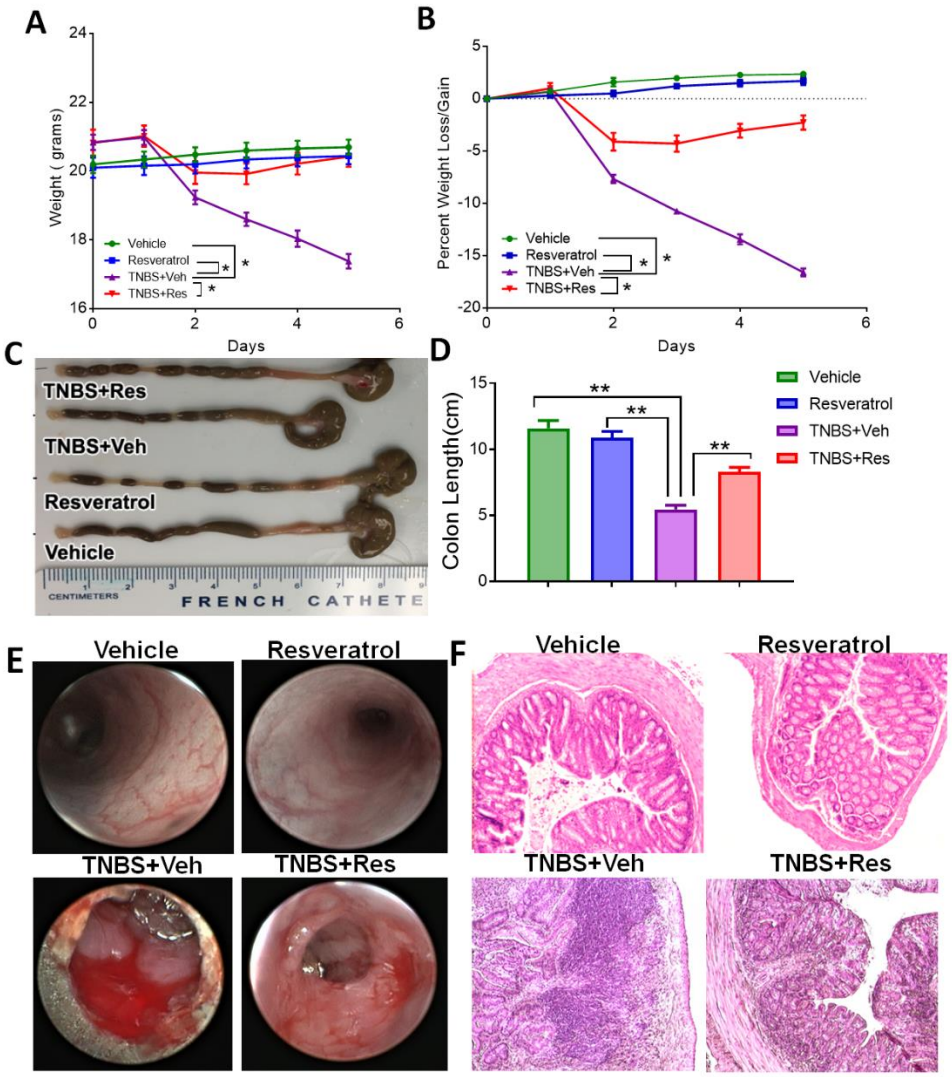

Figure 4.1 Treatment with resveratrol reduces clinical parameters in TNBS-induced colitis. BALB/c mice were injected intrarectally with 1mg of TNBS to induce colitis. Mice treated with resveratrol were given 100mg/kg in vehicle (1% CMC) by oral gavage 24 hours prior to the TNBS injection as well as daily up until the experimental end point (day 4). Experimental groups consisted of: Vehicle (n=5), Resveratrol (n=5), TNBS+Veh (n=5), and TNBS+Res (n=5). Initial clinical parameters consisted of evaluating weight (A), percent weight loss (B) and colon length (C-D). (E) Representative colonoscopies are shown from experimental groups during peak of disease (day 3). (F) Representative colon sections from fixed and paraffin-embedded tissue sections stained with H&E at 20x objective. Significance (p-value: *<0.05, **<0.01, ***<0.005, ****<0.001) was determined by using one-way ANOVA and post-hoc Tukey's test for bar graphs and Mann-Whitney test for weight data. Data are representative of at least 3 independent experiments.

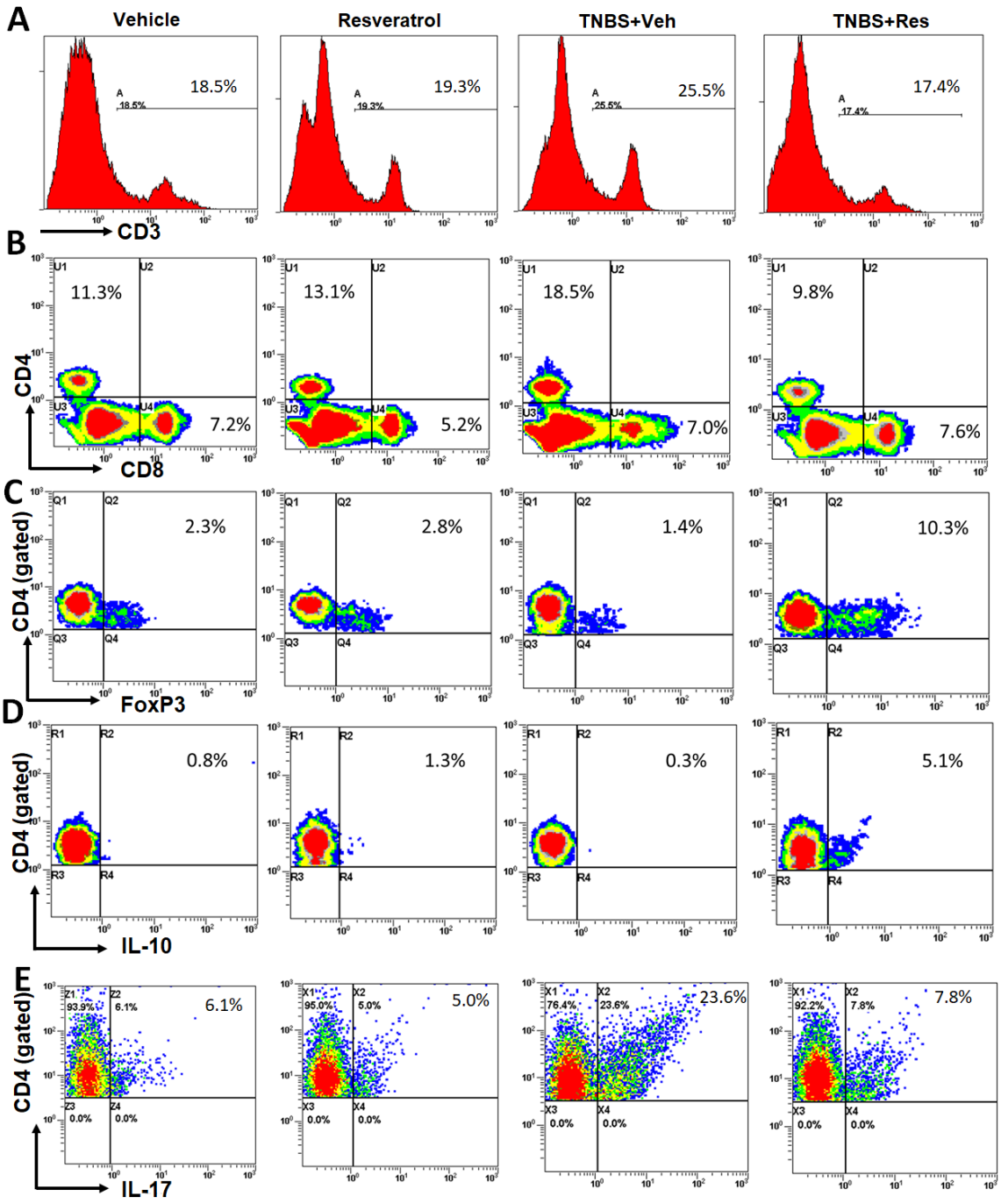

Figure 4.2 Treatment with resveratrol alters T cell subsets in the MLN of TNBS-induced mice. TNBS disease and treatment with resveratrol were performed as described in Figure 4.1 legend. MLNs were excised from experimental groups (n=5 per experimental group), stained with T cell-specific antibodies, and analyzed by flow cytometry. Representative T cell subset staining by flow cytometry was as follows: (A) CD3+ positive histogram plot; (B) CD4+ and CD8+ dot plot; (C) CD4+-gated FoxP3+ dot plot; (D) CD4+-gated IL-10 dot plot; (E) CD4+-gated IL-17 dot plot.

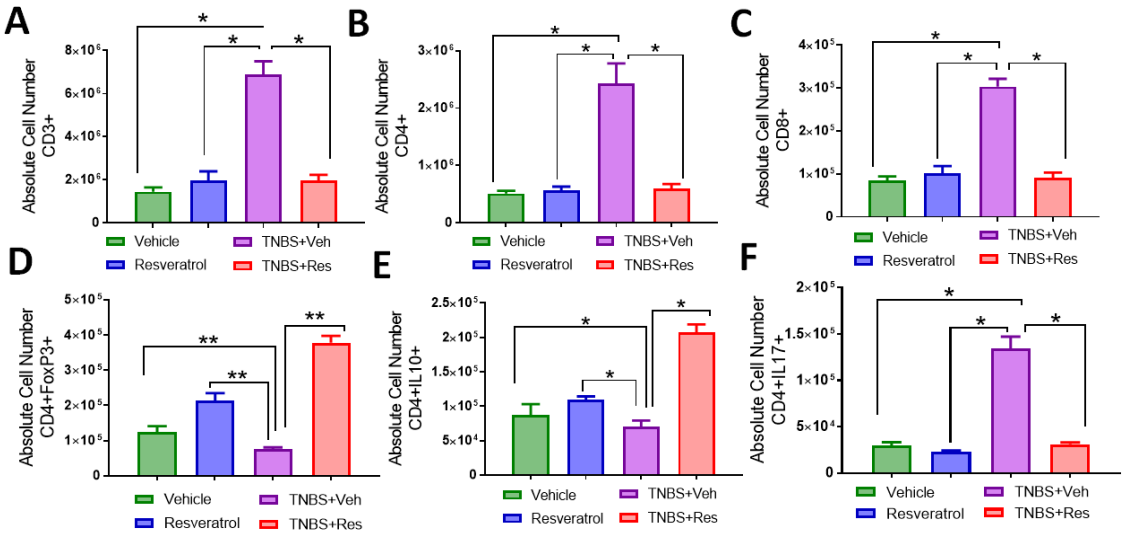

Figure 4.3 Treatment with resveratrol increases absolute cell numbers of anti-inflammatory T cell subsets in the MLN of TNBS-induced mice. TNBS disease and treatment with resveratrol were performed as described in Figure 4.1 legend. MLNs were excised from experimental groups (n=5 per experimental group), stained with T cell-specific antibodies, and analyzed by flow cytometry (as represented in Figure 4.2). Bar graphs depict absolute cell numbers in MLN for all T cells (F), T helper cells (G), cytotoxic T cells (H), Tregs (I), T helper producing IL-10 cells (J), and Th17 cells (K). Significance (p-value: *<0.05, **<0.01, ***<0.005, ****<0.001) was determined by using one-way ANOVA and post-hoc Tukey's test for bar dot graphs. Data are representative of at least 3 independent experiments.

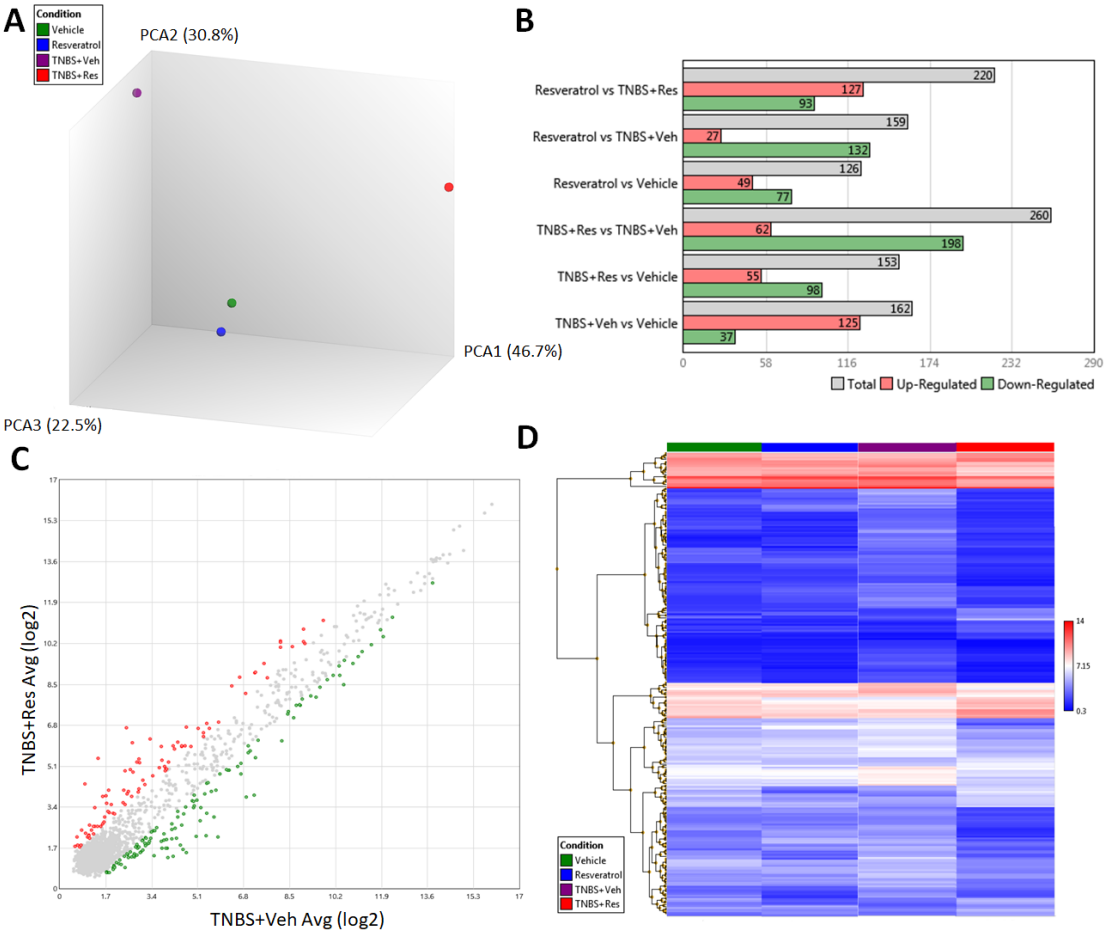

Figure 4.4 Treatment with resveratrol alters the miR profile in TNBS-induced colitis MLN. TNBS disease and treatment with resveratrol were performed as described in Figure 4.1 legend. RNA from MLN of experimental groups was isolated for miR microarray analysis using the murine-specific Affymetrix miRNA 4.0 chip. Experimental groups (Vehicle, Resveratrol, TNBS+Veh, and TNBS+Res) consisted of pools of 5 mice per group. Affymetrix Expression Console Version software was used to generate the following comparisons: (A) 3D PCA plot comparing all experimental groups; (B) multiple bar graph comparisons depicting significantly altered upregulated and downregulated (± 2 fold change) miRs between two experimental groups; (C) scatter plot depicting 260 significantly upregulated (red dots) and downregulated (green dots) miRs out of 3195 total between TNBS+Res and TNBS+Veh; and (D) heat map depicting raw expression values of the 260 aforementioned miRs among the 4 different experimental groups.

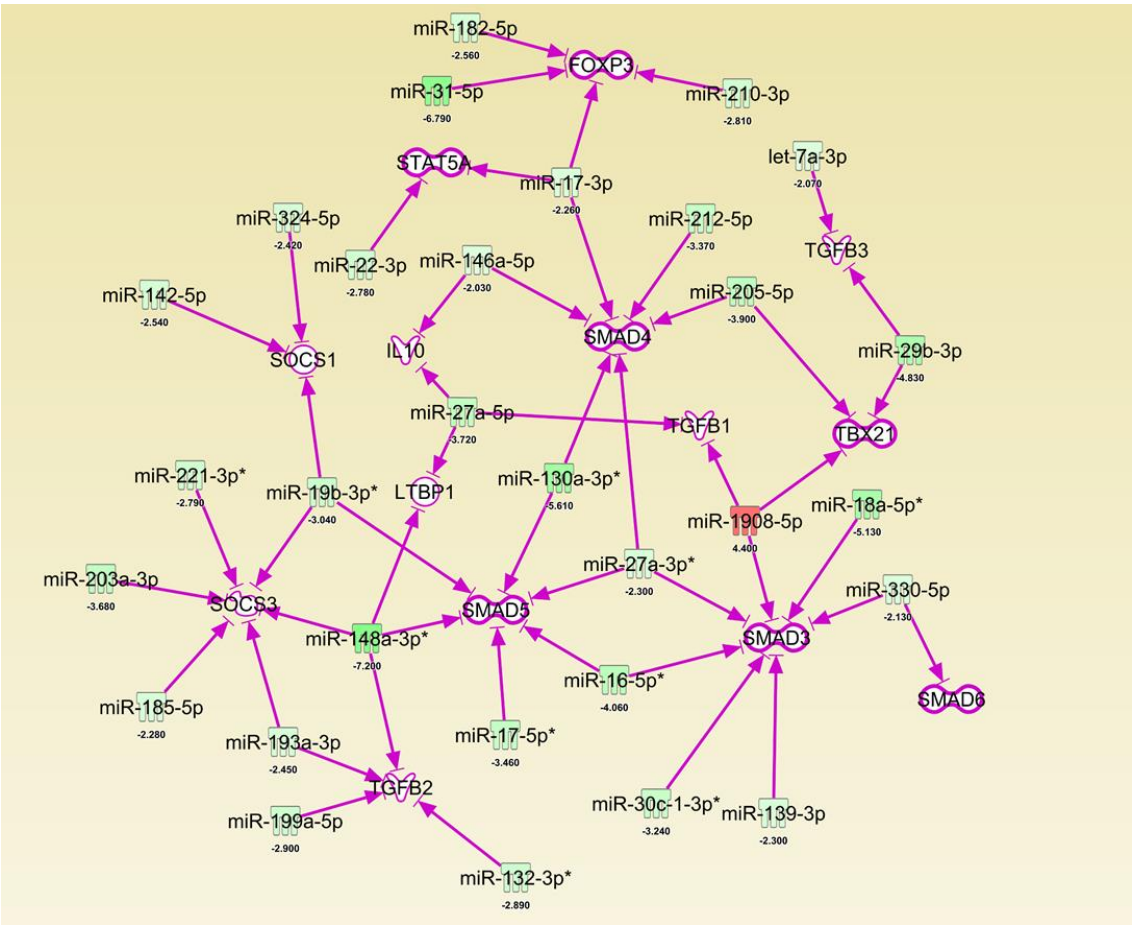

Figure 4.5 Treatment with resveratrol results in downregulation of several miRs that target anti-inflammatory T cell-associated factors. TNBS disease and treatment with resveratrol were performed as described in Figure 4.1 legend. 260 significantly altered miRs between TNBS+Res vs. TNBS+Veh noted in Figure 4.3 legend were subjected to Ingenuity Pathway Analysis (IPA). Depicted is an IPA-generated interaction chart showing significantly altered miRs targeting factors associated with anti-inflammatory T cell responses. Green colors represent downregulated miRs and Red colors represent upregulated miRs. The calculated fold changes between TNBS+Res and TNBS+Veh groups are depicted below each included miR. Purple arrows indicate predicted, highly predicted, and experimentally-proven interactions of the miR with target mRNA shown.

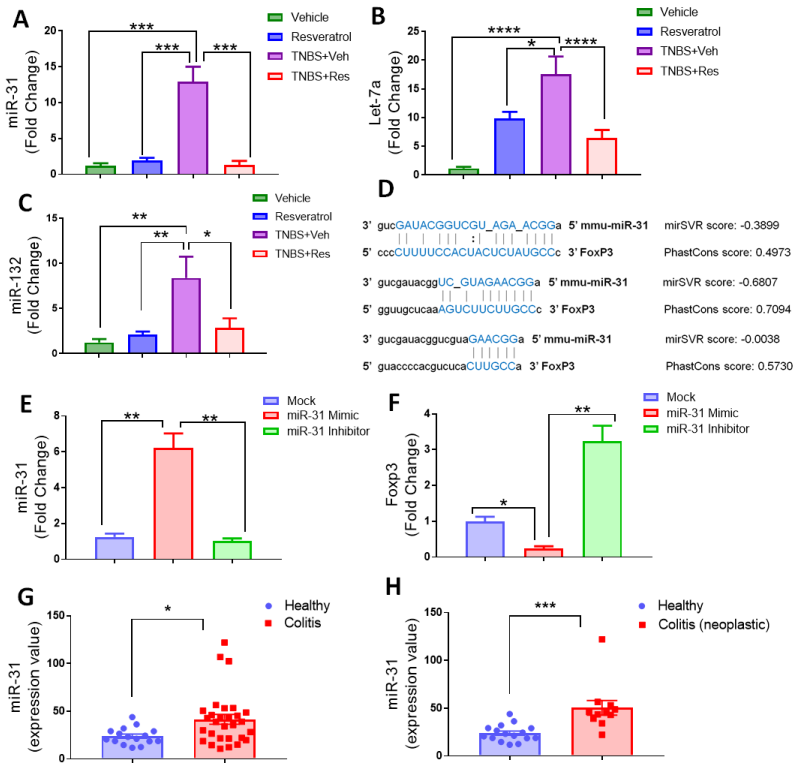

Figure 4.6 Resveratrol prevents FoxP3-targeting miR-31 upregulation in TNBS-induced colitis which correlates with miR-31 upregulation in human UC patients. TNBS disease and treatment with resveratrol were performed as described in Figure 4.1 legend. RNA was isolated from MLN of Vehicle (n=5), Resveratrol (n=5), TNBS+Veh (n=5), and TNBS+Res (n=5) to validate expression levels of miR-31 (A), Let-7a (B), and miR-132 (C). (D) Predicted miR-31 and FoxP3 alignment sites (with mirSVR and Phastcon scores) were obtained from microrna.org. For transfection experiments, single-cell suspensions from normal mouse MLN were seeded ($1x10^5$ cells per well) and activated with SEB (1µg/ml) for 24 hours before collecting total RNA from groups. Experimental groups consisted of transfection reagent only mock (n=5), miR-31 mimic (n=5), and miR-31 inhibitor (n=5). Depicted are PCR-generated expression fold changes for miR-31 (E) and FoxP3 (F). For human samples depicted, raw expression values of miR-31 from colonic biopsies were obtained from GEO data GSE68306. Two comparisons are depicted: (G) Normal Healthy controls (n=16) vs. all UC patients (n=29); and (H) Normal Healthy controls (n=16) vs. UC patients associated with neoplasia (n=11). Significance (p-value: *<0.05, **<0.01, ***<0.005, ****<0.001) was determined by using one-way ANOVA and post-hoc Tukey's test for bar dot graphs when comparing three or more groups. Data are representative of at least 3 independent experiments. For human datasets, significance was determined using an unpaired, two-tailed t test.

CHAPTER 5

SUMMARY AND CONCLUSION

Resveratrol, a natural polyphenol found in various food and beverage products such as grapes, peanuts, and wine, is a potent anti-inflammatory agent capable of preventing or reducing symptoms associated with colitis and colitis-induced CRC by a variety of mechanisms. Using well-established murine models of both colitis (TNBS) and CRC (AOM/DSS), results showed that resveratrol was able to prevent or greatly reduce the symptoms associated with these animal models, which is supported by previously published reports. Highlighted in this disseration is the ability of resveratrol to regulate the gut microbiome and induce epigenetic modifications (e.g. miRs and HDACs) to promote induction of anti-inflammatory T cell subset, Tregs (CD4+FoxP3+).

In the microbiome, resveratrol promotes a microenvironment with increased production of SCFA butyrate, a suppressor of HDACS capable of inducing Tregs. In both the colitis model and CRC model, resveratrol was shown to alter the gut microbiome to favor butyrate production. In particular, in both disease models resveratrol decreased *Bacteriodes acidifaciens* and enriched *Akkermansia muciniphilia* and *Ruminococcus gnavus* species. Fecal transfer experiments provided evidence that the resveratrol-altered microbiome was directly responsible for the anti-inflammatory immune response and subsequent protection against colitis and CRC, a new and exiting finding not previously known. Interestingly, in addition to suppression of HDACs by increased butyrate production, resveratrol was shown to be able to suppress a majority of HDACs

independently of butyrate, and this directly correlated with increased Treg induction. In addition to alterations in the microbiome leading to Treg-promoting HDAC suppression, resveratrol is capable of downregulating several miRs (miR-31, let-7a, and miR-132) that target Treg-related factors (FoxP3, SMAD proteins, STATs, and TGF-β). Transfection experiments confirmed that miR-31 downregulation by resveratrol increased Treg-related transcription factor FoxP3, which was a signficant finding considering that UC patients were shown to have increased expression of this particular miR.

These new findings and mechanisms by which resveratrol regulates inflammation, which has the potential to promote cancer, provide additional evidence to suggest this natural compound can be a beneficial therapeutic or preventative measure against colitis and colitis associated CRC by way of induction of Tregs. The ability of resveratrol to induce Tregs is important not only because this T cell subset has anti-inflammatory properties, but also data presented here shows that increased Tregs correlate with increased survival of CRC patients. Inasmuch, the data and results presented here promote a strong case for this natural compound to be used as a safe alternative to treat and prevent colitis and CRC.

REFERENCES

Abdallah, D.M., and Ismael, N.R. (2011). Resveratrol abrogates adhesion molecules and protects against TNBS-induced ulcerative colitis in rats. Canadian journal of physiology and pharmacology *89*, 811-818.

Abdin, A.A. (2013). Targeting sphingosine kinase 1 (SphK1) and apoptosis by colon-specific delivery formula of resveratrol in treatment of experimental ulcerative colitis in rats. European journal of pharmacology *718*, 145-153.

Agawa, S., Muto, T., and Morioka, Y. (1988). Mucin abnormality of colonic mucosa in ulcerative colitis associated with carcinoma and/or dysplasia. Diseases of the colon and rectum *31*, 387-389.

Ahmed, F.E., Jeffries, C.D., Vos, P.W., Flake, G., Nuovo, G.J., Sinar, D.R., Naziri, W., and Marcuard, S.P. (2009). Diagnostic microRNA markers for screening sporadic human colon cancer and active ulcerative colitis in stool and tissue. Cancer Genomics Proteomics *6*, 281-295.

Akgun, E., Caliskan, C., Celik, H.A., Ozutemiz, A.O., Tuncyurek, M., and Aydin, H.H. (2005). Effects of N-acetylcysteine treatment on oxidative stress in acetic acid-induced experimental colitis in rats. J Int Med Res *33*, 196-206.

Al Bakir, I., Curtius, K., and Graham, T.A. (2018). From Colitis to Cancer: An Evolutionary Trajectory That Merges Maths and Biology. Frontiers in immunology *9*, 2368.

Alghetaa, H., Mohammed, A., Sultan, M., Busbee, P., Murphy, A., Chatterjee, S., Nagarkatti, M., and Nagarkatti, P. (2018). Resveratrol protects mice against SEB-induced acute lung injury and mortality by miR-193a modulation that targets TGF-beta signalling. Journal of cellular and molecular medicine *22*, 2644-2655.

Altamemi, I., Murphy, E.A., Catroppo, J.F., Zumbrun, E.E., Zhang, J., McClellan, J.L., Singh, U.P., Nagarkatti, P.S., and Nagarkatti, M. (2014). Role of microRNAs in resveratrol-mediated mitigation of colitis-associated tumorigenesis in Apc(Min/+) mice. The Journal of pharmacology and experimental therapeutics *350*, 99-109.

Amicarella, F., Muraro, M.G., Hirt, C., Cremonesi, E., Padovan, E., Mele, V., Governa, V., Han, J., Huber, X., Droeser, R.A., *et al.* (2017). Dual role of tumour-infiltrating T helper 17 cells in human colorectal cancer. Gut *66*, 692-704.

Antonelli, E., Villanacci, V., and Bassotti, G. (2018). Novel oral-targeted therapies for mucosal healing in ulcerative colitis. World journal of gastroenterology *24*, 5322-5330.

Ariake, K., Ohkusa, T., Sakurazawa, T., Kumagai, J., Eishi, Y., Hoshi, S., and Yajima, T. (2000). Roles of mucosal bacteria and succinic acid in colitis caused by dextran sulfate sodium in mice. Journal of medical and dental sciences *47*, 233-241.

Arpaia, N., Campbell, C., Fan, X., Dikiy, S., van der Veeken, J., deRoos, P., Liu, H., Cross, J.R., Pfeffer, K., Coffer, P.J., *et al.* (2013). Metabolites produced by commensal bacteria promote peripheral regulatory T-cell generation. Nature *504*, 451-455.

Autenrieth, D.M., and Baumgart, D.C. (2017). [Microbiome and Gut Inflammation]. Deutsche medizinische Wochenschrift *142*, 261-266.

Bacolod, M.D., Das, S.K., Sokhi, U.K., Bradley, S., Fenstermacher, D.A., Pellecchia, M., Emdad, L., Sarkar, D., and Fisher, P.B. (2015). Examination of Epigenetic and other Molecular Factors Associated with mda-9/Syntenin Dysregulation in Cancer Through Integrated Analyses of Public Genomic Datasets. Adv Cancer Res *127*, 49-121.

Becker, W., Nagarkatti, M., and Nagarkatti, P.S. (2018). miR-466a Targeting of TGF-beta2 Contributes to FoxP3(+) Regulatory T Cell Differentiation in a Murine Model of Allogeneic Transplantation. Frontiers in immunology *9*, 688.

Bedoui, S.A., Barbirou, M., Stayoussef, M., Dallel, M., Mokrani, A., Makni, L., Mezlini, A., Bouhaouala, B., Yacoubi-Loueslati, B., and Almawi, W.Y. (2018). Association of interleukin-17A polymorphisms with the risk of colorectal cancer: A case-control study. Cytokine *110*, 18-23.

Bird, J.K., Raederstorff, D., Weber, P., and Steinert, R.E. (2017). Cardiovascular and Antiobesity Effects of Resveratrol Mediated through the Gut Microbiota. Advances in nutrition *8*, 839-849.

Borges, S.C., Ferreira, P.E.B., da Silva, L.M., de Paula Werner, M.F., Irache, J.M., Cavalcanti, O.A., and Buttow, N.C. (2018). Evaluation of the treatment with resveratrol-loaded nanoparticles in intestinal injury model caused by ischemia and reperfusion. Toxicology *396-397*, 13-22.

Bose, D., Zimmerman, L.J., Pierobon, M., Petricoin, E., Tozzi, F., Parikh, A., Fan, F., Dallas, N., Xia, L., Gaur, P., *et al.* (2011). Chemoresistant colorectal cancer cells and cancer stem cells mediate growth and survival of bystander cells. British journal of cancer *105*, 1759-1767.

Buhrmann, C., Shayan, P., Goel, A., and Shakibaei, M. (2017). Resveratrol Regulates Colorectal Cancer Cell Invasion by Modulation of Focal Adhesion Molecules. Nutrients *9*.

Busbee, P.B., Nagarkatti, M., and Nagarkatti, P.S. (2015). Natural indoles, indole-3-carbinol (I3C) and 3,3'-diindolylmethane (DIM), attenuate staphylococcal enterotoxin B-

mediated liver injury by downregulating miR-31 expression and promoting caspase-2-mediated apoptosis. PloS one *10*, e0118506.

Busbee, P.B., Rouse, M., Nagarkatti, M., and Nagarkatti, P.S. (2013). Use of natural AhR ligands as potential therapeutic modalities against inflammatory disorders. Nutrition reviews *71*, 353-369.

Cani, P.D. (2018). Human gut microbiome: hopes, threats and promises. Gut.

Catalanotto, C., Cogoni, C., and Zardo, G. (2016). MicroRNA in Control of Gene Expression: An Overview of Nuclear Functions. Int J Mol Sci *17*.

Chen, D.F., Gong, B.D., Xie, Q., Ben, Q.W., Liu, J., and Yuan, Y.Z. (2010). MicroRNA155 is induced in activated CD4(+) T cells of TNBS-induced colitis in mice. World journal of gastroenterology *16*, 854-861.

Chen, G.Y. (2018). The Role of the Gut Microbiome in Colorectal Cancer. Clin Colon Rectal Surg *31*, 192-198.

Chen, J., Pitmon, E., and Wang, K. (2017). Microbiome, inflammation and colorectal cancer. Semin Immunol *32*, 43-53.

Chen, J., and Vitetta, L. (2018). Inflammation-Modulating Effect of Butyrate in the Prevention of Colon Cancer by Dietary Fiber. Clin Colorectal Cancer.

Chen, L., Yang, S., Liao, W., and Xiong, Y. (2015a). Modification of Antitumor Immunity and Tumor Microenvironment by Resveratrol in Mouse Renal Tumor Model. Cell biochemistry and biophysics *72*, 617-625.

Chen, L., Yang, S., Zumbrun, E.E., Guan, H., Nagarkatti, P.S., and Nagarkatti, M. (2015b). Resveratrol attenuates lipopolysaccharide-induced acute kidney injury by suppressing inflammation driven by macrophages. Molecular nutrition & food research *59*, 853-864.

Chen, M.L., Yi, L., Zhang, Y., Zhou, X., Ran, L., Yang, J., Zhu, J.D., Zhang, Q.Y., and Mi, M.T. (2016). Resveratrol Attenuates Trimethylamine-N-Oxide (TMAO)-Induced Atherosclerosis by Regulating TMAO Synthesis and Bile Acid Metabolism via Remodeling of the Gut Microbiota. mBio *7*, e02210-02215.

Chen, P., Li, Y., Li, L., Yu, Q., Chao, K., Zhou, G., Qiu, Y., Feng, R., Huang, S., He, Y., *et al.* (2019). Circulating microRNA146b-5p is superior to C-reactive protein as a novel biomarker for monitoring inflammatory bowel disease. Aliment Pharmacol Ther *49*, 733-743.

Chen, W., Liu, F., Ling, Z., Tong, X., and Xiang, C. (2012). Human intestinal lumen and mucosa-associated microbiota in patients with colorectal cancer. PloS one *7*, e39743.

Chitrala, K.N., Guan, H., Singh, N.P., Busbee, B., Gandy, A., Mehrpouya-Bahrami, P., Ganewatta, M.S., Tang, C., Chatterjee, S., Nagarkatti, P., *et al.* (2017). CD44 deletion leading to attenuation of experimental autoimmune encephalomyelitis results from alterations in gut microbiome in mice. European journal of immunology *47*, 1188-1199.

Chung, L., Thiele Orberg, E., Geis, A.L., Chan, J.L., Fu, K., DeStefano Shields, C.E., Dejea, C.M., Fathi, P., Chen, J., Finard, B.B., *et al.* (2018). Bacteroides fragilis Toxin Coordinates a Pro-carcinogenic Inflammatory Cascade via Targeting of Colonic Epithelial Cells. Cell Host Microbe *23*, 203-214 e205.

Cobo, E.R., Kissoon-Singh, V., Moreau, F., Holani, R., and Chadee, K. (2017). MUC2 Mucin and Butyrate Contribute to the Synthesis of the Antimicrobial Peptide Cathelicidin in Response to Entamoeba histolytica- and Dextran Sodium Sulfate-Induced Colitis. Infection and immunity *85*.

Conte, M.P., Schippa, S., Zamboni, I., Penta, M., Chiarini, F., Seganti, L., Osborn, J., Falconieri, P., Borrelli, O., and Cucchiara, S. (2006). Gut-associated bacterial microbiota in paediatric patients with inflammatory bowel disease. Gut *55*, 1760-1767.

Cui, X., Jin, Y., Hofseth, A.B., Pena, E., Habiger, J., Chumanevich, A., Poudyal, D., Nagarkatti, M., Nagarkatti, P.S., Singh, U.P., *et al.* (2010). Resveratrol suppresses colitis and colon cancer associated with colitis. Cancer prevention research *3*, 549-559.

Dai, H., Liu, X., Yan, J., Aabdin, Z.U., Bilal, M.S., and Shen, X. (2017). Sodium Butyrate Ameliorates High-Concentrate Diet-Induced Inflammation in the Rumen Epithelium of Dairy Goats. Journal of agricultural and food chemistry *65*, 596-604.

de Almeida, C.V., Taddei, A., and Amedei, A. (2018). The controversial role of Enterococcus faecalis in colorectal cancer. Therap Adv Gastroenterol *11*, 1756284818783606.

de la Lastra, C.A., and Villegas, I. (2005). Resveratrol as an anti-inflammatory and anti-aging agent: mechanisms and clinical implications. Molecular nutrition & food research *49*, 405-430.

de Oliveira, M.R., Chenet, A.L., Duarte, A.R., Scaini, G., and Quevedo, J. (2018). Molecular Mechanisms Underlying the Anti-depressant Effects of Resveratrol: a Review. Mol Neurobiol *55*, 4543-4559.

Diaz-Gerevini, G.T., Repossi, G., Dain, A., Tarres, M.C., Das, U.N., and Eynard, A.R. (2016). Beneficial action of resveratrol: How and why? Nutrition *32*, 174-178.

Edwards, B.K., Noone, A.M., Mariotto, A.B., Simard, E.P., Boscoe, F.P., Henley, S.J., Jemal, A., Cho, H., Anderson, R.N., Kohler, B.A., *et al.* (2014). Annual Report to the Nation on the status of cancer, 1975-2010, featuring prevalence of comorbidity and impact on survival among persons with lung, colorectal, breast, or prostate cancer. Cancer *120*, 1290-1314.

Ehrlich, A.K., Pennington, J.M., Bisson, W.H., Kolluri, S.K., and Kerkvliet, N.I. (2018). TCDD, FICZ, and Other High Affinity AhR Ligands Dose-Dependently Determine the Fate of CD4+ T Cell Differentiation. Toxicol Sci *161*, 310-320.

Elshaer, M., Chen, Y., Wang, X.J., and Tang, X. (2018). Resveratrol: An overview of its anti-cancer mechanisms. Life sciences *207*, 340-349.

Elson, C.O., Beagley, K.W., Sharmanov, A.T., Fujihashi, K., Kiyono, H., Tennyson, G.S., Cong, Y., Black, C.A., Ridwan, B.W., and McGhee, J.R. (1996). Hapten-induced model of murine inflammatory bowel disease: mucosa immune responses and protection by tolerance. Journal of immunology *157*, 2174-2185.

Etxeberria, U., Arias, N., Boque, N., Macarulla, M.T., Portillo, M.P., Martinez, J.A., and Milagro, F.I. (2015). Reshaping faecal gut microbiota composition by the intake of trans-resveratrol and quercetin in high-fat sucrose diet-fed rats. The Journal of nutritional biochemistry *26*, 651-660.

Feng, Y., Dong, Y.W., Song, Y.N., Xiao, J.H., Guo, X.Y., Jiang, W.L., and Lu, L.G. (2018). MicroRNA449a is a potential predictor of colitisassociated colorectal cancer progression. Oncology reports *40*, 1684-1694.

Finnell, J.E., Lombard, C.M., Melson, M.N., Singh, N.P., Nagarkatti, M., Nagarkatti, P., Fadel, J.R., Wood, C.S., and Wood, S.K. (2017). The protective effects of resveratrol on social stress-induced cytokine release and depressive-like behavior. Brain, behavior, and immunity *59*, 147-157.

Foersch, S., Waldner, M.J., and Neurath, M.F. (2012). Colitis and colorectal cancer. Digestive diseases *30*, 469-476.

Galvez, J. (2014). Role of Th17 Cells in the Pathogenesis of Human IBD. ISRN inflammation *2014*, 928461.

Global Burden of Disease Cancer, C., Fitzmaurice, C., Dicker, D., Pain, A., Hamavid, H., Moradi-Lakeh, M., MacIntyre, M.F., Allen, C., Hansen, G., Woodbrook, R., *et al.* (2015). The Global Burden of Cancer 2013. JAMA oncology *1*, 505-527.

Goel, M.K., Khanna, P., and Kishore, J. (2010). Understanding survival analysis: Kaplan-Meier estimate. Int J Ayurveda Res *1*, 274-278.

Gong, W.H., Zhao, N., Zhang, Z.M., Zhang, Y.X., Yan, L., and Li, J.B. (2017). The inhibitory effect of resveratrol on COX-2 expression in human colorectal cancer: a promising therapeutic strategy. Eur Rev Med Pharmacol Sci *21*, 1136-1143.

Guan, H., Singh, N.P., Singh, U.P., Nagarkatti, P.S., and Nagarkatti, M. (2012). Resveratrol prevents endothelial cells injury in high-dose interleukin-2 therapy against melanoma. PloS one *7*, e35650.

Guo, G., Zhou, J., Yang, X., Feng, J., Shao, Y., Jia, T., Huang, Q., Li, Y., Zhong, Y., Nagarkatti, P.S., *et al.* (2018). Role of MicroRNAs Induced by Chinese Herbal Medicines Against Hepatocellular Carcinoma: A Brief Review. Integrative cancer therapies *17*, 1059-1067.

Gwiggner, M., Martinez-Nunez, R.T., Whiteoak, S.R., Bondanese, V.P., Claridge, A., Collins, J.E., Cummings, J.R.F., and Sanchez-Elsner, T. (2018). MicroRNA-31 and MicroRNA-155 Are Overexpressed in Ulcerative Colitis and Regulate IL-13 Signaling by Targeting Interleukin 13 Receptor alpha-1. Genes (Basel) *9*.

Hart, A. (2019). Diet in the etiology of inflammatory bowel disease. Revista espanola de enfermedades digestivas : organo oficial de la Sociedad Espanola de Patologia Digestiva *111*, 3-4.

Hibberd, A.A., Lyra, A., Ouwehand, A.C., Rolny, P., Lindegren, H., Cedgard, L., and Wettergren, Y. (2017). Intestinal microbiota is altered in patients with colon cancer and modified by probiotic intervention. BMJ Open Gastroenterol *4*, e000145.

Hofseth, L.J., Singh, U.P., Singh, N.P., Nagarkatti, M., and Nagarkatti, P.S. (2010). Taming the beast within: resveratrol suppresses colitis and prevents colon cancer. Aging (Albany NY) *2*, 183-184.

Hong, E.H., Heo, E.Y., Song, J.H., Kwon, B.E., Lee, J.Y., Park, Y., Kim, J., Chang, S.Y., Chin, Y.W., Jeon, S.M., *et al.* (2017). Trans-scirpusin A showed antitumor effects via autophagy activation and apoptosis induction of colorectal cancer cells. Oncotarget *8*, 41401-41411.

Hu, G., Li, Z., and Wang, S. (2017). Tumor-infiltrating FoxP3(+) Tregs predict favorable outcome in colorectal cancer patients: A meta-analysis. Oncotarget *8*, 75361-75371.

Huderson, A.C., Rekha Devi, P.V., Niaz, M.S., Adunyah, S.E., and Ramesh, A. (2018). Alteration of benzo(a)pyrene biotransformation by resveratrol in Apc (Min/+) mouse model of colon carcinogenesis. Invest New Drugs.

Jang, S.H., Park, J., Kim, S.H., Choi, K.M., Ko, E.S., Cha, J.D., Lee, Y.R., Jang, H., and Jang, Y.S. (2017). Oral administration of red ginseng powder fermented with probiotic alleviates the severity of dextran-sulfate sodium-induced colitis in a mouse model. Chinese journal of natural medicines *15*, 192-201.

Jiang, W., Su, J., Zhang, X., Cheng, X., Zhou, J., Shi, R., and Zhang, H. (2014). Elevated levels of Th17 cells and Th17-related cytokines are associated with disease activity in patients with inflammatory bowel disease. Inflammation research : official journal of the European Histamine Research Society [et al] *63*, 943-950.

Jobin, C. (2017). Human Intestinal Microbiota and Colorectal Cancer: Moving Beyond Associative Studies. Gastroenterology *153*, 1475-1478.

Jung, M.J., Lee, J., Shin, N.R., Kim, M.S., Hyun, D.W., Yun, J.H., Kim, P.S., Whon, T.W., and Bae, J.W. (2016). Chronic Repression of mTOR Complex 2 Induces Changes in the Gut Microbiota of Diet-induced Obese Mice. Scientific reports *6*, 30887.

Kanauchi, O., Mitsuyama, K., Araki, Y., and Andoh, A. (2003). Modification of intestinal flora in the treatment of inflammatory bowel disease. Current pharmaceutical design *9*, 333-346.

Kang, C.S., Ban, M., Choi, E.J., Moon, H.G., Jeon, J.S., Kim, D.K., Park, S.K., Jeon, S.G., Roh, T.Y., Myung, S.J., *et al.* (2013). Extracellular vesicles derived from gut microbiota, especially Akkermansia muciniphila, protect the progression of dextran sulfate sodium-induced colitis. PloS one *8*, e76520.

Karakoyun, B., Ertas, B., Yuksel, M., Akakin, D., Cevik, O., and Sener, G. (2017). Ameliorative effects of riboflavin on acetic acid-induced colonic injury in rats. Clinical and experimental pharmacology & physiology.

Kespohl, M., Vachharajani, N., Luu, M., Harb, H., Pautz, S., Wolff, S., Sillner, N., Walker, A., Schmitt-Kopplin, P., Boettger, T., *et al.* (2017). The Microbial Metabolite Butyrate Induces Expression of Th1-Associated Factors in CD4(+) T Cells. Frontiers in immunology *8*, 1036.

Khosravi, A., Yanez, A., Price, J.G., Chow, A., Merad, M., Goodridge, H.S., and Mazmanian, S.K. (2014). Gut microbiota promote hematopoiesis to control bacterial infection. Cell Host Microbe *15*, 374-381.

Kim, H.S., and Berstad, A. (1992). Experimental colitis in animal models. Scandinavian journal of gastroenterology *27*, 529-537.

Kim, T.T., Parajuli, N., Sung, M.M., Bairwa, S.C., Levasseur, J., Soltys, C.M., Wishart, D.S., Madsen, K., Schertzer, J.D., and Dyck, J.R.B. (2018). Fecal transplant from resveratrol-fed donors improves glycaemia and cardiovascular features of the metabolic syndrome in mice. Am J Physiol Endocrinol Metab.

Ko, J.H., Sethi, G., Um, J.Y., Shanmugam, M.K., Arfuso, F., Kumar, A.P., Bishayee, A., and Ahn, K.S. (2017). The Role of Resveratrol in Cancer Therapy. Int J Mol Sci *18*.

Kodani, T., Rodriguez-Palacios, A., Corridoni, D., Lopetuso, L., Di Martino, L., Marks, B., Pizarro, J., Pizarro, T., Chak, A., and Cominelli, F. (2013). Flexible colonoscopy in mice to evaluate the severity of colitis and colorectal tumors using a validated endoscopic scoring system. J Vis Exp, e50843.

Koushki, M., Dashatan, N.A., and Meshkani, R. (2018). Effect of Resveratrol Supplementation on Inflammatory Markers: A Systematic Review and Meta-Analysis of Randomized Controlled Trials. Clin Ther.

Langille, M.G., Zaneveld, J., Caporaso, J.G., McDonald, D., Knights, D., Reyes, J.A., Clemente, J.C., Burkepile, D.E., Vega Thurber, R.L., Knight, R., *et al.* (2013). Predictive

functional profiling of microbial communities using 16S rRNA marker gene sequences. Nature biotechnology *31*, 814-821.

Lee, J.Y., Seo, E.H., Oh, C.S., Paik, J.H., Hwang, D.Y., Lee, S.H., and Kim, S.H. (2017). Impact Of Circulating T Helper 1 And 17 Cells in the Blood on Regional Lymph Node Invasion in Colorectal Cancer. J Cancer *8*, 1249-1254.

Lee, S.J., McLachlan, J.B., Kurtz, J.R., Fan, D., Winter, S.E., Baumler, A.J., Jenkins, M.K., and McSorley, S.J. (2012). Temporal expression of bacterial proteins instructs host CD4 T cell expansion and Th17 development. PLoS pathogens *8*, e1002499.

Lee, S.R., Jin, H., Kim, W.T., Kim, W.J., Kim, S.Z., Leem, S.H., and Kim, S.M. (2018). Tristetraprolin activation by resveratrol inhibits the proliferation and metastasis of colorectal cancer cells. Int J Oncol *53*, 1269-1278.

Li, J., Zhang, C.X., Liu, Y.M., Chen, K.L., and Chen, G. (2017). A comparative study of anti-aging properties and mechanism: resveratrol and caloric restriction. Oncotarget *8*, 65717-65729.

Liu, L., Tabung, F.K., Zhang, X., Nowak, J.A., Qian, Z.R., Hamada, T., Nevo, D., Bullman, S., Mima, K., Kosumi, K., *et al.* (2018). Diets That Promote Colon Inflammation Associate With Risk of Colorectal Carcinomas That Contain Fusobacterium nucleatum. Clin Gastroenterol Hepatol *16*, 1622-1631 e1623.

Liu, Z., Bai, J., Zhang, L., Lou, F., Ke, F., Cai, W., and Wang, H. (2017). Conditional knockout of microRNA-31 promotes the development of colitis associated cancer. Biochem Biophys Res Commun *490*, 62-68.

Lopetuso, L.R., De Salvo, C., Pastorelli, L., Rana, N., Senkfor, H.N., Petito, V., Di Martino, L., Scaldaferri, F., Gasbarrini, A., Cominelli, F., *et al.* (2018). IL-33 promotes recovery from acute colitis by inducing miR-320 to stimulate epithelial restitution and repair. Proceedings of the National Academy of Sciences of the United States of America *115*, E9362-E9370.

Lopez, A., Pouillon, L., Beaugerie, L., Danese, S., and Peyrin-Biroulet, L. (2018). Colorectal cancer prevention in patients with ulcerative colitis. Best Pract Res Clin Gastroenterol *32-33*, 103-109.

Marchix, J., Goddard, G., and Helmrath, M.A. (2018). Host-Gut Microbiota Crosstalk in Intestinal Adaptation. Cellular and molecular gastroenterology and hepatology *6*, 149-162.

Martin-Gallausiaux, C., Beguet-Crespel, F., Marinelli, L., Jamet, A., Ledue, F., Blottiere, H.M., and Lapaque, N. (2018). Butyrate produced by gut commensal bacteria activates TGF-beta1 expression through the transcription factor SP1 in human intestinal epithelial cells. Scientific reports *8*, 9742.

Martin, A.R., Villegas, I., Sanchez-Hidalgo, M., and de la Lastra, C.A. (2006). The effects of resveratrol, a phytoalexin derived from red wines, on chronic inflammation induced in an experimentally induced colitis model. British journal of pharmacology *147*, 873-885.

Martinez-Moya, P., Ortega-Gonzalez, M., Gonzalez, R., Anzola, A., Ocon, B., Hernandez-Chirlaque, C., Lopez-Posadas, R., Suarez, M.D., Zarzuelo, A., Martinez-Augustin, O., *et al.* (2012). Exogenous alkaline phosphatase treatment complements endogenous enzyme protection in colonic inflammation and reduces bacterial translocation in rats. Pharmacological research *66*, 144-153.

Maschmeyer, P., Petkau, G., Siracusa, F., Zimmermann, J., Zugel, F., Kuhl, A.A., Lehmann, K., Schimmelpfennig, S., Weber, M., Haftmann, C., *et al.* (2018). Selective targeting of pro-inflammatory Th1 cells by microRNA-148a-specific antagomirs in vivo. J Autoimmun *89*, 41-52.

Meighani, A., Hart, B.R., Bourgi, K., Miller, N., John, A., and Ramesh, M. (2017). Outcomes of Fecal Microbiota Transplantation for Clostridium difficile Infection in Patients with Inflammatory Bowel Disease. Digestive diseases and sciences.

Meisel, M., Mayassi, T., Fehlner-Peach, H., Koval, J.C., O'Brien, S.L., Hinterleitner, R., Lesko, K., Kim, S., Bouziat, R., Chen, L., *et al.* (2017). Interleukin-15 promotes intestinal dysbiosis with butyrate deficiency associated with increased susceptibility to colitis. The ISME journal *11*, 15-30.

Mikhailov, T.A., and Furner, S.E. (2009). Breastfeeding and genetic factors in the etiology of inflammatory bowel disease in children. World journal of gastroenterology *15*, 270-279.

Minacapelli, C.D., Bajpai, M., Geng, X., Van Gurp, J., Poplin, E., Amenta, P.S., Brant, S.R., and Das, K.M. (2019). miR-206 as a Biomarker for Response to Mesalamine Treatment in Ulcerative Colitis. Inflammatory bowel diseases *25*, 78-84.

Miranda, K., Yang, X., Bam, M., Murphy, E.A., Nagarkatti, P.S., and Nagarkatti, M. (2018). MicroRNA-30 modulates metabolic inflammation by regulating Notch signaling in adipose tissue macrophages. International journal of obesity *42*, 1140-1150.

Miyamoto, Y., and Itoh, K. (2000). Bacteroides acidifaciens sp. nov., isolated from the caecum of mice. International journal of systematic and evolutionary microbiology *50 Pt 1*, 145-148.

Molodecky, N.A., Soon, I.S., Rabi, D.M., Ghali, W.A., Ferris, M., Chernoff, G., Benchimol, E.I., Panaccione, R., Ghosh, S., Barkema, H.W., *et al.* (2012). Increasing incidence and prevalence of the inflammatory bowel diseases with time, based on systematic review. Gastroenterology *142*, 46-54 e42; quiz e30.

Mori, G., Rampelli, S., Orena, B.S., Rengucci, C., De Maio, G., Barbieri, G., Passardi, A., Casadei Gardini, A., Frassineti, G.L., Gaiarsa, S., *et al.* (2018). Shifts of Faecal Microbiota During Sporadic Colorectal Carcinogenesis. Scientific reports *8*, 10329.

Morilla, I., Uzzan, M., Laharie, D., Cazals-Hatem, D., Denost, Q., Daniel, F., Belleannee, G., Bouhnik, Y., Wainrib, G., Panis, Y., *et al.* (2018). Colonic MicroRNA Profiles, Identified by a Deep Learning Algorithm, That Predict Responses to Therapy of Patients With Acute Severe Ulcerative Colitis. Clinical gastroenterology and hepatology : the official clinical practice journal of the American Gastroenterological Association.

Necela, B.M., Carr, J.M., Asmann, Y.W., and Thompson, E.A. (2011). Differential expression of microRNAs in tumors from chronically inflamed or genetic (APC(Min/+)) models of colon cancer. PloS one *6*, e18501.

Nishikawa, J., Kudo, T., Sakata, S., Benno, Y., and Sugiyama, T. (2009). Diversity of mucosa-associated microbiota in active and inactive ulcerative colitis. Scandinavian journal of gastroenterology *44*, 180-186.

Nunes, S., Danesi, F., Del Rio, D., and Silva, P. (2018). Resveratrol and inflammatory bowel disease: the evidence so far. Nutrition research reviews *31*, 85-97.

Olaru, A.V., Selaru, F.M., Mori, Y., Vazquez, C., David, S., Paun, B., Cheng, Y., Jin, Z., Yang, J., Agarwal, R., *et al.* (2011). Dynamic changes in the expression of MicroRNA-31 during inflammatory bowel disease-associated neoplastic transformation. Inflammatory bowel diseases *17*, 221-231.

Ong, C., Aw, M.M., Liwanag, M.J., Quak, S.H., and Phua, K.B. (2018). Rapid rise in the incidence and clinical characteristics of pediatric inflammatory bowel disease in a South-East Asian cohort in Singapore, 1994-2015. Journal of digestive diseases *19*, 395-403.

Paramsothy, S., Paramsothy, R., Rubin, D.T., Kamm, M.A., Kaakoush, N.O., Mitchell, H.M., and Castano-Rodriguez, N. (2017). Faecal Microbiota Transplantation for Inflammatory Bowel Disease: A Systematic Review and Meta-analysis. Journal of Crohn's & colitis.

Patnala, R., Arumugam, T.V., Gupta, N., and Dheen, S.T. (2017). HDAC Inhibitor Sodium Butyrate-Mediated Epigenetic Regulation Enhances Neuroprotective Function of Microglia During Ischemic Stroke. Mol Neurobiol *54*, 6391-6411.

Pekow, J., Meckel, K., Dougherty, U., Huang, Y., Chen, X., Almoghrabi, A., Mustafi, R., Ayaloglu-Butun, F., Deng, Z., Haider, H.I., *et al.* (2017). miR-193a-3p is a Key Tumor Suppressor in Ulcerative Colitis-Associated Colon Cancer and Promotes Carcinogenesis through Upregulation of IL17RD. Clinical cancer research : an official journal of the American Association for Cancer Research *23*, 5281-5291.

Peng, R.M., Lin, G.R., Ting, Y., and Hu, J.Y. (2018). Oral delivery system enhanced the bioavailability of stilbenes: Resveratrol and pterostilbene. BioFactors *44*, 5-15.

Pittman, M.E. (2018). Fecal Microbiota and Screening for Colorectal Cancer. Clinical chemistry.

Png, C.W., Linden, S.K., Gilshenan, K.S., Zoetendal, E.G., McSweeney, C.S., Sly, L.I., McGuckin, M.A., and Florin, T.H. (2010). Mucolytic bacteria with increased prevalence in IBD mucosa augment in vitro utilization of mucin by other bacteria. The American journal of gastroenterology *105*, 2420-2428.

Qiao, Y., Sun, J., Xia, S., Tang, X., Shi, Y., and Le, G. (2014). Effects of resveratrol on gut microbiota and fat storage in a mouse model with high-fat-induced obesity. Food Funct *5*, 1241-1249.

Rapozo, D.C., Bernardazzi, C., and de Souza, H.S. (2017). Diet and microbiota in inflammatory bowel disease: The gut in disharmony. World journal of gastroenterology *23*, 2124-2140.

Rezasoltani, S., Asadzadeh-Aghdaei, H., Nazemalhosseini-Mojarad, E., Dabiri, H., Ghanbari, R., and Zali, M.R. (2017). Gut microbiota, epigenetic modification and colorectal cancer. Iran J Microbiol *9*, 55-63.

Riccioni, G., Gammone, M.A., Tettamanti, G., Bergante, S., Pluchinotta, F.R., and D'Orazio, N. (2015). Resveratrol and anti-atherogenic effects. Int J Food Sci Nutr *66*, 603-610.

Rieder, S.A., Nagarkatti, P., and Nagarkatti, M. (2012). Multiple anti-inflammatory pathways triggered by resveratrol lead to amelioration of staphylococcal enterotoxin B-induced lung injury. British journal of pharmacology *167*, 1244-1258.

Sadraei, H., Asghari, G., Khanabadi, M., and Minaiyan, M. (2017). Anti-inflammatory effect of apigenin and hydroalcoholic extract of Dracocephalum kotschyi on acetic acid-induced colitis in rats. Research in pharmaceutical sciences *12*, 322-329.

Salimi, V., Shahsavari, Z., Safizadeh, B., Hosseini, A., Khademian, N., and Tavakoli-Yaraki, M. (2017). Sodium butyrate promotes apoptosis in breast cancer cells through reactive oxygen species (ROS) formation and mitochondrial impairment. Lipids in health and disease *16*, 208.

Samsami-Kor, M., Daryani, N.E., Asl, P.R., and Hekmatdoost, A. (2015). Anti-Inflammatory Effects of Resveratrol in Patients with Ulcerative Colitis: A Randomized, Double-Blind, Placebo-controlled Pilot Study. Archives of medical research *46*, 280-285.

Samsamikor, M., Daryani, N.E., Asl, P.R., and Hekmatdoost, A. (2016). Resveratrol Supplementation and Oxidative/Anti-Oxidative Status in Patients with Ulcerative Colitis: A Randomized, Double-Blind, Placebo-controlled Pilot Study. Archives of medical research *47*, 304-309.

San Hipolito-Luengo, A., Alcaide, A., Ramos-Gonzalez, M., Cercas, E., Vallejo, S., Romero, A., Talero, E., Sanchez-Ferrer, C.F., Motilva, V., and Peiro, C. (2017). Dual

Effects of Resveratrol on Cell Death and Proliferation of Colon Cancer Cells. Nutrition and cancer *69*, 1019-1027.

Satokari, R., Fuentes, S., Mattila, E., Jalanka, J., de Vos, W.M., and Arkkila, P. (2014). Fecal transplantation treatment of antibiotic-induced, noninfectious colitis and long-term microbiota follow-up. Case reports in medicine *2014*, 913867.

Schonauen, K., Le, N., von Arnim, U., Schulz, C., Malfertheiner, P., and Link, A. (2018). Circulating and Fecal microRNAs as Biomarkers for Inflammatory Bowel Diseases. Inflammatory bowel diseases *24*, 1547-1557.

Segata, N., Izard, J., Waldron, L., Gevers, D., Miropolsky, L., Garrett, W.S., and Huttenhower, C. (2011). Metagenomic biomarker discovery and explanation. Genome biology *12*, R60.

Seth, R.K., Kimono, D., Alhasson, F., Sarkar, S., Albadrani, M., Lasley, S.K., Horner, R., Janulewicz, P., Nagarkatti, M., Nagarkatti, P., *et al.* (2018). Increased butyrate priming in the gut stalls microbiome associated-gastrointestinal inflammation and hepatic metabolic reprogramming in a mouse model of Gulf War Illness. Toxicol Appl Pharmacol *350*, 64-77.

Sethi, V., Kurtom, S., Tarique, M., Lavania, S., Malchiodi, Z., Hellmund, L., Zhang, L., Sharma, U., Giri, B., Garg, B., *et al.* (2018). Gut Microbiota Promotes Tumor Growth in Mice by Modulating Immune Response. Gastroenterology *155*, 33-37 e36.

Silva, L.G., Ferguson, B.S., Avila, A.S., and Faciola, A.P. (2018). Sodium propionate and sodium butyrate effects on histone deacetylase (HDAC) activity, histone acetylation, and inflammatory gene expression in bovine mammary epithelial cells. Journal of animal science *96*, 5244-5252.

Simeoli, R., Mattace Raso, G., Pirozzi, C., Lama, A., Santoro, A., Russo, R., Montero-Melendez, T., Berni Canani, R., Calignano, A., Perretti, M., *et al.* (2017). An orally administered butyrate-releasing derivative reduces neutrophil recruitment and inflammation in dextran sulphate sodium-induced murine colitis. British journal of pharmacology *174*, 1484-1496.

Singh, C.K., Kumar, A., Hitchcock, D.B., Fan, D., Goodwin, R., LaVoie, H.A., Nagarkatti, P., DiPette, D.J., and Singh, U.S. (2011a). Resveratrol prevents embryonic oxidative stress and apoptosis associated with diabetic embryopathy and improves glucose and lipid profile of diabetic dam. Molecular nutrition & food research *55*, 1186-1196.

Singh, N.P., Hegde, V.L., Hofseth, L.J., Nagarkatti, M., and Nagarkatti, P. (2007). Resveratrol (trans-3,5,4'-trihydroxystilbene) ameliorates experimental allergic encephalomyelitis, primarily via induction of apoptosis in T cells involving activation of aryl hydrocarbon receptor and estrogen receptor. Molecular pharmacology *72*, 1508-1521.

Singh, N.P., Singh, U.P., Hegde, V.L., Guan, H., Hofseth, L., Nagarkatti, M., and Nagarkatti, P.S. (2011b). Resveratrol (trans-3,5,4'-trihydroxystilbene) suppresses EL4 tumor growth by induction of apoptosis involving reciprocal regulation of SIRT1 and NF-kappaB. Molecular nutrition & food research *55*, 1207-1218.

Singh, N.P., Singh, U.P., Rouse, M., Zhang, J., Chatterjee, S., Nagarkatti, P.S., and Nagarkatti, M. (2016). Dietary Indoles Suppress Delayed-Type Hypersensitivity by Inducing a Switch from Proinflammatory Th17 Cells to Anti-Inflammatory Regulatory T Cells through Regulation of MicroRNA. Journal of immunology *196*, 1108-1122.

Singh, U.P., Murphy, A.E., Enos, R.T., Shamran, H.A., Singh, N.P., Guan, H., Hegde, V.L., Fan, D., Price, R.L., Taub, D.D., *et al.* (2014a). miR-155 deficiency protects mice from experimental colitis by reducing T helper type 1/type 17 responses. Immunology *143*, 478-489.

Singh, U.P., Singh, N.P., Guan, H., Busbee, B., Price, R.L., Taub, D.D., Mishra, M.K., Fayad, R., Nagarkatti, M., and Nagarkatti, P.S. (2014b). The emerging role of leptin antagonist as potential therapeutic option for inflammatory bowel disease. International reviews of immunology *33*, 23-33.

Singh, U.P., Singh, N.P., Singh, B., Hofseth, L.J., Price, R.L., Nagarkatti, M., and Nagarkatti, P.S. (2010). Resveratrol (trans-3,5,4'-trihydroxystilbene) induces silent mating type information regulation-1 and down-regulates nuclear transcription factor-kappaB activation to abrogate dextran sulfate sodium-induced colitis. The Journal of pharmacology and experimental therapeutics *332*, 829-839.

Singh, U.P., Singh, N.P., Singh, B., Hofseth, L.J., Taub, D.D., Price, R.L., Nagarkatti, M., and Nagarkatti, P.S. (2012). Role of resveratrol-induced CD11b(+) Gr-1(+) myeloid derived suppressor cells (MDSCs) in the reduction of CXCR3(+) T cells and amelioration of chronic colitis in IL-10(-/-) mice. Brain, behavior, and immunity *26*, 72-82.

Sitkin, S., and Pokrotnieks, J. (2018). Clinical Potential of Anti-inflammatory Effects of Faecalibacterium prausnitzii and Butyrate in Inflammatory Bowel Disease. Inflammatory bowel diseases.

Slattery, M.L., Mullany, L.E., Wolff, R.K., Sakoda, L.C., Samowitz, W.S., and Herrick, J.S. (2018). The p53-signaling pathway and colorectal cancer: Interactions between downstream p53 target genes and miRNAs. Genomics.

Song, M., Garrett, W.S., and Chan, A.T. (2015). Nutrients, foods, and colorectal cancer prevention. Gastroenterology *148*, 1244-1260 e1216.

Song, M., Sasazuki, S., Camargo, M.C., Shimazu, T., Charvat, H., Yamaji, T., Sawada, N., Kemp, T.J., Pfeiffer, R.M., Hildesheim, A., *et al.* (2018). Circulating Inflammatory Markers and Colorectal Cancer Risk: A Prospective Case-cohort Study in Japan. Int J Cancer.

Sun, B., Jia, Y., Hong, J., Sun, Q., Gao, S., Hu, Y., Zhao, N., and Zhao, R. (2018). Sodium Butyrate Ameliorates High-Fat-Diet-Induced Non-alcoholic Fatty Liver Disease through Peroxisome Proliferator-Activated Receptor alpha-Mediated Activation of beta Oxidation and Suppression of Inflammation. Journal of agricultural and food chemistry *66*, 7633-7642.

Sun, H.L., Zhou, X., Xue, Y.F., Wang, K., Shen, Y.F., Mao, J.J., Guo, H.F., and Miao, Z.N. (2012). Increased frequency and clinical significance of myeloid-derived suppressor cells in human colorectal carcinoma. World journal of gastroenterology *18*, 3303-3309.

Sun, X., and Zhu, M.J. (2018). Butyrate Inhibits Indices of Colorectal Carcinogenesis via Enhancing alpha-Ketoglutarate-Dependent DNA Demethylation of Mismatch Repair Genes. Molecular nutrition & food research *62*, e1700932.

Sung, M.M., Kim, T.T., Denou, E., Soltys, C.M., Hamza, S.M., Byrne, N.J., Masson, G., Park, H., Wishart, D.S., Madsen, K.L., *et al.* (2017). Improved Glucose Homeostasis in Obese Mice Treated With Resveratrol Is Associated With Alterations in the Gut Microbiome. Diabetes *66*, 418-425.

Sykora, J., Pomahacova, R., Kreslova, M., Cvalinova, D., Stych, P., and Schwarz, J. (2018). Current global trends in the incidence of pediatric-onset inflammatory bowel disease. World journal of gastroenterology *24*, 2741-2763.

Tabung, F.K., Liu, L., Wang, W., Fung, T.T., Wu, K., Smith-Warner, S.A., Cao, Y., Hu, F.B., Ogino, S., Fuchs, C.S., *et al.* (2018). Association of Dietary Inflammatory Potential With Colorectal Cancer Risk in Men and Women. JAMA oncology *4*, 366-373.

Tain, Y.L., Lee, W.C., Wu, K.L.H., Leu, S., and Chan, J.Y.H. (2018). Resveratrol Prevents the Development of Hypertension Programmed by Maternal Plus Post-Weaning High-Fructose Consumption through Modulation of Oxidative Stress, Nutrient-Sensing Signals, and Gut Microbiota. Molecular nutrition & food research, e1800066.

Takagi, T., Naito, Y., Mizushima, K., Hirata, I., Yagi, N., Tomatsuri, N., Ando, T., Oyamada, Y., Isozaki, Y., Hongo, H., *et al.* (2010). Increased expression of microRNA in the inflamed colonic mucosa of patients with active ulcerative colitis. J Gastroenterol Hepatol *25 Suppl 1*, S129-133.

Tian, Y., Xu, J., Li, Y., Zhao, R., Du, S., Lv, C., Wu, W., Liu, R., Sheng, X., Song, Y., *et al.* (2019). MicroRNA-31 Reduces Inflammatory Signaling and Promotes Regeneration in Colon Epithelium, and Delivery of Mimics in Microspheres Reduces Colitis in Mice. Gastroenterology.

Tian, Y., Xu, Q., Sun, L., Ye, Y., and Ji, G. (2018). Short-chain fatty acids administration is protective in colitis-associated colorectal cancer development. The Journal of nutritional biochemistry *57*, 103-109.

Timperi, E., Pacella, I., Schinzari, V., Focaccetti, C., Sacco, L., Farelli, F., Caronna, R., Del Bene, G., Longo, F., Ciardi, A., *et al.* (2016). Regulatory T cells with multiple

suppressive and potentially pro-tumor activities accumulate in human colorectal cancer. Oncoimmunology *5*, e1175800.

Tung, Y.C., Lin, Y.H., Chen, H.J., Chou, S.C., Cheng, A.C., Kalyanam, N., Ho, C.T., and Pan, M.H. (2016). Piceatannol Exerts Anti-Obesity Effects in C57BL/6 Mice through Modulating Adipogenic Proteins and Gut Microbiota. Molecules *21*.

Ueno, A., Jeffery, L., Kobayashi, T., Hibi, T., Ghosh, S., and Jijon, H. (2018). Th17 plasticity and its relevance to inflammatory bowel disease. Journal of autoimmunity *87*, 38-49.

van der Beek, C.M., Dejong, C.H.C., Troost, F.J., Masclee, A.A.M., and Lenaerts, K. (2017). Role of short-chain fatty acids in colonic inflammation, carcinogenesis, and mucosal protection and healing. Nutrition reviews *75*, 286-305.

Vieira, R.S., Castoldi, A., Basso, P.J., Hiyane, M.I., Camara, N.O.S., and Almeida, R.R. (2019). Butyrate Attenuates Lung Inflammation by Negatively Modulating Th9 Cells. Frontiers in immunology *10*, 67.

Wagnerova, A., Babickova, J., Liptak, R., Vlkova, B., Celec, P., and Gardlik, R. (2017). Sex Differences in the Effect of Resveratrol on DSS-Induced Colitis in Mice. Gastroenterology research and practice *2017*, 8051870.

Wang, B., Sun, J., Li, X., Zhou, Q., Bai, J., Shi, Y., and Le, G. (2013). Resveratrol prevents suppression of regulatory T-cell production, oxidative stress, and inflammation of mice prone or resistant to high-fat diet-induced obesity. Nutrition research *33*, 971-981.

Wang, F., Liu, J., Weng, T., Shen, K., Chen, Z., Yu, Y., Huang, Q., Wang, G., Liu, Z., and Jin, S. (2017). The Inflammation Induced by Lipopolysaccharide can be Mitigated by Short-chain Fatty Acid, Butyrate, through Upregulation of IL-10 in Septic Shock. Scandinavian journal of immunology *85*, 258-263.

Weber, N., Liou, D., Dommer, J., MacMenamin, P., Quinones, M., Misner, I., Oler, A.J., Wan, J., Kim, L., Coakley McCarthy, M., *et al.* (2018). Nephele: a cloud platform for simplified, standardized and reproducible microbiome data analysis. Bioinformatics *34*, 1411-1413.

Whiteoak, S.R., Claridge, A., Balendran, C.A., Harris, R.J., Gwiggner, M., Bondanese, V.P., Erlandsson, F., Hansen, M.B., Cummings, J.R.F., and Sanchez-Elsner, T. (2018). MicroRNA-31 Targets Thymic Stromal Lymphopoietin in Mucosal Infiltrated CD4+ T Cells: A Role in Achieving Mucosal Healing in Ulcerative Colitis? Inflammatory bowel diseases *24*, 2377-2385.

Wong, S.H., Zhao, L., Zhang, X., Nakatsu, G., Han, J., Xu, W., Xiao, X., Kwong, T.N.Y., Tsoi, H., Wu, W.K.K., *et al.* (2017). Gavage of Fecal Samples From Patients With Colorectal Cancer Promotes Intestinal Carcinogenesis in Germ-Free and Conventional Mice. Gastroenterology *153*, 1621-1633 e1626.

Wu, F., Zikusoka, M., Trindade, A., Dassopoulos, T., Harris, M.L., Bayless, T.M., Brant, S.R., Chakravarti, S., and Kwon, J.H. (2008). MicroRNAs are differentially expressed in ulcerative colitis and alter expression of macrophage inflammatory peptide-2 alpha. Gastroenterology *135*, 1624-1635 e1624.

Wu, S.L., Yu, L., Meng, K.W., Ma, Z.H., and Pan, C.E. (2005). Resveratrol prolongs allograft survival after liver transplantation in rats. World journal of gastroenterology *11*, 4745-4749.

Xu, P., Fan, W., Zhang, Z., Wang, J., Wang, P., Li, Y., and Yu, M. (2017). The Clinicopathological and Prognostic Implications of FoxP3(+) Regulatory T Cells in Patients with Colorectal Cancer: A Meta-Analysis. Front Physiol *8*, 950.

Xu, Y.H., Gao, C.L., Guo, H.L., Zhang, W.Q., Huang, W., Tang, S.S., Gan, W.J., Xu, Y., Zhou, H., and Zhu, Q. (2018). Sodium butyrate supplementation ameliorates diabetic inflammation in db/db mice. J Endocrinol *238*, 231-244.

Yan, G., Liu, T., Yin, L., Kang, Z., and Wang, L. (2018). Levels of peripheral Th17 cells and serum Th17-related cytokines in patients with colorectal cancer: a meta-analysis. Cell Mol Biol (Noisy-le-grand) *64*, 94-102.

Yang, H., Wang, W., Romano, K.A., Gu, M., Sanidad, K.Z., Kim, D., Yang, J., Schmidt, B., Panigrahy, D., Pei, R., *et al.* (2018a). A common antimicrobial additive increases colonic inflammation and colitis-associated colon tumorigenesis in mice. Science translational medicine *10*.

Yang, S., Li, W., Sun, H., Wu, B., Ji, F., Sun, T., Chang, H., Shen, P., Wang, Y., and Zhou, D. (2015). Resveratrol elicits anti-colorectal cancer effect by activating miR-34c-KITLG in vitro and in vivo. BMC Cancer *15*, 969.

Yang, Y., Chen, G., Yang, Q., Ye, J., Cai, X., Tsering, P., Cheng, X., Hu, C., Zhang, S., and Cao, P. (2017). Gut microbiota drives the attenuation of dextran sulphate sodium-induced colitis by Huangqin decoction. Oncotarget *8*, 48863-48874.

Yang, Y., Xu, C., Wu, D., Wang, Z., Wu, P., Li, L., Huang, J., and Qiu, F. (2018b). gammadelta T Cells: Crosstalk Between Microbiota, Chronic Inflammation, and Colorectal Cancer. Frontiers in immunology *9*, 1483.

Yao, J., Wang, J.Y., Liu, L., Zeng, W.S., Li, Y.X., Xun, A.Y., Zhao, L., Jia, C.H., Feng, J.L., Wei, X.X., *et al.* (2011). Polydatin ameliorates DSS-induced colitis in mice through inhibition of nuclear factor-kappaB activation. Planta medica *77*, 421-427.

Yao, J., Wei, C., Wang, J.Y., Zhang, R., Li, Y.X., and Wang, L.S. (2015). Effect of resveratrol on Treg/Th17 signaling and ulcerative colitis treatment in mice. World journal of gastroenterology *21*, 6572-6581.

Youn, J., Lee, J.S., Na, H.K., Kundu, J.K., and Surh, Y.J. (2009). Resveratrol and piceatannol inhibit iNOS expression and NF-kappaB activation in dextran sulfate sodium-induced mouse colitis. Nutrition and cancer *61*, 847-854.

Yu, M., Luo, Y., Cong, Z., Mu, Y., Qiu, Y., and Zhong, M. (2018). MicroRNA-590-5p Inhibits Intestinal Inflammation by Targeting YAP. J Crohns Colitis *12*, 993-1004.

Zeng, Y.H., Zhou, L.Y., Chen, Q.Z., Li, Y., Shao, Y., Ren, W.Y., Liao, Y.P., Wang, H., Zhu, J.H., Huang, M., *et al.* (2017). Resveratrol inactivates PI3K/Akt signaling through upregulating BMP7 in human colon cancer cells. Oncol Rep *38*, 456-464.

Zhang, H., Du, M., Yang, Q., and Zhu, M.J. (2016a). Butyrate suppresses murine mast cell proliferation and cytokine production through inhibiting histone deacetylase. The Journal of nutritional biochemistry *27*, 299-306.

Zhang, L., Xue, H., Zhao, G., Qiao, C., Sun, X., Pang, C., and Zhang, D. (2019). Curcumin and resveratrol suppress dextran sulfate sodiuminduced colitis in mice. Molecular medicine reports.

Zhang, M., Zhou, Q., Dorfman, R.G., Huang, X., Fan, T., Zhang, H., Zhang, J., and Yu, C. (2016b). Butyrate inhibits interleukin-17 and generates Tregs to ameliorate colorectal colitis in rats. BMC gastroenterology *16*, 84.

Zhang, T., Ding, C., Zhao, M., Dai, X., Yang, J., Li, Y., Gu, L., Wei, Y., Gong, J., Zhu, W., *et al.* (2016c). Sodium Butyrate Reduces Colitogenic Immunoglobulin A-Coated Bacteria and Modifies the Composition of Microbiota in IL-10 Deficient Mice. Nutrients *8*.

Zhao, G., Nyman, M., and Jonsson, J.A. (2006). Rapid determination of short-chain fatty acids in colonic contents and faeces of humans and rats by acidified water-extraction and direct-injection gas chromatography. Biomedical chromatography : BMC *20*, 674-682.

Zhao, L., Zhang, Q., Ma, W., Tian, F., Shen, H., and Zhou, M. (2017). A combination of quercetin and resveratrol reduces obesity in high-fat diet-fed rats by modulation of gut microbiota. Food Funct *8*, 4644-4656.

Zhuo, C., Xu, Y., Ying, M., Li, Q., Huang, L., Li, D., Cai, S., and Li, B. (2015). FOXP3+ Tregs: heterogeneous phenotypes and conflicting impacts on survival outcomes in patients with colorectal cancer. Immunol Res *61*, 338-347.

Zou, S., Fang, L., and Lee, M.H. (2018). Dysbiosis of gut microbiota in promoting the development of colorectal cancer. Gastroenterol Rep (Oxf) *6*, 1-12.

Zu, Y., Overby, H., Ren, G., Fan, Z., Zhao, L., and Wang, S. (2018). Resveratrol liposomes and lipid nanocarriers: Comparison of characteristics and inducing browning of white adipocytes. Colloids and surfaces B, Biointerfaces *164*, 414-423.